

**Master's thesis**

Maren Wassås Kveinå

# Carbon Looping for Metallurgical Processes via Boudouard reaction over Magnetite

Master's thesis in Industrial chemistry and biotechnology

Supervisor: De Chen

July 2020

**NTNU**  
Norwegian University of Science and Technology  
Faculty of Natural Sciences  
Department of Chemical Engineering



Norwegian University of  
Science and Technology



Maren Wassås Kveinå

# **Carbon Looping for Metallurgical Processes via Boudouard reaction over Magnetite**

Master's thesis in Industrial chemistry and biotechnology  
Supervisor: De Chen  
July 2020

Norwegian University of Science and Technology  
Faculty of Natural Sciences  
Department of Chemical Engineering







# Preface

This thesis was written as the final part of my masters studies from the Norwegian University of Science and Technology (NTNU) in the spring 2020.

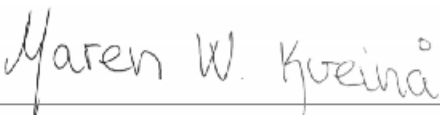
I would like to thank my main supervisor Professor De Chen, for his continued support and guidance in regards to the project. He has been an important motivator throughout this work with his never-ending excitement in regards to the field of science. I would also like to express my gratitude to my co-supervisor Kumar R. Rout for his helpful inputs and for introducing me to connections in the metallurgical industry.

Furthermore, I would like to express my deepest gratitude to Martina Cazzolaro for her guidance and invaluable inputs regarding not only the practical work, but also writing of the thesis and overall moral support. Her work ethic and motivation throughout the entire project has been inspirational. Finally, I am forever grateful for all love and support provided by my closest family and friends.

## Declaration of Compliance

I hereby declare that this is an independent work in compliance with the exam regulations of the Norwegian University of Science and Technology (NTNU).

Maren Wassås Kveinå:



---



# Abstract

The development of efficient and cost-effective technology for the reduction of CO<sub>2</sub> emissions in the metallurgical industry is a major objective for a future low-emission society. Carbothermal reduction of metal oxides produces CO-rich oven gas, which is typically oxidized and emitted to the atmosphere. This thesis aims to explore a novel strategy to decrease the CO<sub>2</sub> emissions through closing the carbon loop; converting the CO-rich gas to C and CO<sub>2</sub> via the Boudouard reaction.

Aspen Plus™ was used to evaluate the thermodynamic equilibrium product distribution when a CO-rich oven gas (from the FeMn process) was fed to a Gibbs reactor. Investigations on the effect of temperature as well as partial pressures of CO<sub>2</sub> and H<sub>2</sub> in the feed were performed. The results show higher CO conversion and C yield obtained by decreasing temperature and P<sub>CO<sub>2</sub></sub> in the feed as well as increasing P<sub>H<sub>2</sub></sub> in the feed to H<sub>2</sub>/CO ≈ 1.

Experiments were conducted feeding the same CO-rich gas mixture to a chemical vapor deposition setup for the production of carbon nanofibers in the presence of magnetite catalyst. Investigating the effect of temperature, catalyst loading and partial pressure of CO<sub>2</sub> and H<sub>2</sub> in the feed on the conversion of CO, H<sub>2</sub>, CO<sub>2</sub> and yield of carbon, compared to the Aspen Plus™ results. The experiments conversion of CO and yield of C is dependent on temperature as well as feed composition. The highest C yield (23.7 %) was obtained feeding CO<sub>2</sub>/CO = 0 at a temperature around 600°C. Furthermore, characterization of the produced carbon by X-ray diffraction and Raman spectroscopy suggests formation of carbon with very small crystallite dimensions.

The potential reduction in CO<sub>2</sub> emissions and required reducing agent were estimated by a mass balance approach on both Aspen Plus™ and experimental results. The results show potential in reducing the ton CO<sub>2</sub> emitted per ton metal produced by 10.8 and 3.7 %. Finally, the potential reduction of ton fresh reducing agent were estimated to 21.7 and 7.3 %. Even higher reduction potential was found by halving P<sub>CO<sub>2</sub></sub> in feed.



# Sammendrag

Utvikling av en effektiv og økonomisk gunstig teknologi for reduksjon av CO<sub>2</sub> utslipp i metallindustrien er et mål for å oppnå et fremtidig lav-utslipp samfunn. Karbotermisk reduksjon av metalloksider produserer en ovngass rik på CO, som typisk blir oksidert og slippet ut i atmosfæren. Målet med denne masteroppgaven er å utforske en ny strategi for å minske CO<sub>2</sub> utslipp gjennom å resirkulere karbon; omgjøring av den CO-rike ovngassen til C og CO<sub>2</sub> via Boudouard reaksjonen og implementering av karbon fangst.

Aspen Plus™ ble benyttet for å estimere produkt distribusjonen ved termodynamisk likevekt, når en typisk CO-rik ovngass fra FeMn prosessen brukes som føde. Effekten av temperatur og partiell trykk av CO<sub>2</sub> og H<sub>2</sub> i føden ble undersøkt. Resultatene viser at høyere omdanning av CO og utbytte av C oppnås når temperaturen og partiell trykket av CO<sub>2</sub> minskes og partiell trykket av H<sub>2</sub> økes. Høyest karbon utbytte ble funnet for H<sub>2</sub>/CO ≈ 1.

Eksperimenter ble utført hvor den samme CO-rike ovngassen ble brukt som føde til et kjemisk dampavsetningsoppsett for produksjon av karbon nanofiber ved bruk av magnetitt katalysator. Det ble gjennomført undersøkelser på effekt av temperatur, mengde katalysator og P<sub>CO2</sub> og P<sub>H2</sub> i føden på omdanningen av CO, CO<sub>2</sub>, H<sub>2</sub> og utbytte av C. Resultatene ble sammenlignet med resultatene fra Aspen Plus™. Funnene viser at omdanning av CO og utbytte av C er avhengig av temperatur og fødekomposisjon. Høyest karbonutbytte (27.3 %) ble funnet ved CO<sub>2</sub>/CO = 0 og temperatur rundt 600°C. Røntgen-diffraksjon og Raman spektroskopi karakterisering av produsert karbon antydte veldig små krystalitt-dimensjoner.

Videre ble potensiell reduksjon av CO<sub>2</sub> utslipp og reduksjonsmiddel estimert ved bruk av massebalanse for både Aspen Plus™ og eksperimentelle resultater. Reduksjonen av tonn CO<sub>2</sub> utslipp/tonn metall ble funnet til 10.8 og 3.7 %. Reduksjonen av tonn reduksjonsmiddel/tonn metall ble estimert til 21.7 og 7.3 %. Enda høyere reduksjonspotensiale ble funnet ved å halvere P<sub>CO2</sub> i føden.



# Contents

<b>1</b>	<b>Introduction</b>	<b>1</b>
1.1	Background . . . . .	1
1.2	Project objective and scopes . . . . .	3
<b>2</b>	<b>Literature review</b>	<b>6</b>
2.1	Metallurgical industries overview . . . . .	6
2.1.1	Blast furnaces . . . . .	11
2.1.2	Electric arc furnaces . . . . .	14
2.2	Reducing agents . . . . .	17
2.2.1	Mechanical stability and particle size . . . . .	19
2.2.2	Composition . . . . .	20
2.2.3	Reactivity . . . . .	20
2.3	Oven gas . . . . .	21
2.4	Carbon capture . . . . .	23
2.5	Carbon materials . . . . .	25
2.5.1	Carbon nanomaterials . . . . .	26
<b>3</b>	<b>Method</b>	<b>35</b>
3.1	Synthesis of carbon nanofibers . . . . .	35
3.2	Catalyst . . . . .	39
3.2.1	Homemade catalyst . . . . .	39
3.2.2	Commercial catalyst . . . . .	40
3.2.3	GC analysis . . . . .	41

3.3	Characterization . . . . .	43
3.3.1	XRD analysis . . . . .	43
3.3.2	Raman spectroscopy . . . . .	45
3.4	Aspen Plus . . . . .	46
<b>4</b>	<b>Results and Discussion</b>	<b>49</b>
4.1	Aspen Plus simulation results . . . . .	49
4.1.1	CO <sub>2</sub> effect . . . . .	51
4.1.2	H <sub>2</sub> effect . . . . .	54
4.1.3	Temperature effect . . . . .	58
4.1.4	Main findings based on thermodynamic anal- ysis . . . . .	60
4.2	Experimental results . . . . .	61
4.2.1	CO <sub>2</sub> effect . . . . .	62
4.2.2	H <sub>2</sub> effect . . . . .	65
4.2.3	Temperature effect . . . . .	68
4.2.4	WHSV effect . . . . .	70
4.2.5	Main findings comparing Aspen Plus and ex- perimental results . . . . .	72
4.3	Characterization . . . . .	74
4.3.1	X-Ray Diffraction . . . . .	74
4.3.2	Raman spectroscopy . . . . .	77
4.4	Case study . . . . .	80
4.4.1	Challenges and opportunities in implement- ing the carbon-loop . . . . .	85
<b>5</b>	<b>Conclusion</b>	<b>86</b>
<b>6</b>	<b>Future work</b>	<b>89</b>
<b>A</b>	<b>Detailed experiment summary</b>	<b>i</b>
<b>B</b>	<b>Commercial catalyst specifics</b>	<b>iv</b>



<b>C</b>	<b>Internal standard and air-correction calculations</b>	<b>viii</b>
<b>D</b>	<b>Procedure for choosing GC data</b>	<b>xi</b>
<b>E</b>	<b>Case study calculation example</b>	<b>xiii</b>
<b>F</b>	<b>Detailed Risk assessment</b>	<b>xv</b>



# List of Figures

1.1	Scheme of metallurgical processes with carbon looping and carbon capture. . . . .	5
2.1	Schematic illustration of Blast furnace [1]. . . . .	11
2.2	Manganese reaction pathway [60]. . . . .	15
2.3	Publications on CNTs in the time period 1991-2004 [94]. . . . .	27
2.4	Carbon nanofiber structures, Platelet, Fishbone and Ribbon CNFs, respectively [77]. . . . .	28
2.5	Schematic illustration of methods for production of carbon nanomaterials [94]. . . . .	29
2.6	Schematic representation of proposed mechanism of CNF growth [5]. . . . .	31
3.1	Schematic representation of CVD synthesis apparatus. . . . .	36
3.2	Size distribution of magnetite produced by Rana Gruber Minerals AS. . . . .	40
3.3	Flowsheet of Aspen Plus simulation. . . . .	47
4.1	CO, H <sub>2</sub> , CO <sub>2</sub> conversion and C yield of Aspen Plus simulation exploring the CO <sub>2</sub> effect. . . . .	52
4.2	CO, H <sub>2</sub> , CO <sub>2</sub> conversion and C yield of Aspen Plus simulation exploring the H <sub>2</sub> effect. . . . .	55

4.3	CH <sub>4</sub> and H <sub>2</sub> O yield (based on CO fed) of Aspen Plus simulation exploring the H <sub>2</sub> effect. . . . .	56
4.4	Temperature effect on conversion of CO, H <sub>2</sub> , CO <sub>2</sub> and yield of C for temperatures ● 500°C, ● 550°C, ● 600°C, ● 650°C, ● 700°C. . . . .	58
4.5	Temperature effect on yield of CH <sub>4</sub> and H <sub>2</sub> O for temperatures ● 500°C, ● 550°C, ● 600°C, ● 650°C, ● 700°C. . . . .	59
4.6	CO, H <sub>2</sub> , CO <sub>2</sub> conversion and C yield exploring CO <sub>2</sub> effect, Experimental vs. Aspen. . . . .	62
4.7	CO, H <sub>2</sub> , CO <sub>2</sub> conversion and C yield exploring H <sub>2</sub> effect, Experimental vs. Aspen. . . . .	65
4.8	CO, H <sub>2</sub> , CO <sub>2</sub> conversion and C yield of Aspen Plus simulations exploring various defined product components. . . . .	67
4.9	Temperature effect on product distribution. . . . .	68
4.10	Product distribution exploring WHSV, compared to Aspen Plus; ● WHSV = 29.83, ● WHSV = 9.97, ● WHSV = 5.97 and ● Aspen Plus. . . . .	70
4.11	XRD graph . . . . .	75
4.12	Crystalline size of homemade and commercial catalyst at various CO <sub>2</sub> /CO ratios. . . . .	76
4.13	Raman plots . . . . .	77
4.14	Intensity ratio I <sub>D</sub> /I <sub>G</sub> versus CO <sub>2</sub> /CO ratio. . . . .	78
4.15	Schematic representation of the carbon-loop . . . . .	80



# List of Tables

2.1	Reduction reactions of manganese oxides, silicon oxides and iron oxides and the standard free energies of formation of these chemical reactions (T [K]) in different temperature ranges. . . . .	8
2.2	Required chemical and physical properties of blast furnace coke in current operation; db = dry based.	18
2.3	Main gaseous compositions in blast furnace gas. . .	21
2.4	Gaseous composition, flow and temperature of typical oven gas from FeMn and SiMn production process.	22
3.1	Summary of all CNF syntheses; H' = Homemade catalyst, C'' = Commercial catalyst. . . . .	38
3.2	Summary of all conditions for Aspen Plus simulation, *temperature intervals of 50°C. . . . .	48
4.1	Gas mixture similar to a typical oven gas mixture produced in the FeMn process. . . . .	49
4.2	Feed gas mixture compositions of Aspen Plus simulation exploring the CO <sub>2</sub> effect. . . . .	51
4.3	Product gas mixture compositions of Aspen Plus simulation exploring the CO <sub>2</sub> effect. . . . .	52
4.4	Feed gas mixture compositions of Aspen Plus simulation exploring the H <sub>2</sub> effect. . . . .	54

4.5	Product gas mixture compositions of Aspen Plus simulation exploring the H <sub>2</sub> effect. . . . .	55
4.6	Reaction equation and enthalpy for RWGS and methanation reactions. . . . .	57
4.7	Feed gas mixture compositions of C synthesis by CVD exploring the CO <sub>2</sub> effect. . . . .	62
4.8	Product gas mixture compositions of C synthesis by CVD exploring the CO <sub>2</sub> effect. . . . .	63
4.9	Feed gas mixture compositions and H <sub>2</sub> /CO ratios of C synthesis by CVD and Aspen Plus exploring the H <sub>2</sub> effect. . . . .	65
4.10	Product gas mixture compositions of C synthesis by CVD and Aspen exploring the H <sub>2</sub> effect. . . . .	66
4.11	Feed condition used for researching the WHSV effect on product distribution. . . . .	71
4.12	WHSV based on L <sub>CO</sub> fed and grams carbon produced per grams catalyst. . . . .	71
4.13	XRD sample names and feed conditions. . . . .	74
4.14	Size estimation by Scherrer equation. . . . .	75
4.15	D-bond and G-bond intensity and I <sub>D</sub> /I <sub>G</sub> ratio for Raman samples. . . . .	78
4.16	Normalized mass fraction and ton of species i per ton of metal produced in and out of the Gibbs reactor (Aspen) and CVD reactor setup (Exp.). . . . .	81
4.17	Percentage CO <sub>2</sub> and C reduction potential. . . . .	83





# Chapter 1

## Introduction

### 1.1 Background

Climate change caused by mankind is considered as one of the major issues of the 21st century. Researchers and scientists all over the world mainly agree that radical decrease in greenhouse gas (GHG) emissions is necessary to avoid further climate damage. The Norwegian Industry have produced a framework for a future low-emission society, with ambitions that between 2050-2100, global man-made emissions should not exceed what can be absorbed in nature through carbon capture, use, and storage [90]. According to the Norwegian environment Directorate, Miljødirektoratet, the Norwegian industry, excluding oil and gas sector, accounted for 23% of the total GHG emissions in 2018. The biggest contributor to GHG emissions in the industry sector was the metallurgical industries, who alone accounted for 5,1 Mt<sub>CO2</sub> of the total 12 Mt<sub>CO2</sub> emitted from this sector in Norway [43]. The government is using legislation to increase the pressures on the industry to improve the resource utilization and reducing waste generation and emissions. The incentive is to reach the demand for increased produc-

tion worldwide without a rise in global emissions. This has caused the industry to focus its attention on research and development of new technologies to close the material loops through re-use of materials [59].

The majority of the CO<sub>2</sub> emissions in the metallurgical industries originates from the utilization of coal and coke from fossil fuels as reducing agents [60]. To fulfil upcoming national regulation, the metallurgical industry must reduce the total CO<sub>2</sub> emissions by introducing more effective processes, carbon capture and storage (CCS) or renewable carbon sources. Much effort has been devoted to researching biomass and its derivatives as reduction agents, however, limited knowledge of charcoal properties and its high costs limits its attraction [85]. Specific properties are demanded for the fuels and reducing agents applied in metallurgical industries. Use of biomass and its derivatives may be a possible solution to reduce GHG emissions in the industry. However, it will be challenging to retain the high throughput and quality of the products [85]. Highly reactive and mechanically stable reducing agents are required in blast furnaces, while low reactive and mechanically stable reducing agents are required in iron sintering [20, 92]. This emphasizes the importance of understanding and researching various metallurgical processes and the properties necessary for the applied reducing agents.

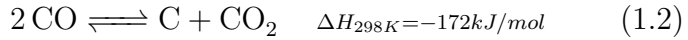
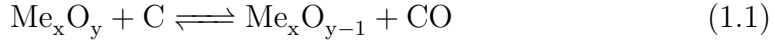
When carbon is used to reduce metal-oxides, a CO rich gas is produced, often referred to as oven gas. Today, this gas is usually fully oxidised to CO<sub>2</sub> and emitted to the atmosphere, thus causing much GHG emissions from the metallurgical industries. China is one of the main manufacturers of carbon black, used as reducing agent, and, because of supply shortage, the carbon black prices has continued to increase [95]. Securing reducing agent is essential in

order to perform the reduction of metal oxides, hence, researching new ways of producing reducing agents are important for the future low-emission society and ensuring cost efficiency in the metallurgical industries.

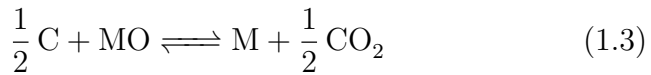
## 1.2 Project objective and scopes

The work presented in this thesis aims to explore and develop a novel strategy to decrease CO<sub>2</sub> emissions from the metallurgy industry through closing the carbon loop; instead of oxidising CO and releasing CO<sub>2</sub> to the atmosphere, CO and CO<sub>2</sub> would be used as starting materials for the production of new reducing agent. The aim of this master project has been 1) to research the thermodynamic equilibrium product distribution by feeding gas mixtures similar to a typical oven gas to an RGibbs reactor model in Aspen Plus V9™ ; 2) to investigate the equilibrium conditions and products formed when a typical oven gas mixture is fed to a carbon-vapor deposition laboratory set-up in the presence of catalyst to produce carbon, compared to the thermodynamic equilibrium results from Aspen Plus™ and; 3) investigating the viability and possibility of implementing a carbon-looping system to decrease CO<sub>2</sub> emissions in metallurgical processes.

This work proposes a carbon looping method for the metal industry to decrease CO<sub>2</sub> emissions. The oven gases are rich in CO, (1.1) [69] that can be used to produce carbon through the Boudouard reaction (1.2) [33]. By recycling carbon back to the metal oxide reduction process, a “carbon-loop” would be created, illustrated in figure 1.1.



The Boudouard reaction is exothermic and reversible at all temperatures. The formation of C and CO<sub>2</sub> is favoured at low temperatures (typically below 700°C), but is limited by thermodynamics. Likewise, the formation of CO is favoured at high temperatures, because the large positive entropic term (T·ΔS) is higher than the enthalpic component, thus making the Gibbs free energy negative (ΔG = ΔH - T·ΔS) [72]. The reaction has been utilized for the production carbon with various structures [79]. The carbon produced from catalytic Boudouard reaction is believed to have advantages of high mechanic strength, high carbon content, high crystallinity, making it a good candidate for application in various metallurgy industries [72]. Sum of reaction 2.1 and 1.2 (if x = y = 1) would result in equation 1.3. Based on the stoichiometry of this equation, the carbon looping method could, possibly, allow a reduction of CO<sub>2</sub> emissions up to 50% and decrease up to 50% the need for fresh carbon.



The scheme in figure 1.1 highlights the four steps of the metal oxide reduction process where Boudouard reaction and a carbon sorption (with CaO) and desorption are implemented.

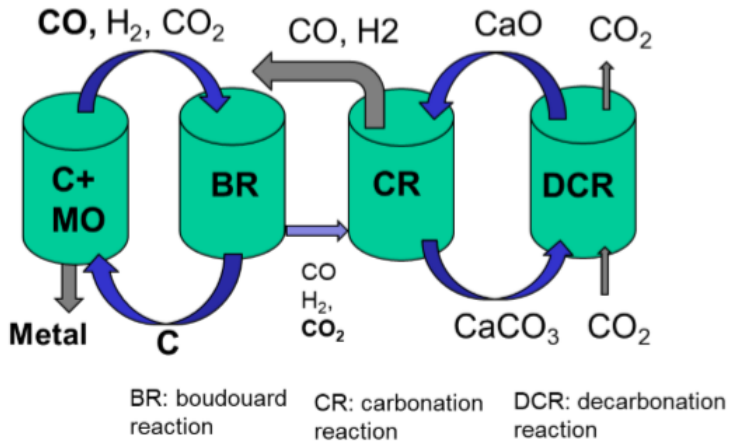


Figure 1.1: Scheme of metallurgical processes with carbon looping and carbon capture.

Coupling the Boudouard reaction with  $\text{CO}_2$  capture would enhance the conversion of  $\text{CO}$  (in the Boudouard reaction) due to the equilibrium shift; its storage, could potentially zero the  $\text{CO}_2$  emissions of the process. Hence, providing a major step towards a low-emission future in the metallurgical industries.

# Chapter 2

## Literature review

### 2.1 Metallurgical industries overview

Most metals are produced through carbothermic processes, which is defined as reduction of metal oxides using carbon reducing agents at high temperatures, typically around 2000°C [60]. The major technologies are blast furnaces and electric arc furnaces. Electrolytic reduction is also a common technology, however, it is mainly applied in the production of aluminum. Blast furnaces are commonly applied for production of iron and steel, while alloying elements like manganese and silicon are mainly produced in electric arc furnaces. A major concern the recent years for carbothermic processes has been the high CO<sub>2</sub> emissions. According to the World Steel Association, metallurgical processes contribute to approximately 10% of the anthropogenic CO<sub>2</sub> emissions [4]. The majority of the emissions comes from direct and indirect emissions, where direct emissions are those emitted from the metallurgical plant and generated by the reduction of metal-oxides or through generating heat required for the process and indirect emissions are linked to electricity and heat purchases [24].

Development of new technologies to reduce the overall GHG emissions in the metallurgical industries has been a topic of interest in recent years. For example the carbothermic reduction of alumina as an alternative process for production of aluminum [7][6], shifting indirect CO<sub>2</sub> emissions from its power input to direct ones and electrolysis as an alternative technology to reduce metal-oxides [7].

Equation 2.1 and 2.2 shows the basic principle of carbothermal reduction processes, in which the oxidation state of the metal-oxide is reduced by one. The reducing agents are carbon and carbon monoxide and acts in both solid and gaseous state. The reductions occur at different temperature ranges and is dependent on the reactivity and the free enthalpy of formation, dividing the furnace in different reaction zones. Table 2.1 gives an overview of the main reactions for the reduction of manganese oxides, silicon-oxides and iron-oxides, along with the temperature range they occur [16, 48, 75, 76].

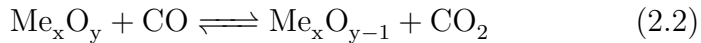
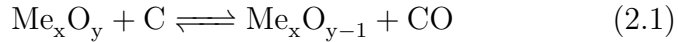


Table 2.1: Reduction reactions of manganese oxides, silicon oxides and iron oxides and the standard free energies of formation of these chemical reactions (T [K]) in different temperature ranges.

Reaction	Formation enthalpy [kJ/mol]	Temperature range [°C]
manganese-oxide [76]		
$3\text{Mn}_2\text{O}_3 + \text{C} = 2\text{Mn}_2\text{O}_4 + \text{CO}$	- 0.25 - 0.17T	25-1100
$3\text{Mn}_2\text{O}_3 + \text{CO} = 2\text{Mn}_3\text{O}_4 + \text{CO}_2$	- 170.71 - 0.004T	25-1100
$\text{Mn}_3\text{O}_4 + \text{C} = 2\text{MnO} + \text{CO}_2$	110.96 - 0.21T	25-1244
	84.35 - 0.20T	1244-1700
$\text{Mn}_3\text{O}_4 + \text{CO} = 3\text{MnO} + \text{CO}_2$	110.96 - 0.21T	25-1244
	84.35 - 0.20T	1244-1700
$\text{MnO} + \text{CO} = \text{Mn} + \text{CO}_2$	102.38 + 0.01T	25-1227
	116.73 + 0.01T	1227-1727
$\text{MnO} + \text{C} = \text{Mn} + \text{CO}$	287.6 - 0.16T	25-1227
silicon-oxide [48, 75]		
$\text{SiO}_2 + 3\text{C} = \text{SiC} + 2\text{CO}$	625	1250-2000
$\text{SiO}_2 + \text{C} = \text{SiO} + \text{CO}$	664	1500
$\text{SiO}_2 + 2\text{C} = \text{Si} + 2\text{CO}$	687	2000
$\text{SiO} + 2\text{C} = \text{SiC} + \text{CO}$	-74	1500
$\text{SiO} + 3\text{CO} = \text{SiC} + 2\text{CO}$	-397	1500
$2\text{SiO}_2 + \text{SiC} = 3\text{SiO} + \text{CO}$	1380 to 1416	1500
$\text{SiO} + \text{SiC} = 2\text{Si} + \text{CO}$	167	2000
$2\text{SiO} = \text{SiO}_2 + \text{Si}$	-599	2000
$2\text{Si} + \text{CO} = \text{SiC} + \text{SiO}$	166.3	1500
iron-oxide [16, 98]		
$3\text{C}(\text{s}) + \text{Fe}_2\text{O}_3(\text{s}) = 2\text{Fe}(\text{s}) + 3\text{CO}(\text{g})$	462 - 0.507T	700-1200
$3\text{CO}(\text{g}) + \text{Fe}_2\text{O}_3(\text{s}) = 2\text{Fe}(\text{s}) + 3\text{CO}_2(\text{g})$	- 26.37 - 0.004T	700-1200
reverse Boudouard reaction [76]		
$\text{C}(\text{s}) + \text{CO}_2(\text{g}) = 2\text{CO}(\text{g})$	170.82 - 0.18T	25-1727



For the carbothermal reduction reactions to occur, large amounts of carbon at high temperature are necessary. Carbonaceous charge is necessary in metallurgical furnaces, as it provides the required temperature in the furnace. As an example, production of pure metals in blast furnaces requires about four times more metallurgical coke compared to electric arc furnaces [62]. Due to the high process temperatures, energy and mass flow analysis is essential to understand the metallurgical processes and to avoid losses. In the last 50 years, heat recovery and improvements of the available technologies have reduced the energy consumption in steel production by approximately 60% [4]. A case study in Japan by Kuramochi assessed that the best available technologies (BAT) with replacement of coke (by for example waste plastics) and an increased usage of steel scrap, made it possible to reduce the total emissions in the Japanese steel production by 12% by 2030 [47]. To further decrease GHG emissions, new technologies and processes must be developed, including the implementation of carbon capture and storage (CCS) [2].

To understand the severity of air pollution from metallurgy industries, one must focus on the amount of coke necessary for the production of 1 ton of various metals. For an integrated steel-making operation in a blast furnace, the amount of coke used per tonne crude steel produced are approximately 350 to 400 kg, while the amount of nut coke and tuyere injectant used per tonne steel produced is around 200 to 250 kg [55]. Approximately 900 kg of coal and 100 kg of coke per tonne hot metal are used in smelting-reduction technologies (e.g. COREX), leading to 2.3 tonne CO<sub>2</sub> emissions per tonne steel [32]. Based on the high amounts of coke and coal used in the industry, recycling some of the carbon will have a positive impact on the necessity of fresh fossils and carbon

emissions, which may result in a positive impact on the daily plant operation costs and the global environment.

The metallurgical processes in general involves production of pure metal, gases such as carbon monoxide and carbon dioxide, and slag. The formation of carbon monoxide occurs through the reaction of solid carbon with the metal-oxide. In production of high carbon ferro-manganese (HC FeMn) the pressure of CO is about 100kPa in electric arc furnaces, and 35kPa in blast furnaces [63]. Carbon dioxide may also react with solid carbon, as shown in table 2.1, forming additional carbon monoxide at the expense of solid carbon. The reverse Boudouard reaction is highly endothermic ( $\Delta H = 172.5 \text{ kJ/mol}$ ), increasing the power requirement in the electric arc furnace. Annually, the reverse Boudouard reaction alone correlates to 500,000 tonnes of  $\text{CO}_2$  emissions in the FeMn and SiMn production, corresponding to approximately 30% of the annual emissions [49].

The next sections will give further description on the blast furnace and EAF, with emphasis on principle of the processes, and their main differences.

### 2.1.1 Blast furnaces

Blast furnaces are the most common metallurgical furnaces for production of iron and steel and other pure metals, like copper and lead. In 2004, 74% of the steel was produced in the basic oxygen furnace (BOF) [4, 30]. In steel production the energy requirements related to metallurgical coke and coal are around 40 to 50% [57], in which the properties of the metallurgical coke are essential for a stable furnace operation [93]. The quality of the feedstock, plant size and heat recovery greatly affects the energy efficiency of the blast furnace technology [30].

The blast furnace is operated as a counter-current furnace, in which blast and oxygen are injected at the bottom of the furnace, while coke and ore are charged in layers at its top. A schematic illustration of a blast furnace is shown in figure 2.1. Due to the counter-current operation, it is possible to obtain high heat recovery from the produced gases within multiple temperature and reaction zones in the furnace [85].

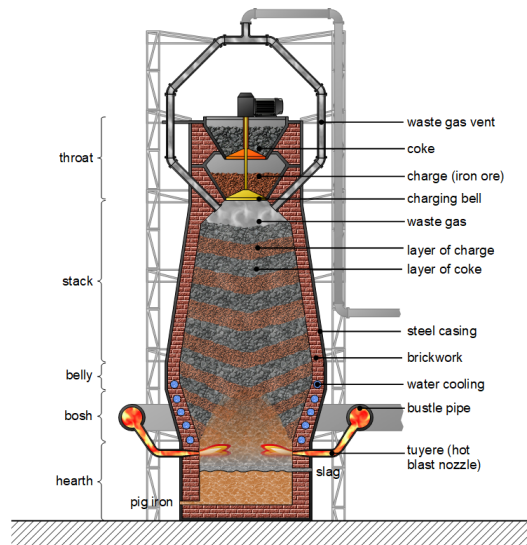


Figure 2.1: Schematic illustration of Blast furnace [1].

The oxygen and fuel are injected into the blast furnace through nozzles at the bottom of the blast furnace. The carbon sources applied in the process are coal, natural gas and oil, in which coke is placed in the front of the nozzles and is partly combusted to CO. This creates voidage and weakens the coke bed structure. The number of tuyeres depends on the size of the blast furnace, from 42 in larger furnaces to 12 in smaller ones [28]. The combustion and reaction of the blast takes place at the lower half of the blast furnace. The particle size distribution and the reactivity of the reducing agent are key parameters affecting the flow and fuel combustion at the bottom area [9]. In fact, previous studies have presented that the conditions in the bottom area are essential for an efficient combustion of the blast [31].

Various carbon sources are applied in the blast furnace, namely metallurgical coke, coal, oil and natural gas. They are applied in the process both as reducing agents and energy carriers [84]. Metallurgical coke is the main carbon source, fed to the top of the blast furnace. In order to obtain a stable operation, properties like high mechanical stability, low amounts of volatile matter, low reactivity and good gas permeability for the coke is required. However, the blast should provide a high heating value and high reactivity to form carbon monoxide, thus, the different carbon feedstocks used in the blast furnace require specific properties. The best available technique to reduce coke consumption was found to be partial replacement of coke by the injected blast [83].

The maximum injection of pulverized coal per tonnes pig iron varies between 270 to 290 kg depending on the blast furnace type [47, 70]. The pulverized coal injection (PCI) can replace coal at a rate of 0.85 to 0.95 of coke per kg pulverized coal for a PCI consumption of 180 to 200 kg per tonnes pig iron [47, 61]. Ribbened,

Thoren and Sternhufud assumed a lower limit of 290 kg coke per tonnes hot metal [70]. However, according to recent studies, it is found that modern blast furnaces usually operates with the consumption of 286 to 320 kg metallurgical coke per tonnes hot metal and a PCI of 170 to 220 kg per tonnes of hot metal [57]. In order to reduce the carbon consumption by the Boudouard reaction in the blast furnace, a high gasification threshold temperature of the metallurgical coke is important. However, the blast furnace reaction efficiency can be improved by utilizing metallurgical coke with lower gasification threshold temperature and thus, reduce the coke consumption [26]. Thus, properties such as high mechanical stability and chemical resistance is important if metallurgical coke is to be replaced by renewable carbon sources (charcoal, charcoal-coke blends, charcoal pellets or biocoke).

### 2.1.2 Electric arc furnaces

Electric arc furnaces (EAF) are furnaces that heats charged material by means of an electric arc. They can be operated with an alternating current (AC) or direct current (DC). In ferroalloy industries, electric arc furnaces operated with direct current started relatively recently, i.e. the last 30 years [40, 46], while alternate current has been used since the beginning of the 20th century. In modern society, electric arc furnaces are used in about 20 different industrial fields [46]. In Norway, electric arc furnaces are typically operated with an alternate current. Actually, in southern Norway, three out of four metallurgical processes are operated as carbothermal processes, with the fourth being an electrolytic process. The four processes are the production of silicon (Si) by Elkem, Silicon carbide (SiC) by Saint-Gobain, silicon manganese (SiMn) by Elkem and production of aluminum (Al) by Alcoa, respectively.

The heat in the carbothermal processes operated as EAF is provided by electricity and reduction of carbonaceous material [73]. In most EAF processes three electrodes are installed and operated with alternating current, while very large rectangular-shaped furnaces are operated with six electrodes [19]. Research has shown that the power input is at its highest capacity when a three electrode-circuit exhibits a similar electric resistance [18]. For submerged arc furnaces, typically used in manganese production, the resistance of the carbon material limits the allowable electrode penetration into the hearth [18]. The electricity supply or furnace transformers are limiting the power rating in EAF's [18]. For example, Eramet Norway Kvinesdal uses three smelting furnaces operated with 30 MW to produce 180 000 tonnes of SiMn [25]. A power consumption of about 3.4 kWh is used to produce 1 kg SiFe (Eramet Porsgrunn) while Eramet Kvinesdal use 4.2 kWh. In Porsgrunn, approximately

35% of the thermal energy input was recovered from the CO gas by supplying it to Yara’s ammonia factory at Herøya [60]. The production of silicon and ferrosilicon typically occurs in submerged arc furnaces operated at between 12 and 24 MW [19], resulting in a power consumption of 10 to 13 kWh per kg<sub>Si</sub> [13, 14, 19]. This power input represents about 45% of the energy necessary for the furnace [14], while the remaining energy demand is covered by carbonaceous materials.

Figure 2.2 is a schematic representation of the working principle of an EAF by the reduction pathway of manganese. Similar to the blast furnace, the EAF emits several GHG emissions. The amount and composition of the emissions depends on the quality of the charge, but may consist of volatile organic compounds (VOC), particulate matter, carbon dioxide, carbon monoxide, nitrogen oxides, dioxins, sulfur oxides and furans [36].

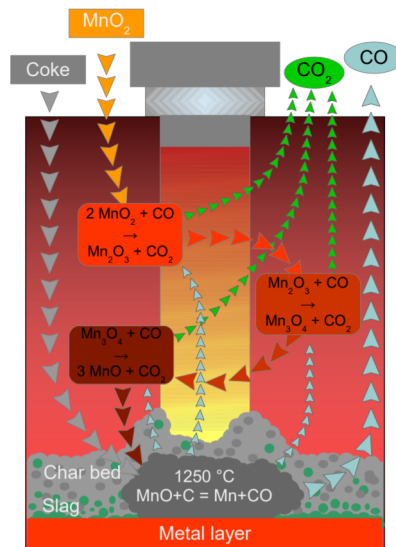


Figure 2.2: Manganese reaction pathway [60].

In Norway the production of ferroalloys (i.e. ferrosilicon/silicon and ferromanganese) is a significant land-based industry. Eramet Norway is a well known and established world wide producer of manganese alloys. In reference to sustainability they have stated that they consider themselves as a "part of the solution" company because they produce metals essential for the energy transition, such as lithium and nickel. However, according to their annual report from 2017, their overall carbon footprint from scope 1 (on-site direct emissions) and 2 (indirect emissions linked to electricity and heat purchases) summarized to 4.29 Mt (volume in millions of tons of CO<sub>2</sub> emitted by all group sites), a value which have been overall stable the recent years [60]. The majority of the CO<sub>2</sub> emissions originates from the utilization of coal and coke from fossil fuels as reducing agents [60]. In order to achieve an effective and stable production, the carbonaceous materials are selected based on their properties and economics. Further description of the reducing agent properties for various carbonaceous reduction processes are provided in the next section.



## 2.2 Reducing agents

The main function of the reducing agent in metallurgical industries is to react with the metal oxides producing pure metals. However, the reducing agents also have other important function, e.g. it improves the gas distribution in the furnace, enhances the permeability of the burden and acts as a SiO gas trap in silicon production [73]. Reducing agents can be obtained from gaseous, liquid or solid sources, depending on the metallurgical process and the necessary properties of the reducing agent. Solid reducing agents are the most abundant in cabothermal reduction processes. In order to obtain a stable operation of the furnace and to ensure a high production rate and quality of product, the metallurgical furnaces require specific properties of the feedstock [64].

In blast furnaces and manganese production, the main reducing agent is metallurgical coke. In order to understand the quality of reducing agents, several standards have been developed, such as the CSR (coke strength after reaction), CRI (coke reactivity index), fixed carbon content or element analysis. The required properties of metallurgical coke used in blast furnaces are summarized in table 2.2. The main criteria for reducing agents in the ferroalloy production is the chemical composition, such as volatile matter content, ash content, ash composition and the reactivity towards CO<sub>2</sub> and SiO [73]. Moreover, high conversion rates, low levels of impurities, high bulk density and energy density is key properties. Low impurity-levels in carbonaceous reductants are important not only for optimal function of the reducing agent, but also to minimize impurities in the produced oven gas from the process. High amounts of sulfur and phosphorus is highly undesired [44, 67]. This emphasizes the importance of understanding and analysing the reducing agents and utilizing the standards. However, a problem

with the developed standards is that they are based on fossil fuels like coke and coal, meaning they may not be directly adopted to renewable reducing agents.

Table 2.2: Required chemical and physical properties of blast furnace coke in current operation; db = dry based.

Chemical property	European range
Moisture (wt.%)	1 - 6
Volatile matter (wt.%, db)	<1,0
Ash (wt.%,db)	8 - 12
Sulfur(wt.%,db)	0,5 - 0,9
Phosphorus (wt.%,db)	0,02 - 0,06
Alkalies (wt.%,db)	<0,3
Particle size, mechanical strength and reactivity	
Mean size (mm)	47 - 70
M40 (+60mm)	>78 - >88
M10 (+60mm)	<5 - <8
I40	53 - 55
I20	>77,5
CSR	74,1
CRI	17,7

In EAF's the properties of the reducing agents are different from the blast furnace. Electrical resistivity of the reducing agent is a key parameter especially in submerged arc furnaces. The total electrical resistivity is dependent on the reducing agent, volume fraction, carbon content and particle size [73]. Moreover, the resistance of the reducing agent is affected by the ash distribution, microstructure, macroscopic cracks and graphitization of the reducing agent. Specific surface area is also of high importance

and an essential feature is that the surface area is accessible for chemisorption of the gas-vapor phase [91]. In electric arc furnaces, more than 70 % of the operating plant cost is related to electricity and reducing agent costs [73], meaning recycling of the reducing agent could benefit both operating cost and total GHG emissions.

### **2.2.1 Mechanical stability and particle size**

The mechanical stability of the reducing agent is commonly evaluated and measured by the CRI and CSR. These analyses provide information on the chemical and mechanical stresses in the shaft of the blast furnace. As shown in table 2.2, CRI and CSR have minimum values for application in a blast furnace. In the EAF the optimal CRI and CSR values are not well documented [67]. The strength of the coke is actually one of the limiting factors in regards to introducing renewable carbon sources as reducing agents into the metallurgical industry. According to G. Surup et al. charcoal can be blended into the coal mixture to produce biocoke with very similar properties as metallurgical coke, but the coke strength can decrease after only adding 5wt.% of charcoal [54, 85]. However, blending with only 2 % of high-density polyethylene can improve the mechanical strength [29]. The desired particle size of the reducing agent is, as presented in table 2.2, around 40-70 mm in order to achieve good distribution of the gases in a blast furnace [21].

### 2.2.2 Composition

Metallurgical coke is usually made from low ash, low sulfur coal, with special coking properties, which is heated to produce carbon and inherent ash while also driving off most of the volatile matter. The final product is nearly pure carbon at various particle sizes [17]. The amount of ash, sulfur and alkalis in the blast furnace coke should be low in order to achieve optimal operation. The range of these composites are listed in table 2.2 [21]. The coking coal is calcined at about 1000°C, and it is at this temperature most of the volatile matter is removed. Petroleum coke which is made from the residues left from refining exhibit similar behaviour upon heating as the coking coal but are usually calcined at slightly higher temperatures (1200-1400 °C). The same goes for baked anodes. Graphitization of coking coal and petroleum coke occurs only at higher temperatures, around 3000°C [17].

### 2.2.3 Reactivity

The typical measurement of reactivity in metallurgical coke is the coke reactivity index (CRI). The procedure for CRI analysis of coke is heating to 1100°C in CO<sub>2</sub>, sometimes referred to as Boudouard reactivity test. Kamalpour et al. researched four different cokes for application in ferromanganese production in a submerged arc furnace. They concluded that coke selected for use in ferromanganese production should be more reactive than those normally used in the iron blast furnace [41]. They argued that higher reactivity for coke in submerged arc furnaces enhanced the stability of the furnace operation and increased productivity. Their reasoning being that more reactive coke would enable Boudouard-controlled reactions occurring higher in the shaft making the heat utilisation in the submerged arc more effective. Thus reducing the capacity of

the gases lower in the furnace which enabled the final high temperature reduction of MnO to Mn to be main reaction in the mixed slag zone. They also argued that less reactive coke could cause poor reducing conditions and larger coke beds in the furnace. Thereby causing poor furnace control, unstable alloy and slag compositions, and increased consumption of electricity in the furnace [41].

## 2.3 Oven gas

When metal oxides react with carbonaceous reducing agents in carbothermal processes, a CO rich gas is produced, typically referred to as oven gas. The main composites of the oven gas is CO, CO<sub>2</sub>, H<sub>2</sub> and N<sub>2</sub>. Based on the type of process and reducing agent applied, traces of impurities such as sulfur and volatile components may also be present. Moisture in the form of H<sub>2</sub>O is also typically found in oven gases. Table 2.3 presents some typical compositions of various blast furnace oven gases [12]. In table 2.4, typical oven gas composition from the FeMn and SiMn processes are presented, provided by co-supervisor Kumar R. Rout.

Table 2.3: Main gaseous compositions in blast furnace gas.

Composition (vol%)					
Blast furnace gas (BFG)					
CO	CH <sub>4</sub>	CO <sub>2</sub>	H <sub>2</sub>	N <sub>2</sub>	H <sub>2</sub> O
22.1	–	24,4	5.2	44.6	3.7
27	0.5	16	3.5	51	2
30.3	–	19,2	6.3	44.2	–
20	–	18	0	62	–
25	–	18	0	57	–
25	–	18	2	55	–

Table 2.4: Gaseous composition, flow and temperature of typical oven gas from FeMn and SiMn production process.

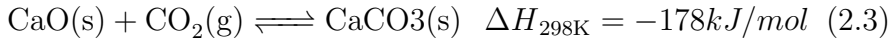
Process	Gas flow [Nm <sup>3</sup> /h]	Temperature [°C]	Composition [mol%]				
			CO	CO <sub>2</sub>	H <sub>2</sub>	O <sub>2</sub>	N <sub>2</sub>
FeMn	10 000	150-250	62	24	8,5	0,5	5
SiMn	7 000	500-600	60	12	6	-	22

Today, the oven gas from the various carbonaceous processes are usually burned to emit CO<sub>2</sub>. However, in Eramet Norway Porsgrunn, some of the oven gas produced are sold to Yara in a cooperation with Herøya Industripark [60]. Moreover, the production of hydrogen as a product from the blast furnace gas has received much attention [12]. Generally, it is an increasing desire to find alternative uses for oven gases to produce valuable products like industrial intermediates and fuels synthesized from CO or CO<sub>2</sub>, thus reducing emissions from the industry [68].

## 2.4 Carbon capture

In order to achieve the goals of a low-emission society, carbon capture and storage (CCS) and carbon capture and utilization (CCU) has been presented as a necessary step. The capturing of carbon dioxide is not a new technology as removal of carbon dioxide from gas streams has been a vital unit operation for many decades in order to avoid corrosion and improve calorific value of gas streams [38]. Post combustion carbon capture using amine-based solvents (for example monoethanolamine (MEA) scrubbing) are scientifically well-established but are known to be quite energy intensive [80]. Thus, other methods for carbon capture with lower energy penalties are attractive. Options such as membrane separation, molecular sieves or desiccant adsorption are proposed and researched [66]. Another alternative to amine-based solvents are solid sorbents operating at high temperature. Calcium looping (CaL) is a solid sorbent carbon capture technology where limestone ( $\text{CaCO}_3$ ) is utilized. It may be an attractive technology as limestone is readily available and a relatively inexpensive material [38].

One of the first reports where CaL was proposed as a carbon capture technology was in 1999 [78]. Then, they proposed a process consisting of two fluidized bed reactors connected by solid transportation lines. The carbon dioxide was to be captured by CaO at 873 K and the produced  $\text{CaCO}_3$  transported to a regenerator where it was decomposed to CaO at 1223K [78]. The principle of the process is the same today, with calcium oxide (CaO) reacting with carbon dioxide ( $\text{CO}_2$ ) to produce carbon carbonate ( $\text{CaCO}_3$ ), see equation 2.3. However the properties and design of the process has developed over the years [22].



One of the challenges of utilizing the CaL technologies are that limestone loses its capacity to capture  $\text{CO}_2$  through long-term cycling, and a large amount of fresh limestone is required to maintain an acceptable  $\text{CO}_2$  capture efficiency [27]. Jayarathna et al. proposed an Aspen Plus<sup>™</sup> Process simulation of carbonate looping using a fluidized bed reactor (carbonator) in which the forward reaction 2.3 occurs at  $650^\circ\text{C}$ . The  $\text{CaCO}_3$  is separated from the cleaned  $\text{CO}_2$  rich gas by a gas/solid separator. The purified gas can then be released to the atmosphere. In a second reactor, the calciner,  $\text{CaCO}_3$  decomposes into  $\text{CaO}$  and  $\text{CO}_2$  at  $900^\circ\text{C}$ . As this is the reverse of reaction 2.3, i.e. an endothermic process, a significant flow of thermal energy is required in order to get the reaction to occur. The regenerated  $\text{CaO}$  is separated from the  $\text{CO}_2$  in a gas/solid separator and recycled back to the carbonator [38]. A research focus regarding the CaL technology has been lowering the energy penalties and cost associated with the separation step [71].



## 2.5 Carbon materials

Carbon's abundance, its unique diversity of organic compounds, and its ability to form polymers enables this element to serve as a common element in everyday life [37].

The decomposition of hydrocarbon molecules in gaseous phase for the production of carbon, is called gas-phase carbonization. Carbon blacks can be produced utilizing gases rich in hydrocarbons. Furthermore, if some metallic particles, for example Fe or Ni, are present in a carbonization system, various carbon materials are produced; carbon nanotubes (CNTs), carbon fibers (vapor-grown carbon fibers), carbon nanofibers (CNFs) with various nanotextures and morphologies/alignments. From the carbon vapor produced by electric-arc discharge or laser ablation, carbon nanotubes (CNT) and fullerenes are formed. The structures of the carbon materials may differentiate extensively: however, for some the structures are very similar, and characterization techniques are necessary to distinguish them [37]. The rest of this section will focus its attention on carbon nanomaterials, especially carbon nanofibers.

### 2.5.1 Carbon nanomaterials

The past decades there has been a significant increase in research efforts on various carbon nanostructures. In 1985 fullerenes was discovered by Kroto et al. [45]. The fullerene is a carbon molecule in which the carbon atoms are connected by single and double bonds (sp<sup>2</sup> carbon atoms) forming a closed-cage structure. Not long after, the carbon nanotubes were discovered by Iijima [34, 35] resulting in an increased interest in the material. CNTs can be defined as two-dimensional hexagonal lattice of carbon atoms forming a hollow cylinder. They are allotropes of carbon, specifically a class of fullerenes. The single-walled carbon nanotube (SWCNT) can be classified as an elongated fullerene. In the 1970's, carbon filaments with very small diameters were prepared in conditions similar to the current chemical vapor deposition (CVD) method, commonly applied today for production of carbon nanofibers (CNF) [23]. The discovery of these new materials caused much excitement. Figure 2.3 shows the number of publications on carbon nanotubes (CNT) from 1991-2004, illustrating the huge increase in attraction to the subject [94].

Carbon nanofibers are cylindrical nanostructures with graphene layers arranged as cups, plates or stacked cones. They are relatively recently discovered carbon materials with easily controlled structural and textural properties with strong resistance to acid/base environment [96]. CNFs share some similarities with carbon nanotubes, and the distinction between the two is not clearly defined only by name. However, they have notably different nanostructures and properties, making it possible to distinguish them with characterization techniques [94].

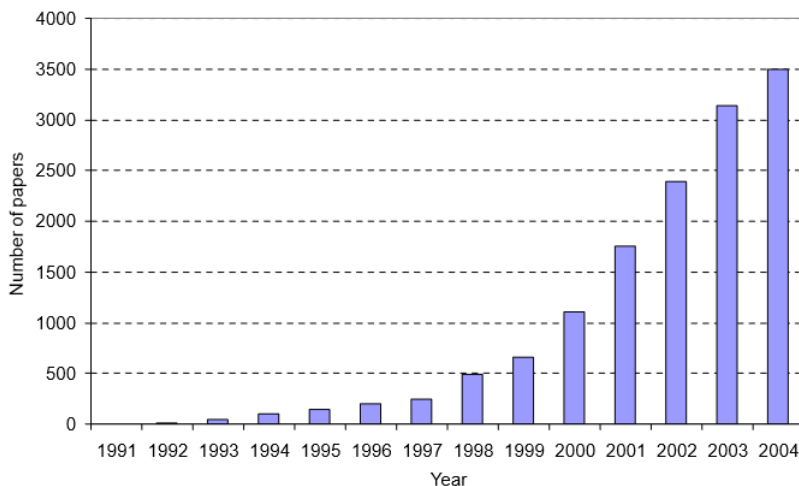


Figure 2.3: Publications on CNTs in the time period 1991-2004 [94].

The most notable difference between CNFs and CNTs are the configuration of the underlying planes that are created by the alignment of the carbon atoms. CNTs display an axial alignment of concentric cylindrical planes with hollow cores. They can be classified as single-walled carbon nanotubes (SWCNTs) or multi-walled carbon nanotubes (MWCNTs) depending on the number of axially aligned cylindrical tubes. CNFs are named and distinguished according to their graphenesheet orientation, which is characterized by the angle between the fiber axis and the graphene sheets [97]. The various carbon nanostructures have major differences concerning chemical and physical properties. For example, the alignment of the graphite layers on the CNFs cause only edge sites to be exposed, making them unstable because of the dangling bonds of the fiber edges. Moreover, they will be ideal candidates in gas adsorption. The large number of edge sites is one of the most outstanding features of CNFs and provide anchoring sites for catalyst precursors [97]. The tubular structure will have different proper-

ties due to its surface primarily consisting of basal planes, causing high electrical conductivity [94]. Figure 2.4 illustrates the different structures of Platelet, Fishbone and Ribbon carbon nanofibers, respectively.

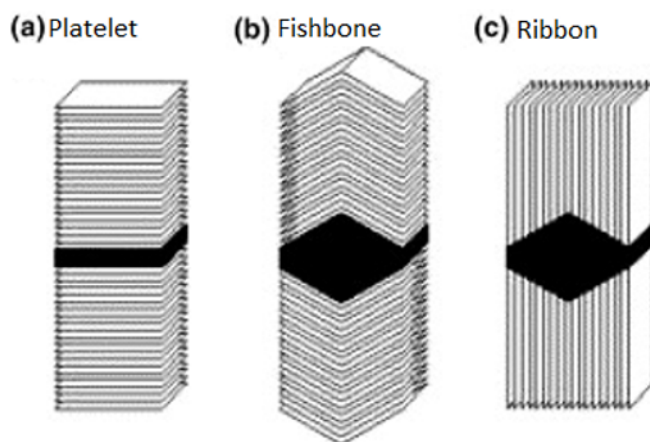


Figure 2.4: Carbon nanofiber structures, Platelet, Fishbone and Ribbon CNFs, respectively [77].

In platelet nanofiber the graphite sheets are stacked perpendicular to the fiber axis. In fishbone nanofiber the graphite sheets are arranged with an angle to the fiber axis. The distance between the interlayers are similar to the interlayer distance in graphite, approximately 0.34 nm [94].

The CNF arrangements presented in figure 2.4 has been observed through analytical methods like HRTEM. The various types of carbon nanofibers are characterised by the angle ( $\alpha$ ) with respect to their fiber axis. For the fishbone CNF the angle with respect to fiber axis is ( $0 < \alpha < 90$ ) whilst for ribbon or tube ( $0 = \alpha$ ) [97]. Research show that selective synthesis of a desired structure of CNFs is achievable by utilizing correct conditions, carbon source and catalyst [96].

### Synthesis of carbon nanomaterials

There are different techniques for synthesizing carbon nanostructures. The three main ones are arc-discharge, laser ablation, and chemical vapor deposition (CVD). A schematic representation of the three methods are shown in figure 2.5.

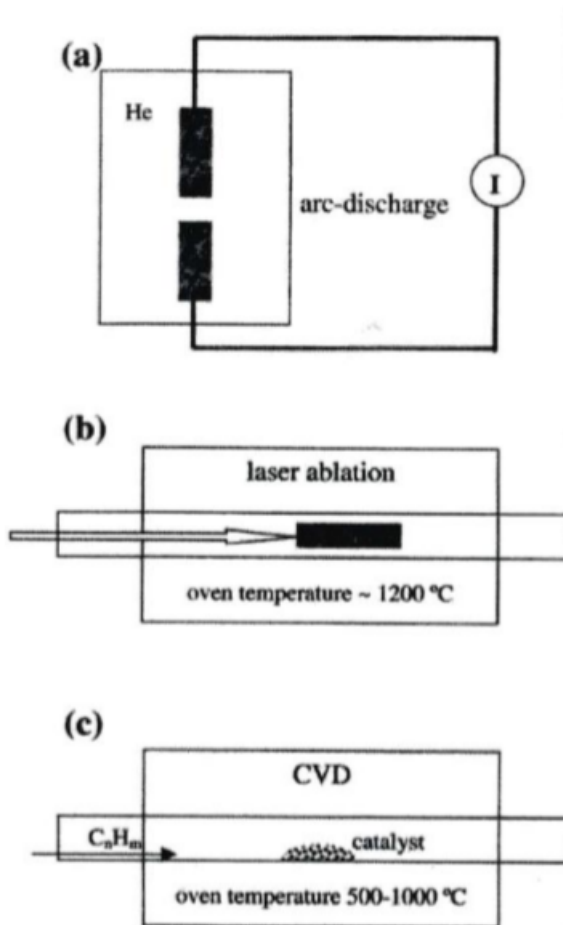


Figure 2.5: Schematic illustration of methods for production of carbon nanomaterials [94].

Arc-discharge, illustrated in 2.5 (a), is a process in which arc discharge between two graphite electrodes is ignited in an inert gas. The graphite anode applied in the process is hollow and packed with a mixture of transition metal and graphite powder which is vaporized by the electric arc. One electrode is consumed, resulting in the production of various carbon nanostructures such as SWNT, MWNT and fullerenes. The temperature in the synthesis is very high (2000-3000°C) yielding highly graphitized tubes [87].

In laser ablation, 2.5 (b), a laser beam vaporizes graphite and nucleates CNTs in front of a target which is graphite mixed with small amounts of transition metal particles. The target functions as a catalyst and is positioned at the end of a quartz tube enclosed furnace which is heated to  $\approx 1200^\circ\text{C}$ . Argon flow through the reactor while product deposits on the cooler section of the tube furnace in direction of the gas flow. The products formed are SWNTs and MWNTs at relatively high yields [81].

Chemical vapor deposition (CVD), 2.5 (c), is a process where a reactor is loaded with metal catalyst and fed with carbon-containing gas or gas mixture producing CNFs and CNTs. A furnace is used to heat the reactor to operating temperatures around 500-1000°C. The carbon is formed on the surface of the catalyst particles. High yields of carbon is formed by CVD. The synthesis method separates itself from the two previously mentioned as it can produce both CNTs and CNFs at high yields. Moreover, the process has relatively low cost and energy requirements for large-scale synthesis [10].

### Growth mechanism of carbon nanofibers

The growth mechanism of CNFs by CVD has been extensively investigated and is now commonly agreed to occur through three steps [5]. First the decomposition of the carbon-containing gas occurs on the metal catalyst surface at the gas particle interface. Then, in the second step, the carbon dissolves in the particles and diffuses on the surface or through the bulk of the metal particle. In the final step, the carbon precipitates at the other side of the particle in the form of CNFs. For most cases, the rate determining step is believed to be the diffusion through the catalyst particle (step 2). The experimental research agreement between the measured activation energies of filament growth and those for carbon diffusion has been used as reasoning for this theory [5]. A schematic representation of the mechanism of carbon filament formation was proposed by R. T. K. Baker and is shown in figure 2.6.

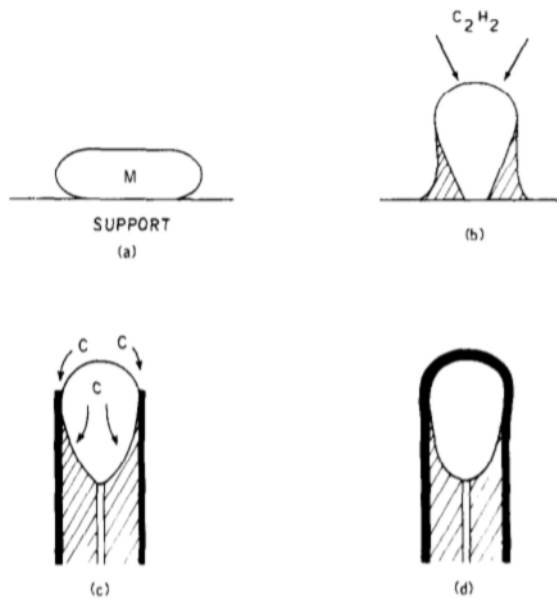


Figure 2.6: Schematic representation of proposed mechanism of CNF growth [5].

The model for the growth of CNFs by Baker et al. is developed with the belief that the temperature gradient inside the particle caused by the exothermic decomposition of the hydrocarbons at the exposed front faces, and endothermic decomposition of carbon at the rear faces (which are initially in contact with the support surface) is the driving force for carbon diffusion. Some limitations in the proposed model was presented by Baker et al; it does not sufficiently describe the formation of the graphitic skin of the filaments; it does not account for the synthesis of filaments from decomposition of methane on metal catalyst, as it is an endothermic process; the model does not explain the structural or chemical nature of either the bulk or surface of the catalyst particles and; does not interpret the possible deviations occurring in filament grow characteristics [5].

The rate-determining step can be reversed in some cases. In CNF production from acetylene decomposing on  $\alpha$ -Fe catalyst, the diffusion of carbon is the rate-limiting step. However, when CNFs are formed from several more stable hydrocarbons, the carbon diffusion is not the rate-limiting step. In those cases the surface reactions are believed to be rate-limiting [15].

The nucleation of fishbone or platelet carbon nanofiber, in which it is proposed that each layer is segregated separately due to supersaturation, differentiates from a parallel tube. Moreover, for growth of fishbone/platelet carbon nanofiber hydrogen is required to be sufficiently present on the specific surface planes of the catalyst particle in order to saturate the bonds at the edges of the nanofiber, and initiate the segregation of graphite layers. This causes each graphite layer to nucleate separately [94].



## Characteristics and applications of carbon nanofibers

The different configurations of the graphene layers of carbon nanofibers results in major differences in physical and chemical properties. The alignment of the graphite layers in CNFs results in only edge sites to be exposed which makes them unstable because of the dangling bonds of the fiber edges. This makes them ideal candidates in gas adsorption. Moreover, the large number of edge sites provide anchoring sites for catalyst precursors [97], and is considered one of the most outstanding features of CNFs. The tubular structure will have different properties due to its surface primarily consisting of basal planes, making the electrical conductivity of this configuration to be higher. Furthermore, the material has a resistance to strong acid/base environment [96].

The unique properties of CNFs has made them interesting in many applications. In catalysis, they have been extensively researched as a support material. For example, Ledoux et al. [65, 88] found that for cinnamaldehyde hydrogenations, Pd imbedded inside carbon nanotubes or supported on carbon nanofibers has a much higher activity compared to activated charcoal. They attributed those findings on the mesoporous CNF structures inhibiting mass-transfer effect and the peculiar Pd interaction with carbon. Salman et al. [74] examined the hydrogenation of crotonaldehyde to crotyl alcohol by using Ni catalyst supported on commercial alumina compared to different types of graphite nanofiber and found notably higher activity when carbon nanofiber support was applied. However, even though the research on preparation, characterization and application of CNFs are extensive, much effort is still required in order to produce CNFs with high purity and well-controlled configurations. Moreover, further understanding regarding the elucidate mechanism responsible for the enhanced activity of CNF supported

catalyst compared to the conventional ones.

Many applications of CNFs other than catalyst support is extensively researched. They have been proposed as catalysts [97], gas storage materials [52, 53], electrodes for fuel cells [8], and polymer additives [50]. All these are attributed to their unique physical and chemical properties. According to Jing-Hong Zhou et al. the morphology and microstructure of CNF's can be tuned depending on the feedstock and catalyst applied in the synthesis of the fibers. They synthesized seven carbon nanofibers with various feedstocks, catalysts, and synthesis time, yielding CNF's with sizes ranging from 20 to 200 nm and angles between the graphene layers resulting in tubular, fishbone and platelet carbon nanofibers, making their application potential quite extensive [96].

# Chapter 3

## Method

In this chapter, the materials, the established method, and the experimental configuration used to investigate the possible implementation of the novel carbon-looping idea for reduction of CO<sub>2</sub> from the metallurgical industry will be presented. A detailed risk analysis for the experimental work is presented in Appendix F.

### 3.1 Synthesis of carbon nanofibers

In order to explore the strategy to decrease CO<sub>2</sub> emissions from the metallurgy industry through closing the carbon loop, carbon nanofibers were prepared via chemical vapour deposition using a CO-rich gas mixture as precursor in the presence of magnetite catalyst. The apparatus for CNF synthesis is schematically represented in figure 3.1. The mass flow controllers (MFC) were used to adjust the amount of gas flow introduced to the reaction, hence, they include flow-range limits. A pressure relief valve was implemented in order to secure against pressure buildup in the reactor. Additionally, a valve was placed under the reactor in order to perform gas sampling. The gas product flowed through a bubble flask before

being released through the vent. Furthermore, the setup was enclosed in a ventilated box for gas-leakage safety. The reactor used in the setup was a vertical quartz reactor with 4 cm diameter and 50 cm length with a quartz sinter placed in the middle, in which catalyst could be loaded. Surrounding the quartz catalyst was a temperature controlled oven.

A weighed amount of catalyst was introduced to the reactor for each synthesis. First the catalyst was reduced in 80/20 ml/min Ar/H<sub>2</sub> mixture, however, due to a change of MFC for N<sub>2</sub>/Ar limiting the flow range, see figure 3.1, the reducing procedure was later changed to 20/5 ml/min Ar/H<sub>2</sub>. The temperature was raised to 600°C for the reduction, with a 5°C/min temperature ramp, and held at 600°C for 6 hours. A summary of all the experiment conditions, including synthesis temperature, feed composition, catalyst mass, weight hourly space velocity (WHSV) and short descriptions of the experiment sets, are presented in table 3.1. Details on catalyst mass and WHSV values, including calculation example of WHSV, is included in Appendix A. All experiments were performed with a synthesis time of 48 hours.

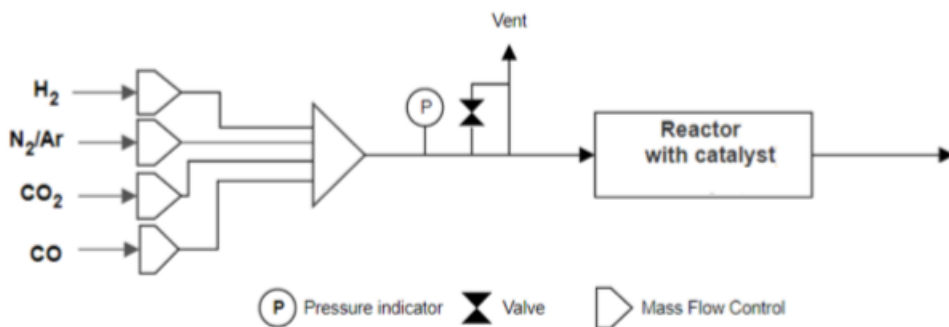


Figure 3.1: Schematic representation of CVD synthesis apparatus.

Two magnetite catalysts were tested in the syntheses, referred to as homemade and commercial catalyst. The effect of WHSV [ $L_{CO}/(g_{cat} \cdot hr)$ ] was investigated for the commercial catalyst, keeping temperature and feed compositions constant. Moreover, the effect of  $CO_2$  and  $H_2$  in the feed was explored by changing their partial pressures keeping temperature and WHSV constant. Finally, temperature investigations were performed conducting syntheses in the temperature range 400-800 °C, at constant feed composition and WHSV. The gaseous product were collected below the reactor outlet using a valve to transport the gas flow into Supel-Inert Foil Gas Sampling Bags from SigmaAldrich™ with a 2L volume capacity. The analysis of the product gas were performed repeatedly throughout the duration of the CNF synthesis, usually 4 or 5 times. The amount of CNF produced in the synthesis was gravimetrically measured after the system had been cooled to ambient temperature under flowing Ar.

## Carbon Looping for Metallurgical Processes via Boudouard reaction over Magnetite

---

Table 3.1: Summary of all CNF syntheses; H' = Homemade catalyst, C'' = Commercial catalyst.

Exp.	Temp. [°C]	Cat.	mcat. [g]	WHSV [Lco/gcat*hr]	Mole fraction				Descript.		
					CO	CO2	H2	N2			
1	600	H'	0.1	30	0.80	0.00	0.20	0.00	PCO2		
2					0.69	0.13	0.10	0.08	&		
3					0.50	0.38	0.07	0.05	PH2		
4					0.57	0.22	0.15	0.06	effect		
5					0.49	0.19	0.27	0.05			
6					0.62	0.24	0.09	0.06			
7					0.62	0.24	0.09	0.06			
8	800				0.62	0.24	0.09	0.06	Temp.		
9	400				0.62	0.24	0.09	0.06	effect		
10	575				0.62	0.24	0.09	0.06			
11	625				0.62	0.24	0.09	0.06			
12	600	C''	0.1	30	0.62	0.24	0.09	0.06	PCO2		
13					0.62	0.12	0.09	0.18	&		
14					0.62	0.24	0.13	0.01	PH2		
15					0.09	0.62	0.00	0.09	0.30	effect	
16					0.3	10	0.62	0.24	0.09	0.06	WHSV
17					0.5	6	0.62	0.24	0.09	0.06	effect
18					575	0,1	30	0.62	0.24	0.09	0.06
19	652				0.62	0.24	0.09	0.06	effect		
20	650				0.62	0.24	0.09	0.06			

## 3.2 Catalyst

Two catalysts were tested for CNF production in the CVD-setup (figure 3.1). One, later called "homemade catalyst", was prepared according to the procedure of Young Soo et al. [42]. The other one, later called "commercial catalyst" was provided by Rana Gruber Minerals AS. More detailed information regarding the two catalysts will be provided in the following subsections.

### 3.2.1 Homemade catalyst

For carbon preparation via CVD with CO and H<sub>2</sub>, unsupported magnetite Fe<sub>3</sub>O<sub>4</sub> in the form of nanoparticles was used as catalyst. The catalyst was prepared following the procedure described by Young Soo et al. The magnetite produced by this method will be narrow in size distribution and, according to TEM analysis by Young Soo et al., have average particle diameter ~ 10nm [42]. Purified deoxygenated water (25 mL) and HCl (0,85 mL, 12,1 M) was combined before FeCl<sub>3</sub> (5,2 g) and FeCl<sub>2</sub> (2,0 g) was added under continuous stirring. The prepared solution was added drop wise to an aqueous solution of NaOH (1,5 M, 250 mL) under vigorous stirring. An instant black precipitate was generated and the paramagnetism was checked by placing a magnet near the precipitate. The supernatant was decanted from the precipitate, before the precipitate was added to centrifugal vials with deoxygenated water and centrifuged at 4000 rpm for 10 minutes. The solution was then decanted and this was repeated three times. HCl (500 mL, 0,01 M) was added under continuous stirring to neutralize the anionic charges on the nanoparticles. The solution was then separated by centrifugation at 4000 rpm for 1 hour and peptized by adding water. This was filtered while washing with purified deoxygenated water before vacuum drying at 70°C.

### 3.2.2 Commercial catalyst

Commercially produced magnetite catalyst (by Rana Gruber Minerals AS) was applied as catalyst in some of the CNF syntheses. The catalyst used in this project, called CM-5 by Rana Gruber, has a narrow size distribution between 0.1 and 1 micron. The SEM analysis results on size distribution performed by Rana Gruber is presented in figure 3.2 as a graph relating the weight cumulus passing (cum.-%) as a function of particle size (micron). Further information and specifics about the magnetite catalyst is given in Appendix B.

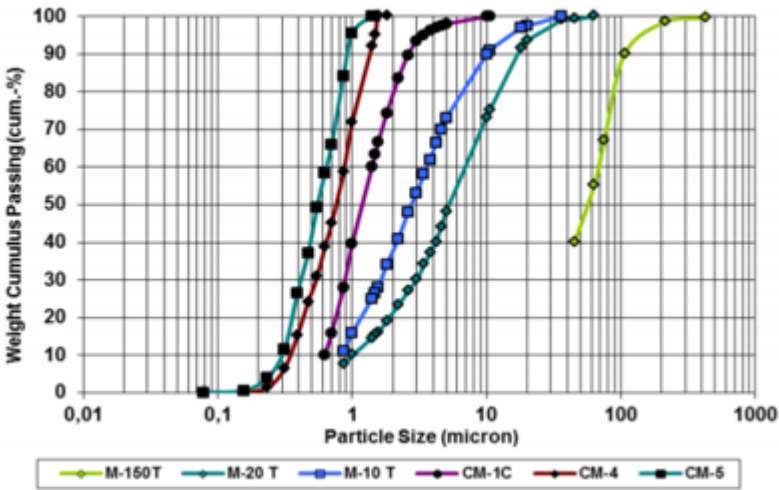


Figure 3.2: Size distribution of magnetite produced by Rana Gruber Minerals AS.

The commercial catalyst was used in some of the CNF syntheses for comparison to the CNFs produced by the homemade catalyst (amount produced, size distribution and crystallinity). Moreover, the CM-5, which is the catalyst produced by Rana Gruber with the smallest size distribution (figure 3.2) was chosen in order to have the same particle diameter of the homemade catalyst.



### 3.2.3 GC analysis

The GC system 7820 A by Agilent Technologies is well fitted for use in small-to medium-sized labs. It features retention time locking (RTL) improving data consistency by maintaining exact retention times and electronic pneumatics regulation (EPR) providing simplicity of manual operation. The GC system includes both FID and TCD detectors.

The analyses were performed with a runtime of 15.867 minutes and a setpoint temperature of 45°C that was held for 6 minutes before it was increased to 190°C with a rate of 75°C/min. This temperature was held for 6 minutes before it returned back to the setpoint at the same rate. The pressure was set to 6.8112 psi and the split ratio 25:1.

The GC system was used to analyse and determine the composition of the CVD product gas. As mentioned, the gaseous product were collected from the CVD-setup using Supel-Inert Foil Gas Sampling Bags by SigmaAldrich™ with a 2L volume capacity before the samples were manually injected into the GC. Three injections were performed for each sample in order to flush impurities in the inlet of the GC. In order to quantify the components measured in the GC analysis, internal standard calibration was used where N<sub>2</sub> acted as internal standard. The calibration were performed using a calibration cylinder containing a gas mixture of methane, ethane, ethene, propane, n-butane, n-pentane, n-hexane, propene, carbon monoxide, hydrogen, nitrogen and carbon dioxide at known concentrations. Furthermore, all results were corrected for air contamination according to the amount of O<sub>2</sub> measured in the GC. This was done based on the assumption that O<sub>2</sub> would not be a product in the CVD synthesis, and the probability of air con-

tamination being present due to the sample collection procedure (sampling bags). Examples of internal standard and air correction calculations, along with raw data from the GC analysis is given in Appendix C.

Since usually 4 or 5 gaseous product samples were collected for each CNF synthesis, a procedure for choosing which sample to include in the results chapter was made. For each synthesis, the conversion of CO vs. synthesis time (hours into the synthesis) were plotted to see the overall trend behaviour. For some samples, the results fluctuated, hence, average values were used. However, for some samples the trend were quite stable over the duration of the synthesis, for the exception of one outlier. For those cases, the values for one of the stable samples were used. Example plots and further explanation is provided in Appendix D.

### 3.3 Characterization

In order to investigate the possibility of applying the produced carbon nanofiber into the carbothermal reduction of metal oxides process, they had to be characterized. Four selected samples was analysed using X-ray diffraction and Raman spectroscopy; two of which prepared by the homemade catalyst, and two with the commercial catalyst. The samples chosen are those obtained from experiment 2, 7, 12 and 13, see table 3.1. Details on the technologies and sample preparation is given in the following sections.

#### 3.3.1 XRD analysis

A D8 A25 DaVinci X-ray Diffractometer with  $\text{CuK}\alpha$  radiation and LynxEye<sup>TM</sup> SuperSpeed Detector with a 90 position sample changer was used for analysing the crystalline structure of the CVD produced CNFs. X-ray diffraction (XRD) analysis is a fundamental method for evaluating carbon structure, in which the crystalline structure causes a beam of incident X-rays to diffract into many specific directions [86]. The angles and intensities of these diffracted beams are measured by the diffractometer making it possible to reveal chemical composition and crystalline size information. Identification of phases is achieved by comparison of the acquired data to that in reference databases, in this case the ICDD-4+PDF-database provided by the Diffrac.Eva V5 analysis software.

The samples were prepared by grounding them to fine powder before they were placed in closed powder specimen holders. The sample was patted down in the holders using a glass slide in order to achieve a level height. Each analysis was programmed for a  $5\text{-}75^\circ$   $2\theta$  for 15 minutes, with a low crystallinity step size of  $0,044^\circ/\text{step}$ .

The Scherrer equation was used to relate the crystalline size to the broadening of a peak in the diffraction pattern. The Scherrer equation can be written as:

$$\tau = \frac{K\lambda}{\beta\cos\theta}$$

where:

- $\tau$  is the mean size of the ordered (crystalline) domains, which may be smaller or equal to the grain size, which may be smaller or equal to the particle size;
- $\mathbf{K}$  is a dimensionless shape factor, with a value close to unity. The shape factor has a typical value of about 0.9, but varies with the actual shape of the crystallite;
- $\lambda$  is the X-ray wavelength;
- $\beta$  is the line broadening at half the maximum intensity (FWHM), after subtracting the instrumental line broadening, in radians. This quantity is also sometimes denoted as  $\Delta(2\theta)$ ;
- $\theta$  is the Bragg angle.

The Bragg angle is the angle coherent and incoherent scattering from a crystal lattice. The Scherrer equation is limited to nano-scale crystallites, or more-strictly, the coherently scattering domain size, which can be smaller than the crystallite size [56, 86].

### 3.3.2 Raman spectroscopy

A Horiba Jibin Yvon LabRAM HR800 instrument was used for the Raman spectroscopy characterization of carbon nanofibers. Raman spectroscopy is a standard nondestructive tool for the characterization of crystalline, nanocrystalline, and amorphous carbons [58]. Typically, a sample is illuminated with a laser beam, whilst the electromagnetic radiation from the illuminated spot is collected and sent through a monochromator. Raman spectroscopy was used to gain further information regarding the crystallinity of the CVD prepared CNFs.

The samples were placed on glass slides and pressed down lightly to achieve a flat surface. All samples were analysed at 3 different spots with a laser excitation wavelength of 633nm. No filters were used because carbon gives a clear Raman scattering, and the signal was not saturated (above 40000 usi). The Raman shift range was varied for some of the samples in order to obtain a good Raman spectra quality, but mainly ranging from 1000-2800cm<sup>-1</sup>.

### 3.4 Aspen Plus

Aspen Plus V9<sup>TM</sup> is a plant wide simulation tool tailored for chemical processes, containing comprehensive physical property models and library of unit operation models providing fast and reliable process simulation functions, and advanced calculation methods [82].

The RGibbs reactor model is a simple reactor model where the only fixed variables are the temperature, pressure and inlet flow. It is the only Aspen Plus<sup>TM</sup> reactor model that allows handling of solid, liquid and gas phase equilibrium. This type of reactor applies the method of direct minimization of Gibbs free energy at a specified temperature and pressure. It is useful when reactions occurring are not known or are high in number, due to many components participating in the reactions [3]. For the purpose of this project, the Peng Robinson thermodynamic package was applied as the property method. The components present in the product has to be specified in the simulation. The RGibbs reactor was chosen for the estimation of thermodynamic equilibrium composition obtainable by; 1) feeding gas mixtures of CO, CO<sub>2</sub>, H<sub>2</sub> and N<sub>2</sub> in various ratios at constant pressure (1atm) and temperature (600°C) and; 2) application of various operating temperatures keeping the feed composition and pressure constant (1atm). The components specified as present in the product of the reactor were CO, CO<sub>2</sub>, H<sub>2</sub>, N<sub>2</sub>, C<sub>(s)</sub>, CH<sub>4</sub> and H<sub>2</sub>O.

The conditions applied in the simulation were chosen on the basis of a typical oven gas composition for the FeMn process, as listed in table 2.4 in section 2.3. Moreover tuning of the partial pressures of the compounds in the feed gas was done to investigate their effect on the thermodynamic equilibrium product distribution. All simulation conditions are summarized in table 3.2. An illustration of the simulation flowsheet is presented in figure 3.3. Investigations on the effect of various feed compositions were done in two ways; 1) changing the partial pressure of  $\text{CO}_2$  in the feed stream (referred to as "IN" in figure 3.3) by changing the partial pressure of  $\text{N}_2$ , keeping partial pressure of  $\text{CO}$  and  $\text{H}_2$  and total volume flow constant and; 2) feeding additional  $\text{H}_2$  in a separate feed stream (referred to as "H2" in figure 3.3) while keeping the "IN" stream composition and total volume flow constant.

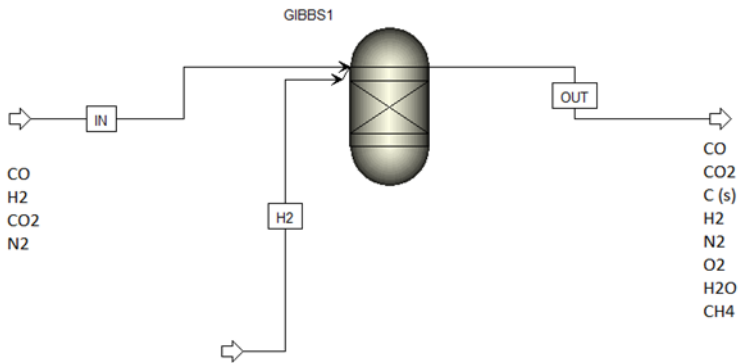


Figure 3.3: Flowsheet of Aspen Plus simulation.

Table 3.2: Summary of all conditions for Aspen Plus simulation, \*temperature intervals of 50°C.

Cond.	Temp.	Pres.	Partial Pressure [bar]				Tot. Flow [ml/min]	Descript.
	[°C]		CO	CO2	H2	N2		
1	600	1	0.800	0.000	0.200	0.000	80.59	PCO2
2			0.62	0.24	0.09	0.06		&
3			0.62	0.00	0.09	0.30		PH2
4			0.62	0.12	0.09	0.18		effect
5			0.62	0.24	0.13	0.01		

Cond.	Temp.	Pres.	Partial pressure [Bar]				Tot. Flow [mol/hr]	Descript.
	[°C]		CO	CO2	H2	N2		
6	500-700*	1	0.62	0.24	0.09	0.06	1.98E-04	Adding
7			0.49	0.19	0.27	0.04	2.48E-04	H2 and
8			0.41	0.16	0.39	0.04	2.99E-04	temp.
9			0.37	0.14	0.46	0.03	3.32E-04	effect
10			0.32	0.12	0.53	0.03	3.83E-04	



# Chapter 4

## Results and Discussion

### 4.1 Aspen Plus simulation results

As mentioned in section 3.4, Aspen Plus V9 was used to estimate the thermodynamic equilibrium product distribution in a Gibbs reactor fed with gas mixtures of CO, CO<sub>2</sub>, H<sub>2</sub> and N<sub>2</sub> in various ratios, with defined possible products (CO, CO<sub>2</sub>, H<sub>2</sub>, N<sub>2</sub>, CH<sub>4</sub> and H<sub>2</sub>O). Originally, the process was simulated with the feed composition of oven gas of a FeMn production process, repeated in table 4.1.

Table 4.1: Gas mixture similar to a typical oven gas mixture produced in the FeMn process.

Cond. [bar]	PCO	PCO2	PH2	PN2
$1_{IND}$	0.620	0.240	0.085	0.055

Note that when the typical oven gas composition is referred to further in this thesis, it will be labeled with subscript (IND) and called "industrial conditions". The effect on product distribution

by varying the partial pressures of CO<sub>2</sub> and H<sub>2</sub> in the feed and process temperature was investigated.

The results are presented as conversions of CO, H<sub>2</sub> and CO<sub>2</sub>, and yield of C, calculated as shown in equation 4.1, 4.2, 4.3 and 4.4, respectively. Note that  $\dot{V}$  is the volumetric flow rate in ml/min and  $\dot{n}$  is the mole flow rate in mol/hr.

$$CO_{conv.} = \frac{\dot{V}_{CO,in} - \dot{V}_{CO,out}}{\dot{V}_{CO,in}} \quad (4.1)$$

$$H2_{conv.} = \frac{\dot{V}_{H2,in} - \dot{V}_{H2,out}}{\dot{V}_{H2,in}} \quad (4.2)$$

$$CO2_{conv.} = \frac{\dot{V}_{CO2,in} - \dot{V}_{CO2,out}}{\dot{V}_{CO,in} + \dot{V}_{CO2,in}} \quad (4.3)$$

$$C_{yield} = \frac{\dot{n}_{C,out}}{\dot{n}_{CO,in}} \quad (4.4)$$

Additionally, the yield of methane and water were calculated based on the CO fed to the system, shown in equation 4.5 and 4.6, respectively.

$$CH4_{yield.} = \frac{\dot{n}_{CH4,out}}{\dot{n}_{CO,in}} \quad (4.5)$$

$$H2O_{yield.} = \frac{\dot{n}_{H2O,out}}{\dot{n}_{CO,in}} \quad (4.6)$$

### 4.1.1 CO<sub>2</sub> effect

Typical oven gases contain carbon dioxide; the effect of the partial pressure of CO<sub>2</sub> in the feed on the thermodynamic equilibrium product distribution was investigated. The conditions that were researched are listed in table 4.2.

Table 4.2: Feed gas mixture compositions of Aspen Plus simulation exploring the CO<sub>2</sub> effect.

Cond. [bar]	PCO	PCO <sub>2</sub>	PH <sub>2</sub>	PN <sub>2</sub>	CO <sub>2</sub> /CO
1 <sub>IND(0xCO<sub>2</sub>)</sub>	0.620	0.000	0.085	0.295	0.000
2 <sub>INS(0.5xCO<sub>2</sub>)</sub>	0.620	0.120	0.085	0.175	0.194
3 <sub>IND</sub>	0,620	0,240	0.085	0.013	0.387

The CO<sub>2</sub>/CO ratios that were investigated was half and zero the partial pressure of CO<sub>2</sub> compared to the industrial condition (see table 4.2). These values were chosen in order to investigate the potential C yield and CO conversion obtainable if CO<sub>2</sub> was partly or fully removed from the industrial gas mixture composition prior to the Boudouard reaction.

In figure 4.1 the conversion of CO (a), H<sub>2</sub> (b), CO<sub>2</sub> (c) and yield of C (d) calculated from the simulation results is presented as a function of CO<sub>2</sub>/CO ratio. The product gas mixture compositions for feed condition 1<sub>IND(0x CO<sub>2</sub>)</sub>, 2<sub>IND (0x CO<sub>2</sub>)</sub> and 3<sub>IND</sub> is tabulated in table 4.3.

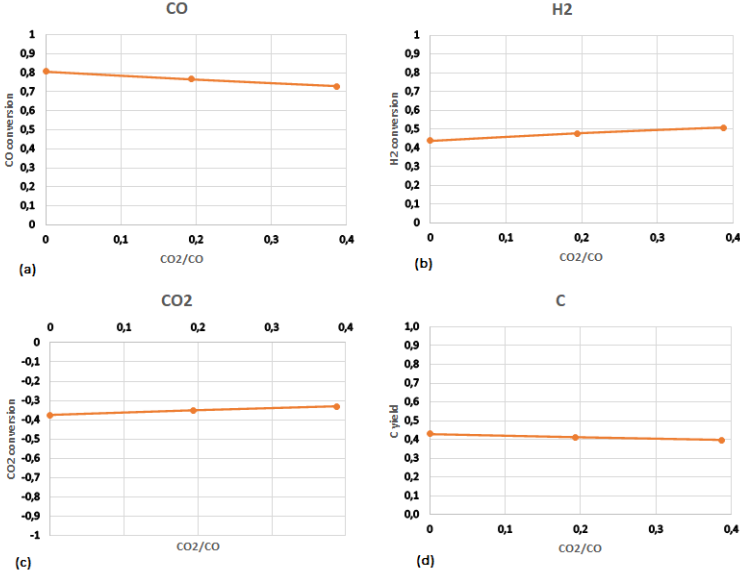


Figure 4.1: CO, H<sub>2</sub>, CO<sub>2</sub> conversion and C yield of Aspen Plus simulation exploring the CO<sub>2</sub> effect.

Table 4.3: Product gas mixture compositions of Aspen Plus simulation exploring the CO<sub>2</sub> effect.

Cond. [bar]	PCO	PCO <sub>2</sub>	PH <sub>2</sub>	PN <sub>2</sub>	PCH <sub>4</sub>	PH <sub>2</sub> O
1 <sub>IND(0xCO<sub>2</sub>)</sub>	0.120	0.234	0.048	0.295	0.001	0.035
2 <sub>IND(0.5xCO<sub>2</sub>)</sub>	0.145	0.339	0.044	0.175	0.001	0.038
3 <sub>IND</sub>	0.168	0.447	0.042	0.055	0.001	0.041

The conversion of CO (a) exhibits a decreasing trend when the partial pressure of CO<sub>2</sub> is increased in the feed. This suggests that CO<sub>2</sub> inhibits the conversion of CO which also results in a decrease in carbon yield (d). According to Le Chatelier's principle, the P<sub>CO</sub> in the products increases at the thermodynamic equilibrium by feeding higher partial pressures of CO<sub>2</sub>, when Boudouard reaction occurs ( $2\text{CO} = \text{C} + \text{CO}_2$ , see table 2.1). The highest C yield (42.9 %) was obtained at P<sub>CO<sub>2</sub></sub>=0. However, for the condition 3<sub>IND</sub> (CO<sub>2</sub>/CO ratio = 0.38, P<sub>CO<sub>2</sub></sub> = 0.24), the carbon yield is still relatively high; 39.6 %. The conversion of CO<sub>2</sub> (c) increases as more CO<sub>2</sub> is fed to the process, which is expected since higher partial pressure of CO<sub>2</sub> will cause lower CO conversion, limiting the formation of CO<sub>2</sub>. The conversion of H<sub>2</sub> (b) increases from 44 to 51 %.

### 4.1.2 H<sub>2</sub> effect

Aspen plus was used to find the H<sub>2</sub>/CO ratio giving the highest C yield and CO conversion at the thermodynamic equilibrium. For this purpose, several H<sub>2</sub>/CO ratios were investigated. The partial pressures of the components in the feed are listed in table 4.4.

Table 4.4: Feed gas mixture compositions of Aspen Plus simulation exploring the H<sub>2</sub> effect.

Cond. [bar]	PCO	PCO <sub>2</sub>	PH <sub>2</sub>	PN <sub>2</sub>	H <sub>2</sub> /CO
1 <sub>IND</sub>	0.620	0.240	0.085	0.055	0.137
2	0.494	0.191	0.271	0.044	0.548
3	0.411	0.159	0.394	0.036	0.960
4	0.369	0.143	0.455	0.033	1.234
5	0.320	0.124	0.527	0.028	1.645

Figure 4.2 shows the conversion of CO (a), H<sub>2</sub> (b), CO<sub>2</sub> (c) and the yield of C (d) for various H<sub>2</sub>/CO ratios. This was simulated by introducing a pure H<sub>2</sub> stream to the Gibbs reactor, thus increasing the H<sub>2</sub> partial pressure in to the system. The partial pressure of the product components are presented in table 4.5.

## Carbon Looping for Metallurgical Processes via Boudouard reaction over Magnetite

---

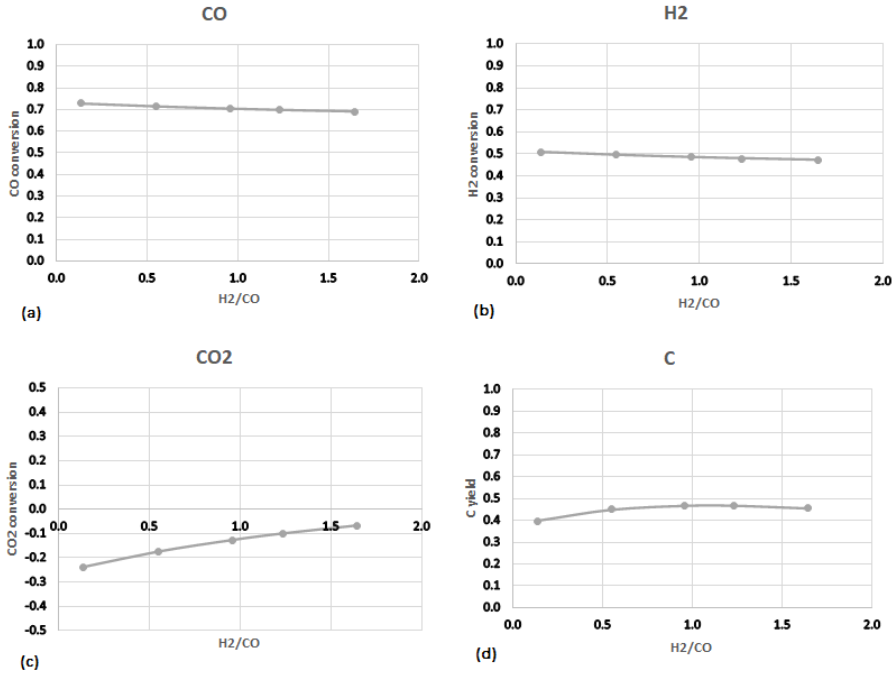


Figure 4.2: CO, H<sub>2</sub>, CO<sub>2</sub> conversion and C yield of Aspen Plus simulation exploring the H<sub>2</sub> effect.

Table 4.5: Product gas mixture compositions of Aspen Plus simulation exploring the H<sub>2</sub> effect.

Cond. [bar]	PCO	PCO <sub>2</sub>	PH <sub>2</sub>	PN <sub>2</sub>	PCH <sub>4</sub>	PH <sub>2</sub> O
1 <sub>IND</sub>	0.168	0.447	0.042	0.055	0.001	0.041
2	0.144	0.319	0.140	0.045	0.011	0.115
3	0.128	0.243	0.213	0.038	0.025	0.151
4	0.119	0.208	0.254	0.035	0.035	0.164
5	0.109	0.169	0.306	0.031	0.049	0.176

The conversion of CO (a) decrease as the partial pressure of H<sub>2</sub> increases. This is an opposite trend of the one of the C yield (d), which has a maximum yield at H<sub>2</sub>/CO ratio at approximately 1. The conversion of CO<sub>2</sub> (c) (negative because CO<sub>2</sub> is produced) increases as the H<sub>2</sub>/CO ratio increases, meaning less CO<sub>2</sub> is produced. The H<sub>2</sub> conversion (b) decreases slightly. The fact that the CO conversion decreases while the formation of C increases suggests that not only the Boudouard reaction occurs in the system. In order to investigate and understand the reactions occurring in the system, the yield of CH<sub>4</sub> and H<sub>2</sub>O is shown as functions of H<sub>2</sub>/CO ratio in figure 4.3 (a) and (b), respectively.

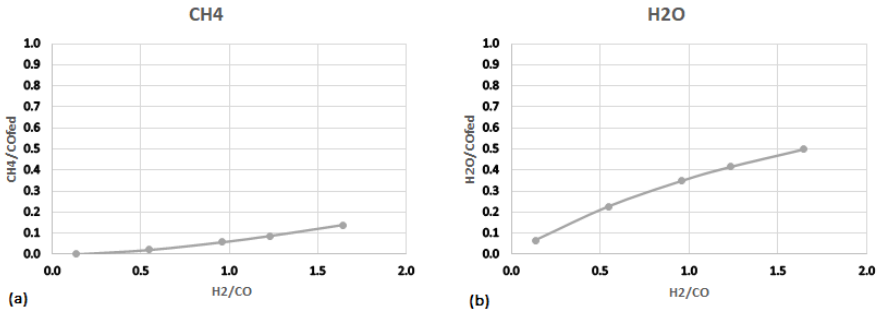


Figure 4.3: CH<sub>4</sub> and H<sub>2</sub>O yield (based on CO fed) of Aspen Plus simulation exploring the H<sub>2</sub> effect.

It appears that both the yield of CH<sub>4</sub> (a) and H<sub>2</sub>O (b) are increasing with increasing H<sub>2</sub>/CO ratio. Higher production of CH<sub>4</sub> at higher partial pressure of H<sub>2</sub> in the feed suggests that methanation is occurring. Methanation reactions, summarized in table 4.6, can occur by H<sub>2</sub> reacting with CO, CO<sub>2</sub> or solid C. This does not explain, and actually contradicts, the decreasing conversion of CO at higher partial pressure of H<sub>2</sub>. However, it might be an explanation to the decreasing production of CO<sub>2</sub> at higher H<sub>2</sub>/CO ratios. Methanation at H<sub>2</sub>/CO ratios higher than 1 may also be why C



yield reaches a plateau.

Table 4.6: Reaction equation and enthalpy for RWGS and methanation reactions.

Reaction	Equation	$\Delta H_{298K}$ [kJ/mol]
RWGS	$\text{CO}_2 + \text{H}_2 = \text{CO} + \text{H}_2\text{O}$	41.1
Methanation	$\text{CO} + 3\text{H}_2 = \text{CH}_4 + \text{H}_2\text{O}$	-206.2
	$\text{CO}_2 + 4\text{H}_2 = \text{CH}_4 + 2\text{H}_2\text{O}$	-164
	$\text{C} + 2\text{H}_2 = \text{CH}_4$	-73

The increased production of  $\text{H}_2\text{O}$  at higher  $\text{H}_2/\text{CO}$  ratios may suggest the reverse water gas shift (RWGS) reaction, listed in table 4.6, where  $\text{CO}_2$  and  $\text{H}_2$  reacts and forms  $\text{CO}$  and  $\text{H}_2\text{O}$ . The RWGS might explain why the conversion of  $\text{CO}$  is decreasing, as  $\text{CO}$  and  $\text{H}_2\text{O}$  are products of this reaction. Additionally, it might explain why less  $\text{CO}_2$  is produced since it would be consumed by the RWGS reaction.

### 4.1.3 Temperature effect

Temperatures ranging from 500-700 °C was applied in the simulation in order to explore the effect on product distribution for the same H<sub>2</sub>/CO ratios investigated in the previous section (table 4.4). The conversions for CO (a), H<sub>2</sub> (b) and CO<sub>2</sub> (c) along with the yield of C (d) are presented in figure 4.4.

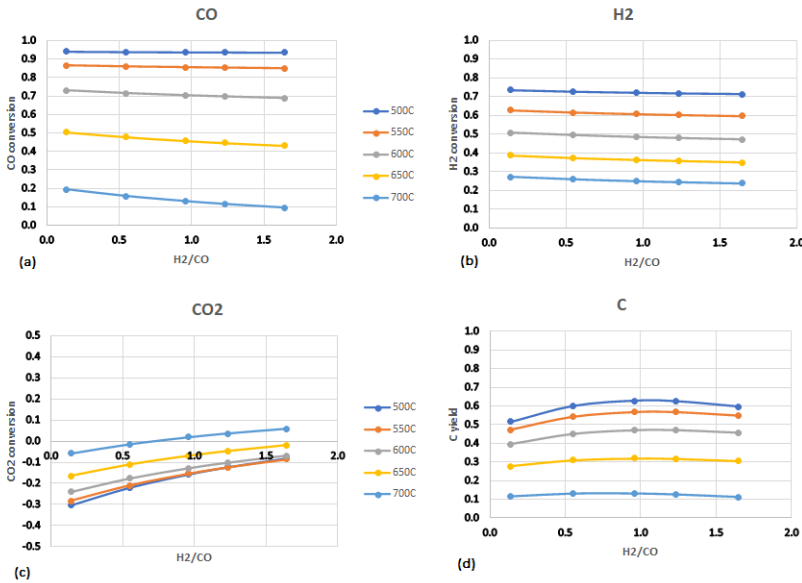


Figure 4.4: Temperature effect on conversion of CO, H<sub>2</sub>, CO<sub>2</sub> and yield of C for temperatures ● 500°C, ● 550°C, ● 600°C, ● 650°C, ● 700°C.

Figure 4.4 (a) shows how CO conversion varies with temperature. The conversion is higher at lower temperatures, which can be expected when Boudouard reaction occurs, due to it's exothermicity. Likewise, in 4.4 (d), the carbon yield is increasing with decreasing temperatures, the conversion of H<sub>2</sub> is higher at lower temperatures, while the conversion of CO<sub>2</sub> is favoured by high temperatures. For the reaction temperature at 700°C for H<sub>2</sub>/CO ratio above approximately 0,65 the conversion of CO<sub>2</sub> becomes positive, meaning CO<sub>2</sub>

is consumed in the process. As discussed in the previous section, the behaviour of the  $\text{CO}_2$  conversion at higher  $\text{H}_2/\text{CO}$  ratios suggests that other reactions are occurring in the system. Also here the yield of  $\text{CH}_4$  (a) and  $\text{H}_2\text{O}$  (b) based on CO fed were investigated (figure 4.5). All three methanation reactions and the RWGS reaction are exothermic (table 4.6), hence they are favoured at low temperatures. It is clear from figure 4.5 that more  $\text{CH}_4$  and  $\text{H}_2\text{O}$  are produced at lower reaction temperatures, supporting the suggestion that these reactions are occurring in the system at higher  $\text{H}_2/\text{CO}$  ratios.

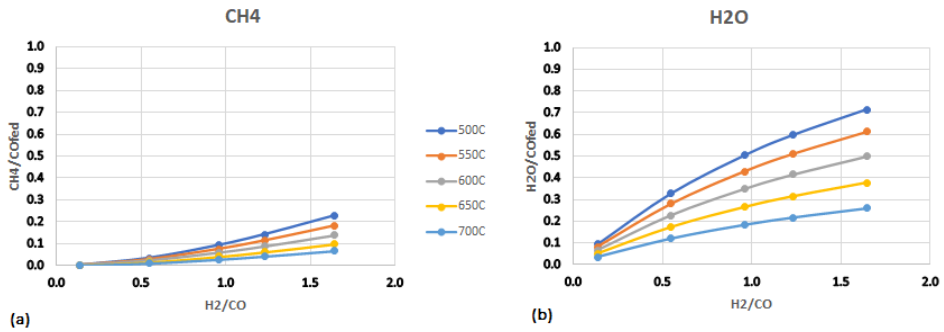


Figure 4.5: Temperature effect on yield of  $\text{CH}_4$  and  $\text{H}_2\text{O}$  for temperatures ● 500°C, ● 550°C, ● 600°C, ● 650°C, ● 700°C.

#### 4.1.4 Main findings based on thermodynamic analysis

According to the thermodynamic analysis in Aspen Plus, it appears that the CO conversion and C yield can be increased by decreasing partial pressure of CO<sub>2</sub> in the feed. Increasing partial pressure of H<sub>2</sub> in the feed seems to increase the C yield until a H<sub>2</sub>/CO ratio of approximately 1. However, the CO conversion decreases with increasing partial pressure of H<sub>2</sub>, which might suggest occurrence of RWGS reaction. Moreover, increasing yield of CH<sub>4</sub> was observed at higher H<sub>2</sub>/CO ratio, suggesting methanation reaction. The methanation reactions are undesirable, as it will inhibit the formation of carbon and produce methane, which is considered a greenhouse gas. The effect of temperature on the system seemed to correlate to the exothermicity of the Boudouard reaction, i.e. higher CO conversion and C yield at lower temperatures. Based purely on the thermodynamic equilibrium results by simulation in Aspen Plus, tuning of the industrial feed condition by lowering the partial pressure of CO<sub>2</sub> and increasing the partial pressure of H<sub>2</sub>, higher CO conversion and C yield could be obtained. Moreover, lowering the operating temperature might have a positive effect for the production of carbon, hence decreasing the total CO<sub>2</sub> emissions in the metallurgical process.

## 4.2 Experimental results

CVD method using CO as C precursor was used for the production of carbon nanofibers. The feed gas composition was varied in order to investigate how the feed components (CO<sub>2</sub>, H<sub>2</sub>) affect the product gas distribution and carbon yield in the presence of magnetite catalyst. Furthermore, the temperature effect was explored while the feed gas composition was held constant. The experimental results were thus compared with the thermodynamic equilibrium results estimated by Aspen Plus.

The results are presented as conversions of CO, H<sub>2</sub> and CO<sub>2</sub>, and yield of C, calculated as shown in equation 4.7, 4.8, 4.9 and 4.10, respectively. Note that  $\dot{V}$  is the volumetric flow rate in ml/min and  $\dot{n}$  is the mole flow rate in mol/hr.

$$CO_{conv.} = \frac{\dot{V}_{CO,in} - \dot{V}_{CO,out}}{\dot{V}_{CO,in}} \quad (4.7)$$

$$H2_{conv.} = \frac{\dot{V}_{H2,in} - \dot{V}_{H2,out}}{\dot{V}_{H2,in}} \quad (4.8)$$

$$CO2_{conv.} = \frac{\dot{V}_{CO2,in} - \dot{V}_{CO2,out}}{\dot{V}_{CO,in} + \dot{V}_{CO2,in}} \quad (4.9)$$

$$C_{yield} = \frac{\dot{n}_{C,out}}{\dot{n}_{CO,in}} \quad (4.10)$$

### 4.2.1 CO<sub>2</sub> effect

The effect of PCO<sub>2</sub> in the feed gas mixture for the preparation of CNFs on the product distribution were researched by feeding the compositions listed in table 4.7. In figure 4.6, the experimental results are plotted together with the Aspen Plus results.

Table 4.7: Feed gas mixture compositions of C synthesis by CVD exploring the CO<sub>2</sub> effect.

Condition [bar]	PCO	PCO <sub>2</sub>	PH <sub>2</sub>	PN <sub>2</sub>	CO <sub>2</sub> /CO
1 <sub>IND(0xCO<sub>2</sub>)</sub>	0.620	0.000	0.085	0.295	0.000
2 <sub>IND(0.5xCO<sub>2</sub>)</sub>	0.620	0.120	0.085	0.175	0.194
3 <sub>IND</sub>	0.620	0.240	0.085	0.013	0.387

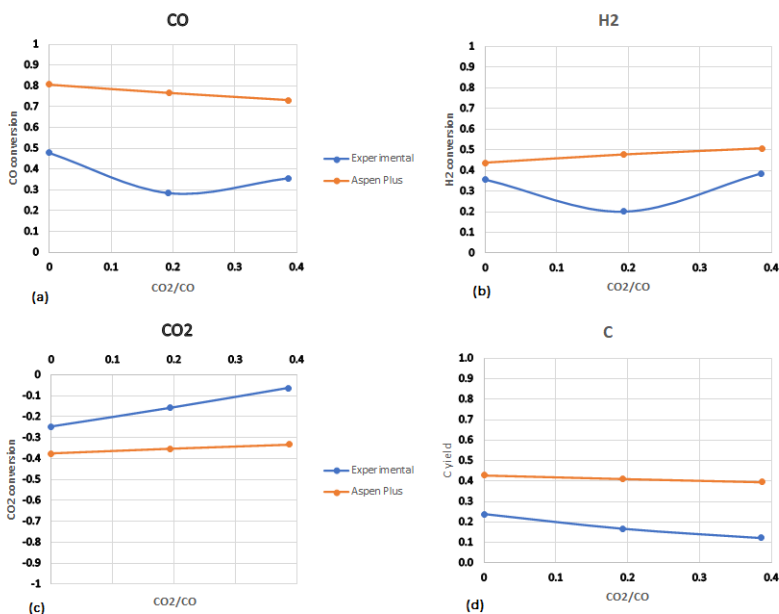


Figure 4.6: CO, H<sub>2</sub>, CO<sub>2</sub> conversion and C yield exploring CO<sub>2</sub> effect, Experimental vs. Aspen.

The experimental results show, like the simulation results, that the conversion of CO (a) decreases with increasing partial pressure of CO<sub>2</sub> in the feed. There is a rapid decrease when CO<sub>2</sub> is introduced to the feed gas mixture, where conversion of CO decreases from 47.9% to 28.5%. However, at higher CO<sub>2</sub>/CO ratio (0.38), the experimental results shows an increase in CO conversion. In comparison to the simulation results, the CO and H<sub>2</sub> conversions obtained experimentally are notably lower, which suggests that the experiments are performed at conditions that are far from the thermodynamic equilibrium. It should be noted that the quantitative analysis of the components in the product gas is obtained by manual injection in a GC from gas sampling bags, which may cause some relative errors associated to the results. Assessing the actual inaccuracies caused by the analysis procedure would be difficult, however, precautions to minimize them were performed; for example by correcting for air contamination. Consequently, the somewhat unexpected observation of increasing CO conversion from CO<sub>2</sub>/CO ratio = 0.194 to 0.387 is difficult to explain. The H<sub>2</sub> conversion (figure 4.6 (b)) exhibit a similar minimum as the CO conversion at CO<sub>2</sub>/CO ratio = 0.193. The product gas compositions of C synthesis by CVD is presented in table 4.8

Table 4.8: Product gas mixture compositions of C synthesis by CVD exploring the CO<sub>2</sub> effect.

Condition [bar]	PCO	PCO <sub>2</sub>	PH <sub>2</sub>	PN <sub>2</sub>
1 <sub>IND(0xCO2)</sub>	0.393	0.187	0.077	0.359
2 <sub>IND(0.5xCO2)</sub>	0.541	0.289	0.083	0.213
3 <sub>IND</sub>	0.389	0.284	0.051	0.054

The CO<sub>2</sub> conversion, figure 4.6 (c), increases with increasing CO<sub>2</sub>/CO ratio, meaning less CO<sub>2</sub> is produced, which is expected considering the La Chatelier's principle. Contrarily to the conversion of CO and H<sub>2</sub> the conversion of CO<sub>2</sub> obtained experimentally is higher than the simulation results, i.e. the simulation predicts more CO<sub>2</sub> in the product gas mixture. The C yield obtained experimentally exhibits a similar trend to the simulation results, with decreasing C yield for increasing CO<sub>2</sub>/CO ratio. The C yield decreases from 23.7 % (P<sub>CO<sub>2</sub></sub>=0) to 12.3% (P<sub>CO<sub>2</sub></sub>=0.387, industrial condition). Note that in the product gas mixture compositions in table 4.8, the partial pressure of N<sub>2</sub> varies from the inlet conditions. This is due to the treatment of the GC results, where it was assumed that the flow of N<sub>2</sub> was constant through the reactor, not the partial pressure. See Appendix C for the details of the calculations.



### 4.2.2 H<sub>2</sub> effect

The effect of H<sub>2</sub> in the gas feed on the product distribution is shown in figure 4.7, together with the Aspen Plus results. The feed conditions are listed in table 4.9.

Table 4.9: Feed gas mixture compositions and H<sub>2</sub>/CO ratios of C synthesis by CVD and Aspen Plus exploring the H<sub>2</sub> effect.

Cond. [bar]	PCO	PCO <sub>2</sub>	PH <sub>2</sub>	PN <sub>2</sub>	H <sub>2</sub> /CO
1 <sub>IND</sub>	0.620	0.240	0.085	0.055	0.137
2 <sub>IND(1.5xH2)</sub>	0.620	0.240	0.130	0.01	0.206

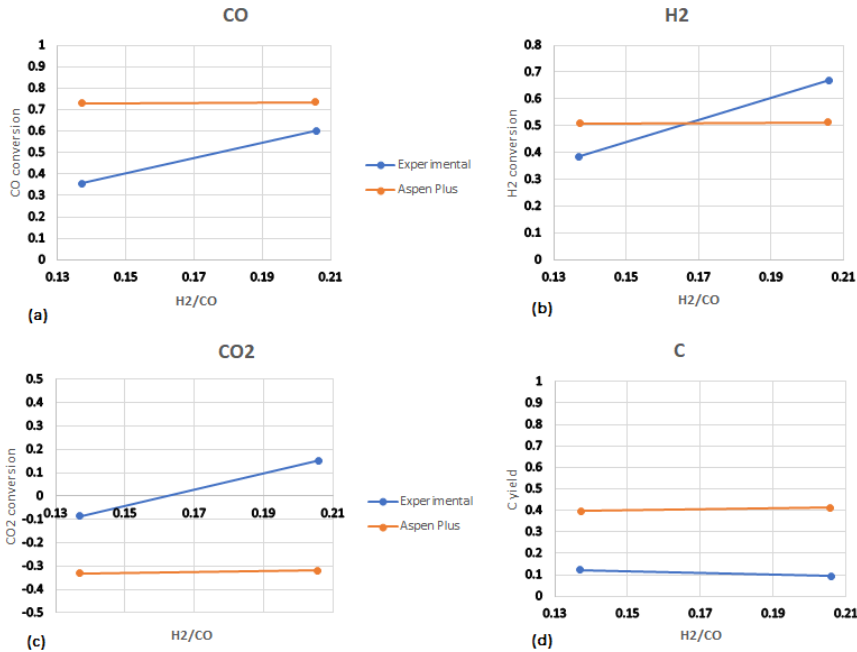


Figure 4.7: CO, H<sub>2</sub>, CO<sub>2</sub> conversion and C yield exploring H<sub>2</sub> effect, Experimental vs. Aspen.

The experimental results show a rapid increase in conversion for CO, H<sub>2</sub> and CO<sub>2</sub> at higher H<sub>2</sub>/CO ratio, whereas the simulation results exhibits more or less unchanged results. While the conversion of CO (a) is notably lower than predicted by the simulation, the conversion of H<sub>2</sub> (b) obtained experimentally exceeds Aspen's prediction at H<sub>2</sub>/CO ratio = 0.206. Likewise, the conversion of CO<sub>2</sub> (c) is much higher than the simulation results for both H<sub>2</sub>/CO ratios, hence, CO<sub>2</sub> is consumed in the process. This suggests that another reaction than the Boudouard reaction is occurring in the system. Furthermore, even though the conversion of CO increased, the C yield obtained experimentally exhibited a slight decrease with increasing H<sub>2</sub>/CO ratio, from 12.3 to 9.4 %. The product gas composition is listed in table 4.10.

Table 4.10: Product gas mixture compositions of C synthesis by CVD and Aspen exploring the H<sub>2</sub> effect.

Cond. [bar]	PCO	PCO <sub>2</sub>	PH <sub>2</sub>	PN <sub>2</sub>
1 <sub>IND</sub>	0.389	0.284	0.051	0.054
2 <sub>IND(1.5xH2)</sub>	0.174	0.102	0.030	0.010

Methanation of CO<sub>2</sub> and H<sub>2</sub> could be a possible explanation of the behaviour of CO<sub>2</sub> at higher H<sub>2</sub>/CO ratios. Unfortunately, the quantification of methane in the product gas could not be performed due to the detection limit of the GC. Consequently, simulations removing H<sub>2</sub>O and CH<sub>4</sub> from the possible products in Aspen Plus were performed as a measure to "force" Boudouard's (No CH<sub>4</sub> and H<sub>2</sub>O) and RWGS (No CH<sub>4</sub>) reactions, respectively. The conversion of CO, CO<sub>2</sub>, H<sub>2</sub> and yield of C for all three simulations with feed conditions listed in table 4.9 are presented in figure 4.8.

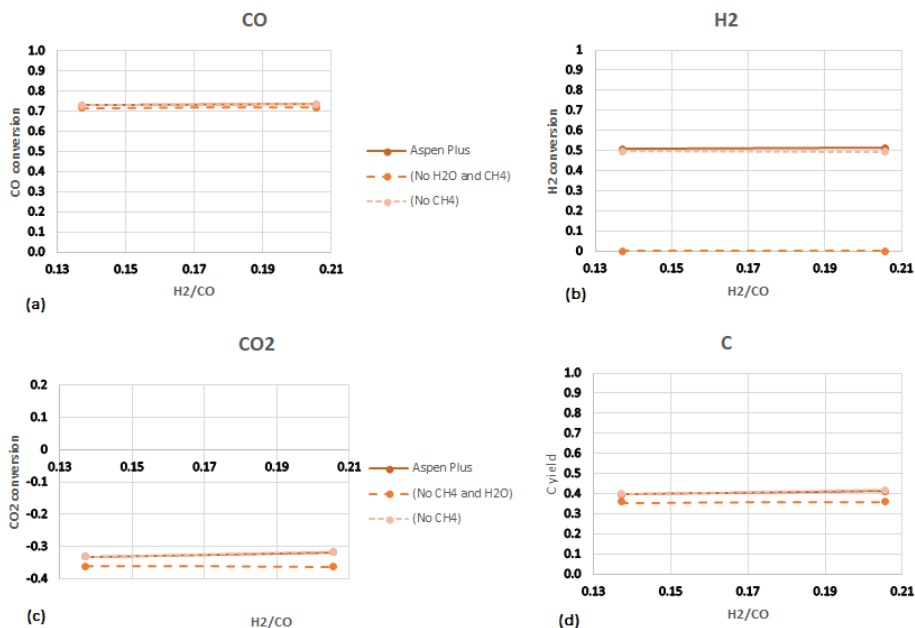


Figure 4.8: CO, H<sub>2</sub>, CO<sub>2</sub> conversion and C yield of Aspen Plus simulations exploring various defined product components.

The conversion of CO (a) in figure 4.8 stayed mainly unchanged comparing the three simulations. When CH<sub>4</sub> and H<sub>2</sub>O was removed as possible products, Aspen Plus predicted zero conversion of H<sub>2</sub>, which is expected since H<sub>2</sub> is the only compound containing H-atoms in the defined products. For that same simulation, a small decrease in CO<sub>2</sub> conversion and C yield was observed. Finally, none of the simulation results exhibit the same trend as the experimental results. Thus, whether or not the experiments are affected by methanation or RWGS can not be suggested purely based on the simulation results.

### 4.2.3 Temperature effect

Figure 4.9 shows the conversion of CO (a), H<sub>2</sub> (b), CO<sub>2</sub> (c) and the yield of C (d) for the homemade and commercial catalyst at various temperatures. The feed condition applied equals the industrial conditions, listed as condition 1<sub>IND</sub> in the previous section (table 4.9), for all reaction temperatures.

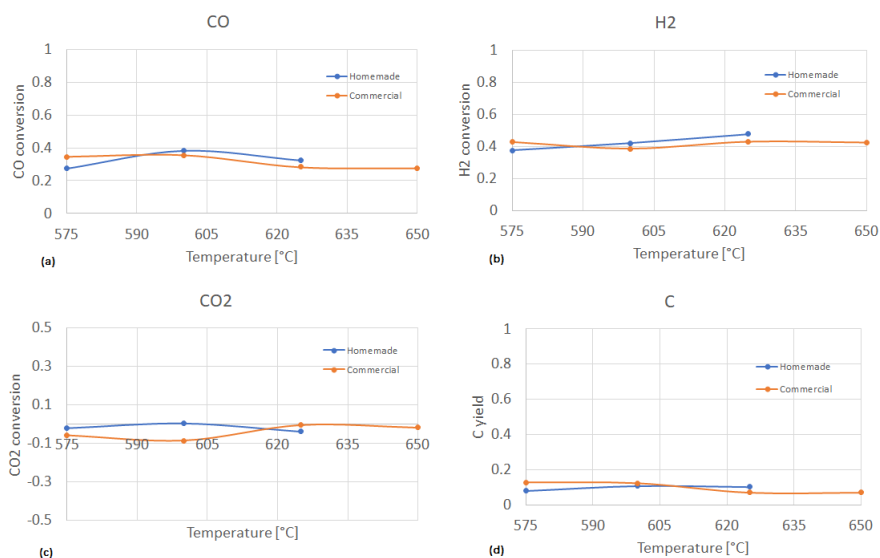


Figure 4.9: Temperature effect on product distribution.

For the commercial catalyst the conversion of CO (a) is more or less unchanged in the temperature interval  $575^{\circ}\text{C} < T < 600^{\circ}\text{C}$ , before decreasing at higher temperatures. However, for the homemade catalyst the CO conversion exhibits a maximum at  $T=600^{\circ}\text{C}$ .

When homemade catalyst was used, the  $H_2$  conversion (b) exhibit an increase with increasing temperature, whilst the experiments where commercial catalyst was used show highest  $H_2$  conversion at  $T=575^\circ C$  before exhibiting a slight fluctuation at increasing temperature. For the syntheses applying homemade catalyst, the  $CO_2$  conversion (fig. 4.9 (c)) is positive at lower temperatures, whilst at  $T=625^\circ C$  decreases and becomes negative. The opposite trend is seen for the commercial catalyst, where the  $CO_2$  conversion exhibits negative values at lower temperatures but increases, and becomes positive, at  $T = 625^\circ C$ . The C yield (d) varied comparing the two catalysts; for the experiments where the homemade catalyst were used, the C yield increases with increasing temperature, whilst for the commercial catalyst the C yield are more or less unchanged in the temperature range  $575^\circ C < T > 600^\circ C$ , before decreasing at higher temperatures. Overall, it seems like lower reaction temperatures ( $575-600^\circ C$ ) is favoured when the commercial catalyst is applied, while higher temperature ( $600-625^\circ C$ ) gave highest C yield when the homemade catalyst was used in the synthesis. Looking purely on the CO conversion (a), it appears that reaction temperature =  $600^\circ C$  is the favourable.

### 4.2.4 WHSV effect

In order to approach the thermodynamic equilibrium conversion of CO in the process, the weight hourly space velocity (WHSV) on the basis of CO fed was decreased. The conversion of CO (a), H<sub>2</sub> (b), CO<sub>2</sub> (c) and C yield (d) for WHSV at 29.83, 9.97 and 5.97 (experiment 12, 16 and 17 in table 3.1) and Aspen Plus results at the same feed condition (repeated in table 4.11) is given in figure 4.10.

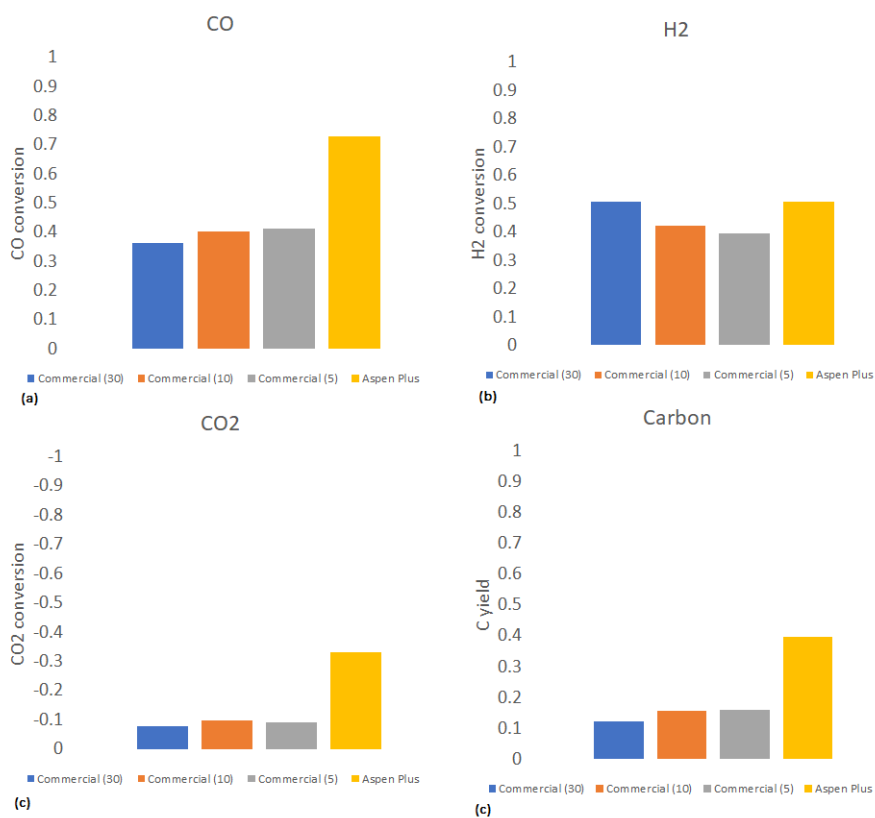


Figure 4.10: Product distribution exploring WHSV, compared to Aspen Plus; ● WHSV = 29.83, ● WHSV = 9.97, ● WHSV = 5.97 and ● Aspen Plus.

Table 4.11: Feed condition used for researching the WHSV effect on product distribution.

Cond. [bar]	PCO	PCO2	PH2	PN2
$1_{IND}$	0.620	0.240	0.085	0.055

Decreasing WHSV did not affect the product distribution much. Slight increase in CO conversion and C yield was observed at lower WHSV but still much lower than predicted by Aspen Plus. Moreover, grams of carbon produced per grams of catalyst loaded decreased with decreasing WHSV, see table 4.12. These results suggests that the experimental results are close to thermodynamic equilibrium, and that a higher CO conversion can not be achieved by increasing the catalyst mass.

Table 4.12: WHSV based on  $L_{CO}$  fed and grams carbon produced per grams catalyst.

WHSV	$g_C/g_{cat.}$
$[L_{CO}/g_{cat.} \cdot hr]$	
29.83	88.0
9.97	37.4
5.97	23.3

#### 4.2.5 Main findings comparing Aspen Plus and experimental results

Aspen Plus analysis feeding industrial conditions (table 4.9) show high CO conversion (72.3 %) and C yield (39.6 %) at thermodynamic equilibrium by the method of direct minimization of Gibbs free energy. However, the overall experimental results suggests a much lower CO conversion (35.7 %) and C yield (12.3 %) obtainable by feeding industrial conditions in CVD-setup for the production of CNFs using magnetite catalyst. Hence suggesting the experiments are performed at conditions that are far from the thermodynamic equilibrium. Moreover, the WHSV was decreased (higher catalyst loading) in order to approach the thermodynamic equilibrium conversion of CO in the process. A slight increase in CO conversion was observed, however the grams of carbon produced per grams of catalyst loaded decreased, suggesting that the thermodynamic equilibrium was reached for the system.

The experimental results do exhibit a positive trend on the CO conversion by decreasing CO<sub>2</sub>/CO ratio and increasing H<sub>2</sub>/CO ratio, similarly to the simulation results, suggesting that it might be favourable to reduce the CO<sub>2</sub> partial pressure in the industrial conditions prior to production of C in the CVD-setup. However, no increase in C yield was observed when increasing H<sub>2</sub>/CO ratio, suggesting other reactions might be occurring enhancing the CO conversion.



According to the thermodynamic equilibrium analysis performed in Aspen Plus, decreasing reaction temperature should enhance both CO conversion and C yield. Researching the reaction temperature in the CVD-setup for the industrial condition did not exhibit the same trend; lower reaction temperature gave a higher CO conversion and C yield for the commercial catalyst, however, the homemade catalyst exhibited an increase in CO conversion and C yield from  $T=575^{\circ}\text{C}$  to  $T=600^{\circ}\text{C}$ . The main findings comparing the Aspen Plus analysis and experimental results indicates that decreasing the partial pressure of  $\text{CO}_2$ , increasing the partial pressure of  $\text{H}_2$  in the industrial condition, whilst keeping a process temperature around  $600^{\circ}\text{C}$  would favour CO conversion and C yield in the process.

## 4.3 Characterization

### 4.3.1 X-Ray Diffraction

X-ray diffraction characterization is performed to investigate structure of the carbon filaments from 4 different samples. The samples investigated, here labeled homemade, homemade 0.5CO<sub>2</sub>, commercial and commercial 0.5 CO<sub>2</sub> corresponding to experiments 2, 7, 12 and 13 in table 3.1. The conditions for each sample are repeated in table 4.13. The XRD patterns for all 4 samples are presented in figure 4.11.

Table 4.13: XRD sample names and feed conditions.

Sample name	Cond.	PCO	PCO <sub>2</sub>	PH <sub>2</sub>	PN <sub>2</sub>	CO <sub>2</sub> /CO
<i>Homemade</i>	1 <sub>IND</sub>	0.620	0.240	0.085	0.055	0.387
<i>Commercial</i>						
<i>Homemade0.5CO<sub>2</sub></i>	2	0.690	0.130	0.010	0.08	0.188
<i>Commercial0.5CO<sub>2</sub></i>	3	0.620	0.120	0.085	0.055	0.194

Three peaks was observed in the XRD analysis for all four samples at  $2\theta = 25^\circ$ ,  $2\theta = 45^\circ$  and  $2\theta = 54.5^\circ$ . Using the diffrac.Eva V5 tool for analysis of the XRD signals gave 92% match with carbon (graphite). The (0 0 2) diffraction peak of the CNF was clear, whatever the type of catalyst and CO<sub>2</sub> partial pressure in feed gas mixture used for the synthesis. This indicates that the CNFs were highly graphitized. The (0 0 4) diffraction peak was also visible at  $2\theta = 54.5^\circ$ , corresponding to perfect graphened layers. No signals of iron carbide or iron oxide are observed, in agreement with Jiao et al. [39]. The Scherrer equation was used to estimate the crysallite size for the peak at  $2\theta = 25^\circ$ , the results can be seen in table 4.14.

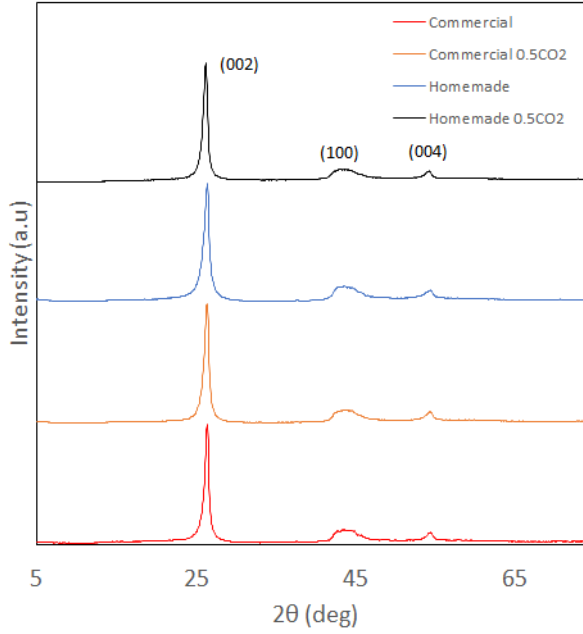


Figure 4.11: XRD graph

Table 4.14: Size estimation by Scherrer equation.

Sample	$2\theta(^{\circ})$	FWHM	nm
Homemade	26.437	0.803	10.61
Commercial	26.433	0.632	13.48
Homemade 0.5CO2	26.246	0.681	12.51
Commercial 0.5CO2	26.390	0.715	11.91

The crystallite sizes of the samples varied from 10.61 to 13.48 nm, with the biggest size found for the commercial catalyst at industrial conditions (table 4.14), while the sample where homemade catalyst was applied at the same feed conditions gave the smallest crystallite size. Thus, the crystallite sizes for the samples varied depending on the catalyst applied in the synthesis. Furthermore, the crystallite sizes varied based on the  $\text{CO}_2/\text{CO}$  ratio in the feed. A plot of crystallite size as a function of  $\text{CO}_2/\text{CO}$  ratio is presented in figure 4.12.

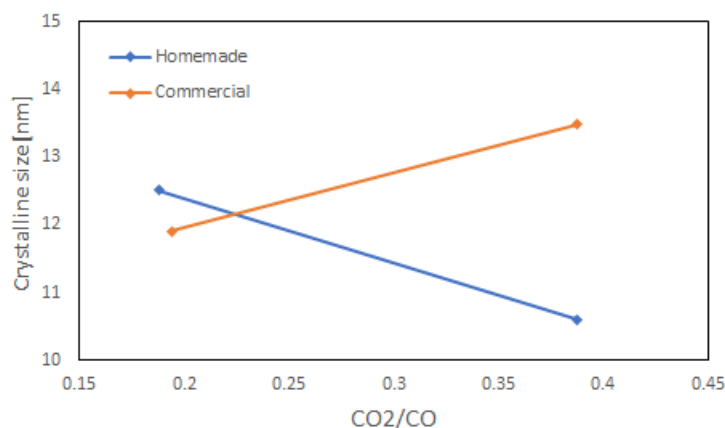


Figure 4.12: Crystalline size of homemade and commercial catalyst at various  $\text{CO}_2/\text{CO}$  ratios.

The samples catalyzed by the homemade catalyst exhibit decreasing crystallite size with increasing  $\text{CO}_2/\text{CO}$  ratio. The opposite trend is observed for the commercial catalyst. Overall, the crystallite size distribution for the four samples, ranging from 10.61 to 13.48nm, is quite narrow, portraying only small variations. The results suggest formation of very small carbon filaments.

### 4.3.2 Raman spectroscopy

Further information about the crystallinity of the carbon filaments was obtained from Raman investigation. Figure 4.13 displays typical Raman spectrum for 4 different samples (sample information in table 4.13), characterized by two main peaks centered at  $1329\text{cm}^{-1}$  (D band) and  $1583\text{cm}^{-1}$  (G band).

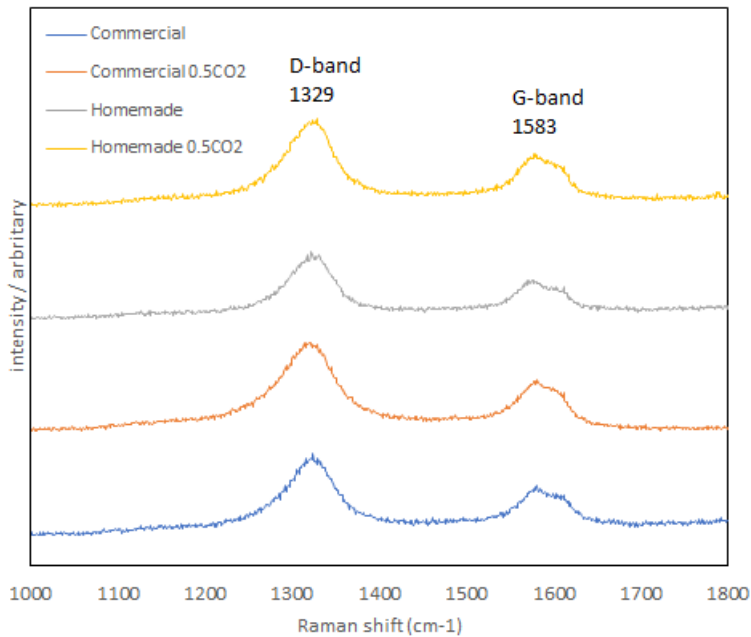


Figure 4.13: Raman plots

According to Nemanich et al. the G band is associated with the  $E_{2g}$  mode (stretching vibrations) in the basal-plane of graphite, while the origin of the D band is described as disorder-induced features exhibited by the finite particle size effect, amorphous carbon or lattice distortion background signals [58]. The positions of both G and D band fits well with Carbon-encapsulated Fe nanoparticles studied and produced by Lu et al. [51]. Typically, the position of the D-band associated with nanocrystalline carbon are  $\approx 1350\text{cm}^{-1}$

but is known to vary strongly with the laser excitation wavelength, which might be an explanation to the lower frequency value for the D-band for these samples.

The ratio ( $I_D/I_G$ ) of the D band intensity to the G band intensity is inversely proportional to crystallite dimension. The bond intensities and  $I_D/I_G$  ratios for all samples are given in table 4.15. The ( $I_D/I_G$ ) ratios as a function of  $CO_2$  in the feed gas mixture of the synthesis is given in figure 4.14.

Table 4.15: D-bond and G-bond intensity and  $I_D/I_G$  ratio for Raman samples.

Sample	$I_D$	$I_G$	$I_D/I_G$
Homemade	406	286	1.42
Commercial	483	342	1.41
Homemade 0.5CO2	462	317	1.46
Commercial 0.5CO2	520	346	1.50

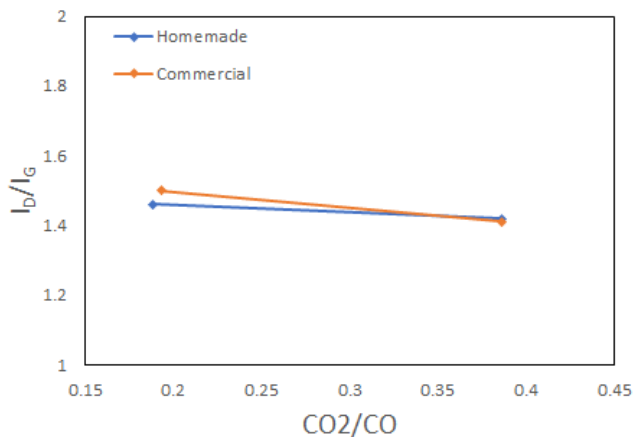


Figure 4.14: Intensity ratio  $I_D/I_G$  versus  $CO_2/CO$  ratio.

Since the  $I_D/I_G$  ratio is inversely proportional to the crystallite dimension, meaning higher ratios indicate smaller dimensions, these results contradicts the findings in the XRD analysis, as they suggests that the sample prepared at industrial conditions catalyzed by the commercial catalyst is smallest in crystallite dimension (table 4.15). Furthermore, increasing  $CO_2/CO$  ratio exhibits a increase in  $I_D/I_G$  for both catalysts, suggesting that the crystallite dimension increases with increasing  $CO_2/CO$  ratio. In the XRD analysis the same trend was evident for the commercial catalyst at various  $CO_2/CO$  ratios, but not for the homemade catalyst. Overall, it seems to be very small variations in the crystallite dimensions of the graphite structures for the four samples, which corresponds well with the XRD analysis results. According to F. Tuinstra and J. L.Koeng, which has correlated the  $I_D/I_D$  ratio to crystallite size for carbon, the ratios presented in figure 4.14 suggests crystalline dimensions of small nanofibers [89], in agreement with the XRD data.

## 4.4 Case study

In order to investigate the viability and emission reducing potential by adding a carbon-loop to a metallurgical process, a case study was performed. The 2006 IPCC Guidelines outline several approaches for calculating CO<sub>2</sub> emissions from ferroalloy production [11]. For practical purposes, this chapter adopts a mass balance approach where all CO emitted is reported as emitted CO<sub>2</sub>. In other words, it is assumed that the  $\text{ton}_{\text{CO}_2}/\text{ton}_{\text{metal}}$  reported by Eramet to equal 1.47 in 2019 [60] can be directly associated to the sum of CO and CO<sub>2</sub> (in tonnes) produced in the industrial condition feed composition (condition 1<sub>IND</sub> in table 4.13) for each ton metal produced. Moreover, the effect of less CO<sub>2</sub> in the feed, in other words; removal of some CO<sub>2</sub> prior to the Boudouard reaction, was investigated (condition 3 in table 4.13). A schematic representation of the process is given in figure 4.15.

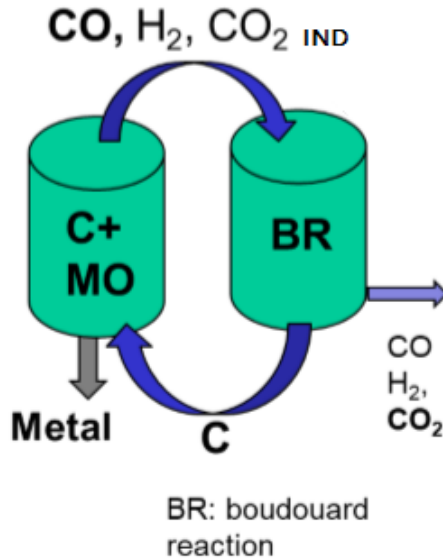


Figure 4.15: Schematic representation of the carbon-loop



Furthermore, for ferroalloys, CO<sub>2</sub> is the primary greenhouse gas, whereas CH<sub>4</sub> and N<sub>2</sub>O are only a few percent of the CO<sub>2</sub>-equivalents emitted [11]. Thus, considering the quantification of CH<sub>4</sub> was problematic due to the detection limit in the GC for the experimental results and, for sake of simplicity, it is assumed the emissions related to CH<sub>4</sub> and N<sub>2</sub> present are negligible. A summary of the key figures for both industrial condition and (0.5x CO<sub>2</sub>) condition is presented in table 4.16. Note that subscript m represents metal (produced).

Table 4.16: Normalized mass fraction and ton of species i per ton of metal produced in and out of the Gibbs reactor (Aspen) and CVD reactor setup (Exp.).

Comp.	In		Out Aspen		Out Exp.	
	mass fraction	ton <sub>i</sub> /ton <sub>m</sub>	mass fraction	ton <sub>i</sub> /ton <sub>m</sub>	mass fraction	ton <sub>i</sub> /ton <sub>m</sub>
IND						
CO	0.622	0.914	0.172	0.253	0.447	0.657
CO <sub>2</sub>	0.378	0.556	0.719	1.058	0.516	0.759
C	0.000	0.000	0.108	0.159	0.037	0.054
Total	1	1.47	1	1.47	1	1.47
Half CO2						
CO	0.767	1.127	0.185	0.271	0.450	0.661
CO <sub>2</sub>	0.233	0.343	0.676	0.994	0.496	0.729
C	0.000	0.000	0.139	0.205	0.055	0.080
Total	1	1.47	1	1.47	1	1.47

The tabulated values for  $\text{ton}_i/\text{ton}_M$  is calculated according to equation 4.11 and 4.12.

$$\dot{m}_{\text{in}} = \dot{m}_{\text{out}} \quad (4.11)$$

$$\frac{\text{ton}_i}{\text{ton}_M} = m_{\text{frac},i} \cdot \frac{\text{ton}_{\text{ovengas}}}{\text{ton}_M} \quad (4.12)$$

Note that the mass fractions are normalized mass fractions obtained from the Aspen Plus<sup>TM</sup> and experimental results for the two feed conditions on the basis of CO and CO<sub>2</sub> being the only species present. The mass flow of C was found by gravimetric measurement of the total carbon produced and dividing by the synthesis time. Whereas the mass flows of CO and CO<sub>2</sub> obtained experimentally was calculated using the ideal gas law, see equation 4.13.

$$\dot{m}_i = \frac{P \cdot \dot{V}_i}{R \cdot T} \cdot M m_i \quad (4.13)$$

Where  $\dot{V}$  (calculated based on internal standard calculation from GC results, as described in Appendix C) is volumetric flow in [ml/min], P is pressure in [atm], [R] is the gas constant in [ml·atm/K·mol] and T is the temperature in [K]. A calculation example is given in Appendix E.

The percentage reduction of total CO<sub>2</sub> emissions by implementation of the carbon-loop can now be estimated by the following equation;

$$\% \text{ red. CO}_2 \text{ emissions} = \frac{\frac{\text{ton}_{\text{CO}_2}}{\text{ton}_M} - \frac{\text{ton}_{\text{CO}_2 + \text{CO}_{\text{IND}}}}{\text{ton}_M}}{\frac{\text{ton}_{\text{CO}_2}}{\text{ton}_M}} \cdot 100\% \quad (4.14)$$

Where the  $\text{ton}_{\text{CO}_2 + \text{CO}_{\text{IND}}}/\text{ton}_M$  is the sum of  $\text{ton}_{\text{CO}_2}/\text{ton}_M$  and  $\text{ton}_{\text{CO}}/\text{ton}_M$  after implementation of the carbon-loop, and  $\text{ton}_{\text{CO}_2}/\text{ton}_M$  is the reported number by Eramet (1.47)[60]. Furthermore, the potential reduction in. required fresh reducing agent can be calculated using equation 4.15. Here, the  $\text{ton}_{\text{red.agent}}/\text{ton}_M$  is given by Eramet to equal 0.734 [60], and  $\text{ton}_{\text{C,produced}}/\text{ton}_M$  is the tonnes of C produced in the Boudouard reaction unit in figure 4.15. The results of equations 4.14 and 4.15 for both Aspen and experimental are presented in table 4.17.

$$\% \text{ red. in required C} = 100 - \frac{\frac{\text{ton}_{\text{red.agent}}}{\text{ton}_M} - \frac{\text{ton}_{\text{C,produced}}}{\text{ton}_M}}{\frac{\text{ton}_{\text{red.agent}}}{\text{ton}_M}} \cdot 100\% \quad (4.15)$$

Table 4.17: Percentage CO<sub>2</sub> and C reduction potential.

Case	IND		Half CO2	
	Aspen	Exp.	Aspen	Exp
CO <sub>2</sub> red. potential [%]	10.8	3.7	13.9	5.5
C red. potential [%]	21.7	7.3	27.9	11.0

According to the calculations, the potential reduction of CO<sub>2</sub> emissions by feeding the industrial condition is 3.7% from the experimental results and 10.8% according to the simulation (thermodynamic equilibrium conditions). The CO<sub>2</sub> reduction potential increases somewhat (5.5% and 13.9%) by halving the P<sub>CO<sub>2</sub></sub> in the feed for experimental and Aspen results, respectively. Moreover, the potential reduction of required reducing agent, which will enhance the overall CO<sub>2</sub> reduction, was estimated to 7.3 and 21.7 % feeding the industrial condition. By halving the partial pressure of CO<sub>2</sub> prior to the Boudouard unit the potential reduction in required reducing agent increased to 11.0 and 27.9%. It is evident in both cases that the thermodynamic equilibrium conditions estimated by Aspen Plus shows much greater potential than what was measured experimentally. However, the overall experimental results suggests, for both conditions, that the carbon-looping would decrease the overall CO<sub>2</sub> emissions. It should be mentioned that inaccuracies are present in the presented case study results. More precise estimations could have been carried out if the process, in its entirety, had been designed in a simulation tool. Unfortunately, Aspen Plus<sup>TM</sup> is not equipped to handle carbothermal processes as it lacks furnace models that fits such operations.

#### 4.4.1 Challenges and opportunities in implementing the carbon-loop

Many challenges regarding implementation of the novel carbon-looping idea have been observed throughout this project; 1) enhancing the conversion of CO and yield of C has proven to be a challenge, resulting in lower CO<sub>2</sub> reducing potential than anticipated; 2) estimating and decreasing the overall inaccuracies in the experimental results, hence evaluating the reproducibility and reliability of the presented data; 3) concluding whether or not the carbon formed in the CVD-setup is fit to use as reducing agent in the metallurgical industries, due to minimal characterization and; 4) assessing the challenges regarding process design (moving the produced carbon to the carbothermal reduction process, without too much product loss) and overall cost effectiveness. However, the presented data suggest a potential of reducing the overall CO<sub>2</sub> emissions for the metallurgical industries by implementation of the novel carbon-looping idea, especially by tuning the feed gas mixture (lowering the partial pressure of CO<sub>2</sub> and possibly increasing the partial pressure of H<sub>2</sub>). Moreover, if the carbon produced can be used as reducing agent, the decrease in the need for fresh reducing agent would further decrease the CO<sub>2</sub> emissions. As mentioned in section 2.2, the reducing agents used in various metallurgical industries has different requirements in order to achieve stable operation. Therefore, carbon produced by CVD using various feed gas mixtures of CO, CO<sub>2</sub> and H<sub>2</sub> should be further characterized in order to imply their potential use in the various processes. However, if further characterizations should result in the carbon produced not being fit to use as reducing agent, it might still be a profitable product as CNFs has chemical and physical properties making them interesting in many other applications (section 2.5.1).

# Chapter 5

## Conclusion

This research aimed to identify the possibility of reducing CO<sub>2</sub> emissions in the metallurgical industries by implementation of a novel carbon-loop; using the CO-rich oven gas from the metallurgical industry to produce C and CO<sub>2</sub> through the Boudouard reaction and the possibility of applying the produced carbon as reducing agent in the carbothermal reduction process, further decreasing CO<sub>2</sub> emissions. Overall, the results presented has suggested that there is potential of reducing the ton CO<sub>2</sub> emissions per ton metal produced in the FeMn process by 3.7 and 10.8 % by experiments and Aspen Plus, respectively. Moreover, by halving the P<sub>CO2</sub> in the feed the potential CO<sub>2</sub> reduction increased to 5.5 and 13.9 %.

The thermodynamic equilibrium product distribution investigations performed in an RGibbs reactor model in Apen Plus™ demonstrated that high C yield and CO conversion could be obtained feeding industrial condition. Moreover, the research showed that decreasing P<sub>CO2</sub> and increasing P<sub>H2</sub> in the feed as well as decreasing the temperature enhanced the C yield and CO conversion. The

highest yield was obtained by feeding the industrial condition zeroing the  $P_{\text{CO}_2}$  and applying a  $\text{H}_2/\text{CO}$  ratio  $\approx 1$  at  $500^\circ\text{C}$ ; resulting in C yield above 60 % and CO conversion above 90 %.

Comparison of the Aspen plus<sup>TM</sup> results with the experimental results obtained (feeding industrial condition gas mixture to a CVD-setup for production of CNFs in the presence of magnetite catalyst) suggested the experimental system was far from the thermodynamic equilibrium condition. However, researching the product distribution by lowering the WHSV suggested the system might be close to thermodynamic equilibrium conditions as the CO conversion did not change much. Furthermore, the investigations on the effect of  $\text{CO}_2$  and  $\text{H}_2$  in the feed composition showed, similar to the Aspen Plus<sup>TM</sup> results, that decreasing  $P_{\text{CO}_2}$  and increasing  $P_{\text{H}_2}$  in the feed enhanced the CO conversion. However, increasing the  $P_{\text{H}_2}$  did not enhance the C yield, suggesting other reactions, such as methanation and RWGS, might be affecting the product distribution. The temperature effect on the product distribution for the homemade and commercial catalyst showed highest CO conversion and C yield obtainable at temperatures around  $600^\circ\text{C}$ . The highest C yield (23.7 %) was found by zeroing the partial pressure of  $\text{CO}_2$  in the feed, keeping a reaction temperature =  $600^\circ\text{C}$ .

Finally, the characterization of the produced carbon by XRD and Raman spectroscopy showed that carbon with very small crystallite dimensions were produced. As presented in the literature review (section 2.5.1), CNFs have chemical and physical properties making them interesting for application as carbothermal reducing agents. The potential reduction of ton fresh reducing agent per ton metal produced was estimated for the industrial condition to 7.3 and 21.7 % by experiments and Aspen Plus<sup>TM</sup> respectively. Lowering the partial pressure of  $\text{CO}_2$  in the feed further enhanced it to

11.0 and 27.9 %.



# Chapter 6

## Future work

The topic of reducing the CO<sub>2</sub> emissions from the metallurgical industries attracts much attention, and the research effort on finding efficient and cost-effective solutions will continue to increase. Much research is necessary in order to estimate the viability of the novel carbon-looping idea. Some selected alleyways that should be pursued are:

- Further research on the possibility of using CVD produced carbon nanofiber as reducing agent in the metallurgical industry by further characterization of the carbon product (for example by S(T)EM analysis) to determine the carbon structure. This will open the possibility of comparing the properties and structure of CVD-produced CNFs with the characteristics of typical reducing agents.
- Evaluation of the economic viability by performing detailed process design and cost evaluation of the process. Preferably, this should be done in a precise simulation tool with models prepared to handle carbothermal processes. Further understanding on the CO<sub>2</sub> reduction potential can be achieved by careful process design.
- Assessing the recyclability of the produced carbon nanofibers by researching various reactor and process configurations for continuous gas/solid separation.
- Considering the proposed carbon-loop is a closed loop, the buildup or

complete consumption of components, for example  $H_2$ , should be explored using simulation tools fitted for carbothermal process simulation.

# Bibliography

- [1] T.-S. - et al. *Ironworks - tec-science*. Oct. 2019. URL: <https://www.tec-science.com/material-science/steel-making/iron-works/>.
- [2] M. Arens et al. “Pathways to a low-carbon iron and steel industry in the medium-term – the case of Germany”. In: *Journal of Cleaner Production* (2017). ISSN: 09596526. DOI: 10.1016/j.jclepro.2015.12.097.
- [3] I. Aspen Technology. *Aspen Plus user guide*. Tech. rep. <https://www.aspentech.com/en/products/engineering/aspen-plus>, 2000.
- [4] W. S. Association et al. “Steel’s contribution to a low carbon future and climate resilient societies”. In: *Worldsteel Climate Change Position Paper*. 2017.
- [5] R. T. K. Baker. “Catalytic growth of carbon filaments”. In: *Carbon* 27.3 (1989), pp. 315–323. DOI: [https://doi.org/10.1016/0008-6223\(89\)90062-6](https://doi.org/10.1016/0008-6223(89)90062-6). URL: <http://www.sciencedirect.com/science/article/pii/0008622389900626%20https://pdf.sciencedirectassets.com/271508/1-s2.0-S0008622300X01169/1-s2.0-0008622389900626/main.pdf?X-Amz-Security-Token=IQoJb3JpZ2luX2%20VjEH4aCXVzLWVhc3QtMSJHMEUCIQD8wRuzMze%2Brrpo9HJhUC1pz>.
- [6] E. Balomenos, D. Pantias, and I. Paspaliaris. “Energy and ex-ergy analysis of the primary aluminum production processes:

- a review on current and future sustainability”. In: *Mineral Processing & Extractive Metallurgy Review* 32.2 (2011), pp. 69–89. ISSN: 0882-7508.
- [7] E. Balomenos et al. “ENEXAL: Novel technologies for enhanced energy and exergy efficiencies in primary aluminium production industry”. In: *Association of Metallurgical Engineers of Serbia* (2009). DOI: 669.71.056.
- [8] C. A. Bessel et al. “Graphite nanofibers as an electrode for fuel cell applications”. In: *Journal of Physical Chemistry B* (2001). ISSN: 15206106. DOI: 10.1021/jp003280d.
- [9] J. M. Burgess. “Fuel combustion in the blast furnace raceway zone”. In: *Progress in Energy and Combustion Science* (1985). ISSN: 03601285. DOI: 10.1016/0360-1285(85)90013-9.
- [10] J.-O. Carlsson and P. M. Martin. “Chapter 7 - Chemical Vapor Deposition”. In: *Handbook of Deposition Technologies for Films and Coatings (Third Edition)*. Ed. by P. M. Martin. Boston: William Andrew Publishing, 2010, pp. 314–363. ISBN: 978-0-8155-2031-3. DOI: <https://doi.org/10.1016/B978-0-8155-2031-3.00007-7>. URL: <http://www.sciencedirect.com/science/article/pii/B9780815520313000077>.
- [11] I. P. O. C. Change. “2006 IPCC guidelines for national greenhouse gas inventories”. In: *Institute for Global Environmental Strategies, Hayama, Kanagawa, Japan* (2006).
- [12] W.-H. Chen et al. “An evaluation of hydrogen production from the perspective of using blast furnace gas and coke oven gas as feedstocks”. In: *International Journal of Hydrogen Energy* 36.18 (2011), pp. 11727–11737. DOI: 10.1016/j.ijhydene.2011.06.049.

- [13] Z. Chen et al. “A Study of the Performance of Submerged Arc Furnace Smelting of Industrial Silicon”. In: *Silicon* (2018). ISSN: 18769918. DOI: 10.1007/s12633-017-9584-3.
- [14] Z. Chen et al. “Effect of raw materials on the production process of the silicon furnace”. In: *Journal of Cleaner Production* (2017). ISSN: 09596526. DOI: 10.1016/j.jclepro.2017.05.037.
- [15] V. V. Chesnokov and R. A. Buyanov. “The formation of carbon filaments upon decomposition of hydrocarbons catalysed by iron group metals and their alloys”. In: *Uspekhi Khimii* (2000). ISSN: 00421308. DOI: 10.1070/rc2000v069n07abeh000540.
- [16] R. Conceição Nascimento, M. Breda Movrão, and J. D. Trani Capocchi. “Reduction-swelling behaviour of pellets bearing iron ore and charcoal”. In: *Canadian metallurgical quarterly* 37.5 (1998), pp. 441–448. ISSN: 0008-4433.
- [17] J. C. Crelling. “Chapter 7 - Coal Carbonization”. In: ed. by I. Suárez-Ruiz and J. C. B. T. .-. A. C. P. Crelling. Burlington: Elsevier, 2008, pp. 173–192. ISBN: 978-0-08-045051-3. DOI: <https://doi.org/10.1016/B978-0-08-045051-3.00007-5>. URL: <http://www.sciencedirect.com/science/article/pii/B9780080450513000075>.
- [18] A. De Waal et al. “Electrical factors affecting the economic optimization of submerged-arc furnaces”. In: *INFACON 6* (1992), pp. 247–252.
- [19] R. Degel et al. “History and new milestones in submerged arc furnace technology for ferro alloy and silicon production”. In: *Proceedings of the Fourteenth International Ferro-Alloys Congress INFACON XIV*. 2015, pp. 7–16.
- [20] A. Demirbas et al. “Sustainable charcoal production from biomass”. In: *Energy Sources, Part A: Recovery, Utilization, and Environmental Effects* 38.13 (2016), pp. 1882–1889.

- [21] M. Díez, R. Alvarez, and C. Barriocanal. “Coal for metallurgical coke production: predictions of coke quality and future requirements for cokemaking”. In: *International Journal of Coal Geology* 50.1-4 (2002), pp. 389–412.
- [22] H. Ebrahimi and M. Rahmani. “A new design for CO<sub>2</sub> capture and usage in a syngas production unit by carbonate chemical looping”. In: *Journal of Natural Gas Science and Engineering* 36 (2016), pp. 241–251. DOI: <https://doi.org/10.1016/j.jngse.2016.10.007>. URL: <http://www.sciencedirect.com/science/article/pii/S187551001630717X>.
- [23] M. Endo and H. Kroto. “Formation of carbon nanofibers”. In: *The Journal of Physical Chemistry* 96.17 (1992), pp. 6941–6944.
- [24] Eramet. *Energy: our actions to cut our CO<sub>2</sub> emissions*. URL: <https://www.eramet.com/en/csr/environment/energy>.
- [25] *Eramet Norway Kvinesdal*. URL: <https://eramet.no/en/our-organization/kvinesdal/>.
- [26] B. D. Flores et al. “Effect of charcoal blending with a vitrinite rich coking coal on coke reactivity”. In: *Fuel Processing Technology* (2017). ISSN: 03783820. DOI: 10.1016/j.fuproc.2016.04.012.
- [27] N. Florin and P. Fennell. “Synthetic CaO-based sorbent for CO<sub>2</sub> capture”. In: *Energy Procedia* 4 (2011), pp. 830–838. DOI: <https://doi.org/10.1016/j.egypro.2011.01.126>. URL: <http://www.sciencedirect.com/science/article/pii/S1876610211001287>.
- [28] M. Geerdes, R. Chaigneau, and I. Kurunov. *Modern blast furnace ironmaking: an introduction (2015)*. Ios Press, 2015.
- [29] S. S. Gornostayev et al. “Textural changes in metallurgical coke prepared with polyethylene”. In: *International Journal*

- of Minerals, Metallurgy and Materials* (2014). ISSN: 1869103X. DOI: 10.1007/s12613-014-0997-3.
- [30] K. He and L. Wang. *A review of energy use and energy-efficient technologies for the iron and steel industry*. 2017. DOI: 10.1016/j.rser.2016.12.007.
- [31] M. Helle and H. Saxén. “Simulation of tuyere-raceway system in blast furnace”. In: *Ironmaking and Steelmaking* (2006). ISSN: 03019233. DOI: 10.1179/174328006X102592.
- [32] C. HU et al. “Comparison of CO<sub>2</sub> emission between COREX and blast furnace iron-making system”. In: *Journal of Environmental Sciences* (2009). ISSN: 10010742. DOI: 10.1016/S1001-0742(09)60052-8.
- [33] J. Hunt et al. “Microwave-Specific Enhancement of the Carbon–Carbon Dioxide (Boudouard) Reaction”. In: *The Journal of Physical Chemistry C* 117.51 (2013), pp. 26871–26880. DOI: 10.1021/jp4076965. URL: <https://doi.org/10.1021/jp4076965>. URL: <https://pubs.acs.org/doi/pdf/10.1021/jp4076965>.
- [34] S. Iijima. “Helical microtubules of graphitic carbon”. In: *Nature* 354.6348 (1991), pp. 56–58. DOI: 10.1038/354056a0. URL: <https://doi.org/10.1038/354056a0>.
- [35] S. Iijima and T. Ichihashi. “Single-shell carbon nanotubes of 1-nm diameter”. In: *Nature* 363.6430 (1993), pp. 603–605. DOI: 10.1038/363603a0. URL: <https://doi.org/10.1038/363603a0>.
- [36] D.-A. Iluțiu-Varvara et al. “An Assessment of Pollution with Volatile Organic Compounds in the Electric Arc Furnaces”. In: *Procedia Technology* (2016). ISSN: 22120173. DOI: 10.1016/j.protcy.2016.01.086.

- [37] M. Inagaki. “Advanced Carbon Materials”. In: *Handbook of Advanced Ceramics*. 2013, pp. 25–60. ISBN: 9780123854698. DOI: 10.1016/b978-0-12-385469-8.00002-2.
- [38] C. K. Jayarathna et al. “Aspen Plus® Process Simulation of Calcium Looping with Different Indirect Calciner Heat Transfer Concepts”. In: *Energy Procedia* 114 (2017), pp. 201–210. DOI: <https://doi.org/10.1016/j.egypro.2017.03.1162>. URL: <http://www.sciencedirect.com/science/article/pii/S1876610217313358>.
- [39] J. Jiao et al. “Preparation and properties of ferromagnetic carbon-coated Fe, Co, and Ni nanoparticles”. In: *Journal of Applied Physics* 80.1 (1996), pp. 103–108. ISSN: 00218979. DOI: 10.1063/1.362765.
- [40] R. T. Jones. “DC ARC furnaces - Past, present, and future”. In: *TMS Annual Meeting*. 2014. ISBN: 9781118889619. DOI: 10.1002/9781118889657.ch10.
- [41] S. Kamalpour and W. J. Rankin. “The Behaviour of coke in submerged arc furnace smelting of ferromanganese”. In: *Proceedings: Tenth International Ferroalloys Congress*. Vol. 1. 2004, p. 4.
- [42] Y. S. Kang et al. “Synthesis and Characterization of Nanometer-Size Fe<sub>3</sub>O<sub>4</sub> and  $\gamma$ -Fe<sub>2</sub>O<sub>3</sub> Particles”. In: *Chemistry of Materials* 8.9 (1996), pp. 2209–2211. DOI: 10.1021/cm960157j. URL: <https://doi.org/10.1021/cm960157j%20https://pubs.acs.org/doi/pdf/10.1021/cm960157j>.
- [43] *Klimagassutslipp fra industri*. June 2020. URL: <https://miljostatus.miljodirektoratet.no/tema/klima/norske-utslipp-av-klimagasser/klimagassutslipp-fra-industri/>.
- [44] L. Kong et al. “Conversion of recycled sawdust into high HHV and low NO<sub>x</sub> emission bio-char pellets using lignin and



- calcium hydroxide blended binders”. In: *Renewable energy* 60 (2013), pp. 559–565.
- [45] H. W. Kroto et al. “C60: Buckminsterfullerene”. In: *Nature* 318.6042 (1985), pp. 162–163. DOI: 10.1038/318162a0. URL: <https://doi.org/10.1038/318162a0>.
- [46] J. Kunze Degel R. “New Trends in Submerged Arc Furnace Technology”. In: *Tenth International Ferroalloys Congress; INFACON X: 'Transformation through Technology'*. 2004. ISBN: 0958466351.
- [47] T. Kuramochi. “Assessment of midterm CO<sub>2</sub> emissions reduction potential in the iron and steel industry: a case of Japan”. In: *Journal of Cleaner Production* (2016). ISSN: 09596526. DOI: 10.1016/j.jclepro.2015.02.055.
- [48] X. Li. “Effects of gas atmosphere on reduction of quartz and its reaction with silicon carbide for silicon production”. In: (2016).
- [49] T. Lindstad, B. Monsen, and K. Osen. “How the ferroalloy industry can meet greenhouse gas regulations”. In: *INFACON XII* (2010).
- [50] K. Lozano and E. V. Barrera. “Nanofiber-reinforced thermoplastic composites. I. Thermoanalytical and mechanical analyses”. In: *Journal of Applied Polymer Science* (2001). ISSN: 00218995. DOI: 10.1002/1097-4628(20010103)79:1<125::AID-APP150>3.0.CO;2-D.
- [51] Y. Lu, Z. Zhu, and Z. Liu. “Carbon-encapsulated Fe nanoparticles from detonation-induced pyrolysis of ferrocene”. In: *Carbon* 43.2 (2005), pp. 369–374. ISSN: 0008-6223. DOI: <https://doi.org/10.1016/j.carbon.2004.09.020>. URL: <http://www.sciencedirect.com/science/article/pii/S0008622304005688>.

- [52] A. D. Lueking et al. “Hydrogen storage in graphite nanofibers: Effect of synthesis catalyst and pretreatment conditions”. In: *Langmuir* (2004). ISSN: 07437463. DOI: 10.1021/1a0349875.
- [53] D. Lupu et al. “Hydrogen uptake by carbon nanofibers catalyzed by palladium”. In: *International Journal of Hydrogen Energy* (2004). ISSN: 03603199. DOI: 10.1016/S0360-3199(03)00055-7.
- [54] J. A. MacPhee et al. “Possible CO<sub>2</sub> mitigation via addition of charcoal to coking coal blends”. In: *Fuel Processing Technology* (2009). ISSN: 03783820. DOI: 10.1016/j.fuproc.2008.07.007.
- [55] J. G. Mathieson et al. “Use of biomass in the iron and steel industry—an Australian perspective”. In: *EECR-METEC In-SteelCon* (2011).
- [56] A. Monshi, M. R. Foroughi, M. R. Monshi, et al. “Modified Scherrer equation to estimate more accurately nanocrystallite size using XRD”. In: *World journal of nano science and engineering* 2.3 (2012), pp. 154–160.
- [57] E. Mousa et al. *Biomass applications in iron and steel industry: An overview of challenges and opportunities*. 2016. DOI: 10.1016/j.rser.2016.07.061.
- [58] R. J. Nemanich and S. A. Solin. “First- and second-order Raman scattering from finite-size crystals of graphite”. In: *Physical Review B* (1979). ISSN: 01631829. DOI: 10.1103/PhysRevB.20.392.
- [59] T. E. Norgate, S. Jahanshahi, and W. J. Rankin. “Assessing the environmental impact of metal production processes”. In: *Journal of Cleaner Production* 15.8 (2007), pp. 838–848. DOI: <https://doi.org/10.1016/j.jclepro.2006.06.018>. URL: <http://www.sciencedirect.com/science/article/pii/S0959652606002320>.

- [60] E. Norway. *Eramet Bærekrafttrapport 2019*. 2020. URL: [https://issuu.com/erametnorway/docs/eramet\\_norsk\\_digital](https://issuu.com/erametnorway/docs/eramet_norsk_digital).
- [61] K. Nozawa et al. “Combustion behaviors of fine coal and its impact on gas permeability at lower part of blast furnace under high pulverized coal rate operation”. In: *ISIJ International* (2011). ISSN: 09151559. DOI: 10.2355/isijinternational.51.1336.
- [62] S. E. Olsen and M. Tangstad. “SILICOMANGANESE PRODUCTION  $\alpha$  PROCESS UNDERSTANDING”. In: (2004).
- [63] S. E. Olsen et al. “Equilibrium in Production of High Carbon Ferromanganese”. In: *at INFACON95 in Trondheim* (1995).
- [64] S. E. Olsen et al. *Production of manganese ferroalloys*. Tapir academic press, 2007. ISBN: 8251921910.
- [65] C. Pham-Huu et al. “Carbon nanofiber supported palladium catalyst for liquid-phase reactions an active and selective catalyst for hydrogenation of cinnamaldehyde into hydrocinnamaldehyde”. In: *Journal of Molecular Catalysis A: Chemical* (2001). ISSN: 13811169. DOI: 10.1016/S1381-1169(01)00055-3.
- [66] J. Pires et al. “Recent developments on carbon capture and storage: an overview”. In: *Chemical engineering research and design* 89.9 (2011), pp. 1446–1460.
- [67] P. C. Pistorius. “Reductant selection in ferro-alloy production: The case for the importance of dissolution in the metal”. In: *Journal of The South African Institute of Mining and Metallurgy* (2002). ISSN: 0038223X.
- [68] Á. A. Ramírez-Santos, C. Castel, and E. Favre. “Utilization of blast furnace flue gas: Opportunities and challenges for polymeric membrane gas separation processes”. In: *Journal of Membrane Science* 526 (2017), pp. 191–204. ISSN: 0376-7388. DOI: <https://doi.org/10.1016/j.memsci.2016>.

- 12.033. URL: <http://www.sciencedirect.com/science/article/pii/S037673881631002X>.
- [69] R. Razaq, C. Li, and S. Zhang. “Coke oven gas: Availability, properties, purification, and utilization in China”. In: *Fuel* 113 (2013), pp. 287–299. DOI: <https://doi.org/10.1016/j.fuel.2013.05.070>. URL: <http://www.sciencedirect.com/science/article/pii/S0016236113004821>.
- [70] M. Ribbenhed, M. Thorén, and C. Sternhufvud. “CO<sub>2</sub> emission reduction costs for iron ore-based steelmaking in Sweden”. In: *Journal of Cleaner Production* (2008). ISSN: 09596526. DOI: [10.1016/j.jclepro.2006.11.007](https://doi.org/10.1016/j.jclepro.2006.11.007).
- [71] N. Rodriguez et al. “Heat requirements in a calciner of CaCO<sub>3</sub> integrated in a CO<sub>2</sub> capture system using CaO”. In: *Chemical Engineering Journal* 138.1-3 (2008), pp. 148–154.
- [72] K. R. Rout, M. V. Gil, and D. Chen. “Highly selective CO removal by sorption enhanced Boudouard reaction for hydrogen production”. In: *Catalysis Science & Technology* 9.15 (2019), pp. 4100–4107. DOI: [10.1039/C9CY00851A](https://doi.org/10.1039/C9CY00851A). URL: <http://dx.doi.org/10.1039/C9CY00851A> <https://pubs.rsc.org/en/content/articlepdf/2019/cy/c9cy00851a>.
- [73] V. Sahajwalla, M. Dubikova, and R. Khanna. “Reductant characterisation and selection: implications for ferroalloys processing”. In: *Proceedings: Tenth International Ferroalloys Congress*. Vol. 1. 2004, p. 4.
- [74] F. Salman, C. Park, and R. T. Baker. “Hydrogenation of crotonaldehyde over graphite nanofiber supported nickel”. In: *Catalysis Today* (1999). ISSN: 09205861. DOI: [10.1016/S0920-5861\(99\)00132-7](https://doi.org/10.1016/S0920-5861(99)00132-7).
- [75] A. Schei, J. K. Tuset, and H. Tveit. *Production of high silicon alloys*. Tapir Trondheim, Norway, 1998. ISBN: 8251913179.

- [76] F. E. Sesen. “Practical reduction of manganese oxide”. In: *Journal of Chemical Technology and Applications* (2017). DOI: 10.35841/chemical-technology.1.1.26-27.
- [77] S. Sharma. “Molecular level analysis of carbon nanofiber reinforced polymer composites”. In: *Journal of Composite Materials* 50 (2015). DOI: 10.1177/0021998315596591.
- [78] T. Shimizu et al. “A Twin Fluid-Bed Reactor for Removal of CO<sub>2</sub> from Combustion Processes”. In: *Chemical Engineering Research and Design* 77.1 (1999), pp. 62–68. DOI: <https://doi.org/10.1205/026387699525882>. URL: <http://www.sciencedirect.com/science/article/pii/S026387629971751X>.
- [79] J. W. Snoeck, G. F. Froment, and M. Fowles. “Steam/CO<sub>2</sub> Reforming of Methane. Carbon Filament Formation by the Boudouard Reaction and Gasification by CO<sub>2</sub>, by H<sub>2</sub>, and by Steam: Kinetic Study”. In: *Industrial & Engineering Chemistry Research* 41.17 (2002), pp. 4252–4265. DOI: 10.1021/ie010666h. URL: <https://doi.org/10.1021/ie010666h>.
- [80] C. Stewart and M.-A. Hessami. “A study of methods of carbon dioxide capture and sequestration—the sustainability of a photosynthetic bioreactor approach”. In: *Energy Conversion and Management* 46.3 (2005), pp. 403–420. ISSN: 0196-8904.
- [81] Y. Suda et al. “Growth of carbon nanofibers on metal-catalyzed substrates by pulsed laser ablation of graphite”. In: *Journal of Physics: Conference Series* 59 (2007), pp. 348–353. DOI: 10.1088/1742-6596/59/1/073. URL: <http://dx.doi.org/10.1088/1742-6596/59/1/073>.
- [82] K. Sun. “Optimization of biomass gasification reactor using Aspen Plus”. MA thesis. Høgskolen i Telemark, 2015.
- [83] H. Suopajarvi. “Bioreducer use in blast furnace ironmaking in Finland”. In: *Techno-economic assessment and CO<sub>2</sub> emis-*

- sion reduction potential. University of Oulu. University on Oulu graduate school. Faculty of technology. PDF-dokumentti. Saatavissa: <http://urn.fi/urn:isbn:9789526207063> [viitattu 23.4. 2018]* (2014).
- [84] H. Suopajarvi et al. "Effect of charcoal and Kraft-lignin addition on coke compression strength and reactivity". In: *Energies* 10.11 (2017), p. 1850.
- [85] G. R. Surup. *Renewable reducing agents for the use in ferroalloy industries*. 2019. ISBN: 9788271179380.
- [86] H. Takagi et al. "XRD analysis of carbon stacking structure in coal during heat treatment". In: *Fuel* 83.17 (2004), pp. 2427–2433. ISSN: 0016-2361. DOI: <https://doi.org/10.1016/j.fuel.2004.06.019>. URL: <http://www.sciencedirect.com/science/article/pii/S0016236104001851>.
- [87] D. S. Tang et al. "Evidence for an open-ended nanotube growth model in arc discharge". In: *Carbon* 38.3 (2000), pp. 480–483. DOI: [https://doi.org/10.1016/S0008-6223\(99\)00249-3](https://doi.org/10.1016/S0008-6223(99)00249-3). URL: <http://www.sciencedirect.com/science/article/pii/S0008622399002493%20https://pdf.science%20directassets.com/271508/1-s2.0-S0008622300X00565/1-s2.0-S0008622399002493/main.pdf?X-Amz-Security-Token=IQoJb3JpZ2luX2VjEAKaCXVzLWVhc3QtMSJHMEUCIE%2FJrCjv7Gae%2B28Jg5MaV>.
- [88] J. P. Tessonnier et al. "Pd nanoparticles introduced inside multi-walled carbon nanotubes for selective hydrogenation of cinnamaldehyde into hydrocinnamaldehyde". In: *Applied Catalysis A: General* (2005). ISSN: 0926860X. DOI: 10.1016/j.apcata.2005.04.034.
- [89] TUINSTRA F and KOENIG JL. "RAMAN SPECTRUM OF GRAPHITE". In: *Journal of Chemical Physics* (1970). ISSN: 00219606. DOI: 10.1063/1.1674108.

- [90] “Veikart for proessindustrien ”. In: (2016), pp. 1–100.
- [91] V. P. Vorob’ev, A. D. Golunov, and A. V. Ignat’ev. “Carbon reductants for the production of manganese ferroalloys”. In: *Russian Metallurgy (Metally)* (2009). ISSN: 00360295. DOI: 10.1134/S0036029509080163.
- [92] K. Weber and P. Quicker. “Properties of biochar”. In: *Fuel* 217 (2018), pp. 240–261.
- [93] H. C. Wilkinson. “The high temperature properties of coke. EUR 10430 EN. Technical coal research”. In: (1986).
- [94] Z. Yu. “Synthesis of Carbon Nanofibers and Carbon Nanotubes”. In: (2005). URL: <https://brage.bibsys.no/xmlui/handle/11250/248111>.
- [95] F. Zhang. *China carbon black prices surge on supply shortage*. ICIS.com, 2018. URL: <https://www.icis.com/explore/resources/news/2018/03/12/10201445/china-carbon-black-prices-surge-on-supply-shortage/>.
- [96] J.-H. Zhou et al. “Structural characterization of carbon nanofibers formed from different carbon-containing gases”. In: *Carbon* 44.15 (2006), pp. 3255–3262. ISSN: 0008-6223. DOI: <https://doi.org/10.1016/j.carbon.2006.06.028>. URL: <http://www.sciencedirect.com/science/article/pii/S0008622306003575>.
- [97] Y. A. Zhu et al. “Modeling of fishbone-type carbon nanofibers: A theoretical study”. In: *Carbon* 43.8 (2005), pp. 1694–1699. DOI: <https://doi.org/10.1016/j.carbon.2005.02.011>. URL: <http://www.sciencedirect.com/science/article/pii/S0008622305001028%20https://pdf.sciencedirectassets.com/271508/1-s2.0-S0008622305X03335/1-s2.0-S0008622305001028/main.pdf?X-Amz-Security-Token=IQoJb3JpZ2luX2VjEAQaCXVzLWVhc3QtMSJIMEYCIQCF3x69XK%20i45SNJK7tGiAR2d>.

- [98] H.-b. Zuo et al. “Direct reduction of iron ore by biomass char”. In: *International Journal of Minerals, Metallurgy, and Materials* 20.6 (2013), pp. 514–521. ISSN: 1674-4799.



# Appendix A

## Detailed experiment summary

# Carbon Looping for Metallurgical Processes via Boudouard reaction over Magnetite

## Summary of experiments

Experiment	Temp (C)	Catalyst	mcat (g)	WHSV(l/hr*gcat)	Description	
1	600	Homemade	0.1003	29.91	Standard	
2			0.1002	29.92	Half CO2	
3			0.1007	29.77	Double CO2	
4			0.1002	29.92	2X H2	
5			0.0997	30.07	4x H2	
6			0.1012	29.62	IND	
7			0.0999	30.01	IND	
8			800	0.1005	29.83	Temp
9			400	0.0999	30.01	
10			575	0.1003	29.89	
11			625	0.1001	29.95	
12	600	Commercial	0.1005	29.83	IND	
13			0.1006	29.80	Half CO2	
14			0.1004	29.86	1.5 xH2	
15			0.0868	34.53	No CO2	
16			0.3008	9.97	WHSV	
17			0.5019	5.97		
18			575	0.1006	29.80	Temp
19			625	0.1002	29.92	
20	650	0.1001	29.95			

Experiment	Time (hr)	C (g) - cat
1	48	18.6232
2		15.0614
3		1.1932
4		8.1346
5		6.7431
6		7.5788
7		5.9133
8		0
9		2.4029
10		5.6838
11		7.2162
12		8.6997
13		11.8217
14		6.6442
15		14.5533
16		10.9201
17		11.1506
18		8.9754
19		4.9392
20	4.9339	

Calculation example: WHSV for experiment 1:

$$\text{WHSV} = \text{Lco}/\text{gcat} \cdot \text{hr}$$

$$\begin{aligned} \text{WHSV (exp1)} &= \\ &= (50\text{ml}/\text{min} \cdot 60\text{min}/\text{hr}) / \\ &= (0,1003\text{g} \cdot 1000\text{ml}/\text{L}) = 29,91 \end{aligned}$$

# Carbon Looping for Metallurgical Processes via Boudouard reaction over Magnetite

---

Experiment 1		
Species	Mole frac	Flow (ml/min)
CO	80	50
H2	20	12.5

Species	Experiment 2		Experiment 3	
	Mole frac	F (ml/min)	Mole frac	F (ml/min)
CO	0.694	50	0.495	50
CO2	0.134	9.65	0.382	38.6
H2	0.095	6.85	0.068	6.85
N2	0.076	5.5	0.055	5.5

Species	Experiment 4		Experiment 5	
	Mole frac	F (ml/min)	Mole frac	F (ml/min)
CO	0.565	49.7	0.489	49.9
CO2	0.218	19.2	0.189	27.3
H2	0.155	13.6	0.268	19.3
N2	0.062	5.5	0.054	5.5

Species	Experiment 6		Experiment 7-12,16-20	
	Mole frac	Flow (ml/min)	Mole frac	Flow (ml/min)
CO	0.62	50	0.62	49.96
CO2	0.24	19.3	0.24	19.34
H2	0.085	6.85	0.085	6.85
N2	0.055	4.44*	0.055	4.43

\* Ar instead of N2

Species	Experiment 13		Experiment 14	
	Mole frac	Flow (ml/min)	Mole frac	Flow (ml/min)
CO	0.620	50	0.620	50
CO2	0.120	9.67	0.239	19.3
H2	0.085	6.85	0.128	10.3
Nr	0.175	14.1	0.012	1
Total		80.62		80.6

Experiment 15		
Species	Mole frac	Flow (ml/min)
CO	0.62	43.4
CO2	0	0
H2	0.085	5.95
Nr	0.295	20.65
Total		70

# Appendix B

## Commercial catalyst specifics

# Carbon Looping for Metallurgical Processes via Boudouard reaction over Magnetite

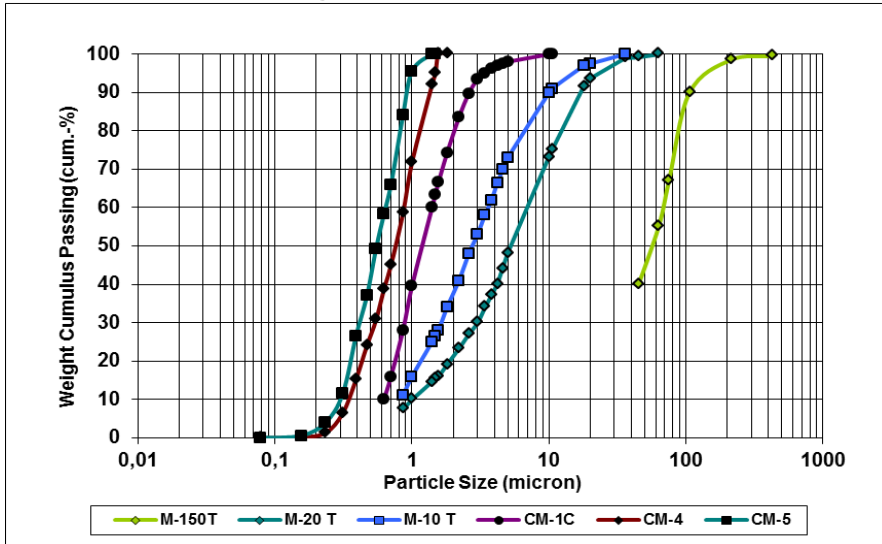


**RANA  
GRUBER**

**Technical Information**  
**COLORANA®**  
Page 1/1

RG Mineral AS  
Postboks 434, N-8601 Mo i Rana  
Tel.: +47 751 37 300, Fax: +47 751 37 302  
e-mail: [market@ranagruber.no](mailto:market@ranagruber.no)  
http: [www.ranagruber.no](http://www.ranagruber.no), [www.colorana.com](http://www.colorana.com)

## Particle Size Distribution Rana Gruber Magnetite Concentrates a. COLORANA®



	RGM COLORANA®	RGAS	RGM COLORANA®	RGM COLORANA®	RGM COLORANA®	RGM COLORANA®	RGM COLORANA®
Product	M-150T	M-40LS	M-20T	M-10T	CM-1C	CM-4	CM-5
Micron	Sieve analysis	Sieve analysis	Laser Dry	Laser Dry	Laser Dry	SEM	SEM
425	99,5						
212	98,5	100					
106	90	93					
75	67	85					
63	55	80	100				
45	40	70	99,5				
36		63	99	100			
20		35	94	98			
18			92	97			
10,5			75	91	100		
5			48	73	98		
3			30	53	93		
2,6			27	48	90		
1,56			16	28	67	100	
1,48			15	26	63	95	100
1			10	16	40	72	96
0,858			7	11	28	59	84
0,702					16	45	66
0,624					10	39	58
0,546						31	49
0,468						24	37
0,39						15	26
0,312						6,4	11,5
0,234						1,3	4
0,156						0,2	0,6

Doc.no.: IP-E-048d

Rev.no.: 003

Date: 2015-03-26

Carbon Looping for Metallurgical Processes via Boudouard reaction over Magnetite



**Product Specification**  
**Technical Data Sheet**  
Page 1/2

P.O.Box 434, N-8601 Mo i Rana  
Tel.: +47 751 37 300, Fax: +47 751 37 302  
e-mail: market @ ranagruber.no

**MO I RANA CONCENTRATE**  
**M - 40 LS**

**PRODUCT:**

**Magnetite Concentrate**

COMPONENTS:  
CHEMICAL FORMULA:  
CHEM. INVENTORY-no.:

Magnetite  
Fe<sub>3</sub>O<sub>4</sub>  
CAS-no: 1309-38-2, 1317-61-9  
EINECS-no.: 215-169-8, 215-277-5  
Natural product, not required  
No labelling, no registration

REACH-registration (1907/2006/EEC):  
CLP/GHS-status (1272/2008/EEC):

**TYPICAL ANALYSIS (Dry basis):**

	%	%	ppm	ppm
<b>Fe<sub>tot</sub></b>	<b>71.5*</b>	CaO 0.1	<b>S</b>	As 2
Fe <sub>2</sub> O <sub>3</sub>	-	MgO 0.1	P 20	Sb <0.5
Fe <sub>3</sub> O <sub>4</sub>	98.7	MnO 0.25	Cu 15	Bi <0.1
<b>SiO<sub>2</sub></b>	<b>0.65*</b>	K <sub>2</sub> O 0.02	Zn 100	Mo 4
Al <sub>2</sub> O <sub>3</sub>	0.2	Na <sub>2</sub> O 0.02	Pb < 0.5	Ni 50
TiO <sub>2</sub>	0.02		Cd < 0.1	V 50
			Cr 40	Co 30
				Hg <0.05

**H<sub>2</sub>O: 7.5 - 9.5\***

**PHYSICAL PROPERTIES:**

Angle of repose	36° to 41°
Stowage factor	average 0.37 m <sup>3</sup> /metric tonne
Specific density	5.2 g/cm <sup>3</sup>
Bulk density	2.7 g/cm <sup>3</sup>
Stamped density	2.9 g/cm <sup>3</sup>
Saturated volume weight	3.1 g/cm <sup>3</sup>

**SIZE DISTRIBUTION (Sieve analysis, dry basis):**

**0.063 mm = 50 to 80 % passing\***

**SAFETY:**

Consult the actual MSDS for this product. The product contains <0.08% RCS, crystalline silica in the thoracic fraction PM10.

Carbon Looping for Metallurgical Processes via Boudouard  
reaction over Magnetite



**Product Specification**  
**Technical Data Sheet**  
Page 2/2

P.O.Box 434, N-8601 Mo i Rana  
Tel.: +47 751 37 300, Fax: +47 751 37 302  
e-mail: market @ ranagruber.no

For a complete outline of regulations and risks connected to the product consult our IP-E-082a  
"Regulatory Information".

Moisture content is guaranteed to be <TML (Transport Moisture Limit).

**\*Specified values on Certificate of Analysis**

# Appendix C

## Internal standard and air-correction calculations



## Carbon Looping for Metallurgical Processes via Boudouard reaction over Magnetite

Excel spreadsheet and equations used for calculating air correction and internal standard calculation on experiment 7 (summary of experiments in appendix A) – for all 5 samples.

	calibration		input		ES		F <sub>OT</sub> _OUT [ml/min]	IS correction		X_CO
	RF	RFf	Area	Fi_IN	xi_OUT*ES	xi_OUT*air corr		Fi_OUT [ml/min]	xi_OUT	
Sample 1	H2	2.60E-02	1.53E+01	1.41E+02	0.037			3.283	0.037	
	CO2	1.54E-03	9.02E-01	1.26E+04	0.193			17.343	0.193	
	N2	1.71E-03	1.00E+00	2.88E+03	0.049	0.049		4.400	0.049	
	CO	1.83E-03	1.07E+00	1.60E+04	0.293			26.332	0.293	47%
	O2	8.98E-08	1.00E+00	3.27E+01	0.000			0.050	0.001	
	sum				0.572			51.408	0.573	
Sample 2	H2	2.60E-02	1.53E+01	1.38E+02	0.036			4.134	0.036	
	CO2	1.54E-03	9.02E-01	1.23E+04	0.189			21.819	0.189	
	N2	1.71E-03	1.00E+00	2.24E+03	0.038	0.038		115.34	0.038	
	CO	1.83E-03	1.07E+00	1.57E+04	0.288			33.182	0.288	34%
	O2	8.98E-08	1.00E+00	3.29E+02	0.000			0.647	0.006	
	sum				0.551			64.183	0.556	
Sample 3	H2	2.60E-02	1.53E+01	1.35E+02	0.035			3.032	0.035	
	CO2	1.54E-03	9.02E-01	1.28E+04	0.198			17.007	0.198	
	N2	1.71E-03	1.00E+00	3.00E+03	0.051	0.051		4.400	0.051	
	CO	1.83E-03	1.07E+00	1.49E+04	0.273			23.527	0.273	53%
	O2	8.98E-08	1.00E+00	2.09E+02	0.000			0.307	0.004	
	sum				0.558			48.273	0.561	
Sample 4	H2	2.60E-02	1.53E+01	1.40E+02	0.037			4.146	0.037	
	CO2	1.54E-03	9.02E-01	1.33E+04	0.205			23.271	0.205	
	N2	1.71E-03	1.00E+00	2.27E+03	0.039	0.039		4.400	0.039	
	CO	1.83E-03	1.07E+00	1.53E+04	0.281			31.821	0.281	36%
	O2	8.98E-08	1.00E+00	8.02E+00	0.000			0.016	0.000	
	sum				0.561			63.653	0.561	
Sample 5	H2	2.60E-02	1.53E+01	1.41E+02	0.037			4.269	0.037	
	CO2	1.54E-03	9.02E-01	1.34E+04	0.206			23.993	0.206	
	N2	1.71E-03	1.00E+00	2.22E+03	0.038	0.038		4.400	0.038	
	CO	1.83E-03	1.07E+00	1.53E+04	0.279			32.519	0.279	35%
	O2	8.98E-08	1.00E+00	1.76E+00	0.000			0.003	0.000	
	sum				0.560			65.184	0.560	

*External standard calculation:*

$$X_{i,out} = \frac{RF_i}{Area_i}$$
$$X_{N_2,out,air\ corr.} = \frac{x_{N_2} - 4x_{O_2}}{1 - 5x_{O_2}}$$

*Internal standard correction:*

$$F_{tot} = \frac{F_{N_2,in}}{x_{N_2,out,air\ corr.}}$$
$$F_{i,out} = \frac{Area_i}{Area_{N_2} * RRF_i * F_{N_2,in}}$$
$$x_{i,out} = \frac{F_{i,out}}{F_{tot,out}}$$

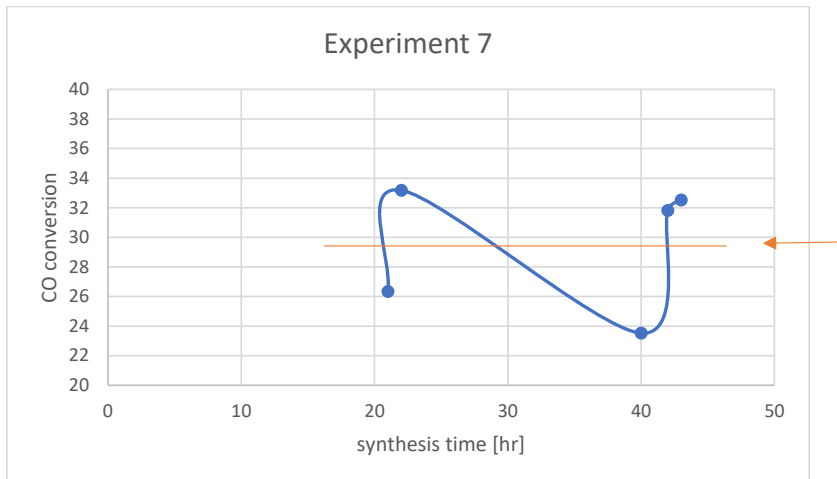
# Appendix D

## Procedure for choosing GC data

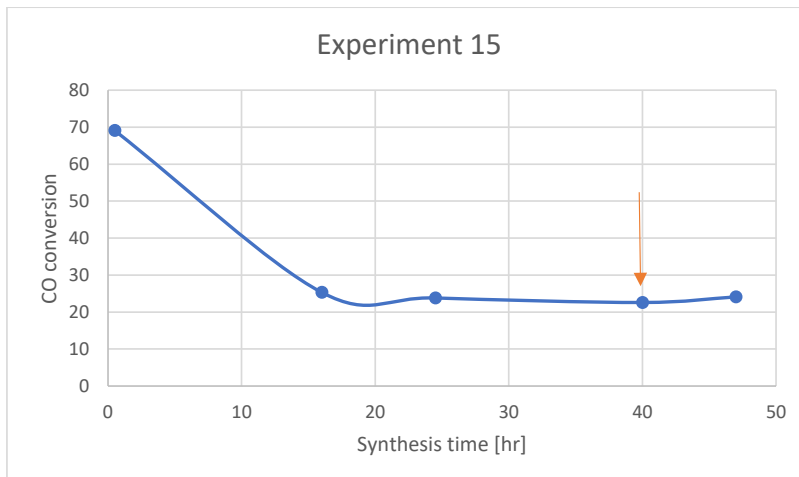
## Carbon Looping for Metallurgical Processes via Boudouard reaction over Magnetite

### Choosing GC – data (shown for experiment 7 and 15 in appendix A)

In those cases (like exp.7) where the CO conversion fluctuated over time, average mole fractions (out) and flows (ml/min, out) were calculated and applied in the results.



In cases like exp. 15, the mole fractions (out) and flows (ml/min, out) of samples obtained late in the synthesis time are used as results.



# Appendix E

## Case study calculation example

# Carbon Looping for Metallurgical Processes via Boudouard reaction over Magnetite

Calculation example Casestudy (industrial condition – experimental results)

---

**Calculating the mass flows:**

$$\dot{m}_{CO} = \frac{P * V_{CO}}{R * T} * Mm_{CO}$$

$$\dot{m}_C = \frac{m_{c,tot}}{\text{synthesis time (min)}}$$

**Calculating normalized mass fractions:**

$$m_{frac,norm} = \frac{m_{frac,i}}{\sum m_{frac,(CO,CO2,C)}}$$

IN			OUT	
Comp (IND)	mfrac,i,norm	Toni/ton <sub>m</sub>	mfrac,i,norm	Toni/ton <sub>m</sub>
CO	0.622	0.941	0.447	0.657
CO2	0.378	0.556	0.516	0.759
C	0.000	0.000	0.037	0.054
Total	1	1.47	1	1.47

**Calculating the ton of species i per ton metal produced:**

$$\frac{ton_i}{ton_M} = m_{frac,i,norm} * \frac{ton_{CO2}}{ton_M} (eramet)$$

$$\frac{ton_{CO}}{ton_M} = 0.447 * 1.47 = 0.657$$

**Calculating the CO2 reduction potential:**

$$\% \text{red. } CO_2 \text{ emissions} = \frac{\frac{ton_{CO2}}{ton_M} (eramet) - \left( \frac{ton_{CO2}}{ton_M} + \frac{ton_{CO}}{ton_M} \right)}{\frac{ton_{CO2}}{ton_M} (eramet)} * 100\%$$

$$\% \text{red. } CO_2 \text{ emissions} = \frac{1.47 - (0.657 + 0.759)}{1.47} * 100\% = 3.7\%$$

**Calculating the reducing agent reduction potential:**

$$\% \text{red. in required C} = 100 - \frac{\frac{ton_{red.agent}}{ton_M} (eramet) - \frac{ton_C}{ton_M}}{\frac{ton_{red.agent}}{ton_M} (eramet)} * 100\%$$

$$\% \text{red. in required C} = 100 - \frac{0.734 - 0.054}{0.734} * 100\% = 7.3\%$$

# Appendix F

## Detailed Risk assessment

# Carbon Looping for Metallurgical Processes via Boudouard reaction over Magnetite



---

<b>ID</b>	34566	<b>Status</b>	<b>Date</b>
<b>Risk Area</b>	Risikovurdering: Helse, miljø og sikkerhet (HMS)	Created	16.09.2019
<b>Created by</b>	Maren Wassås Kveinå	Assessment started	14.01.2020
<b>Responsible</b>	De Chen	Measures decided	
		Closed	

## Risk Assessment:

### Cat\_Master Student\_2020\_Maren Kveinå

---

#### Valid from-to date:

6/12/2019 - 7/30/2020

#### Location:

Chemistry block 5-228

#### Goal / purpose

The goal of the risk assesment is a careful examination of what could cause injury or illness in working with carbon synthesis from oven gas in metal production processes for CO2 emission reduction. The risk assessment will assess whether existing actions are sufficient, or whether new actions must be implemented to reduce the risk.

#### Background

The background for doing the risk assessment is that it is statutory by the government and NTNU. The risk assesment is required to avoid hazardous situations in the work environment by being aware of the consequences related to the laboratory work.

#### Description and limitations



# Carbon Looping for Metallurgical Processes via Boudouard reaction over Magnetite



The risk related to the laboratory work will be limited by preparing an action plan. The Action plan contains risk identification, analysis, evaluation and risk management. This involves identifying and understanding the risk the work may cause - an assessment of causes and sources, the consequences these may have and the likelihood of how frequent they may occur. The evaluation involves the risks that needs to be addressed, as well as the priority of them. The management involves a selection of measures to counteract the greatest dangers listed in the risk assessment.

## PREPARATION OF GROWTH CATALYST:

CNF preparation

- Fe/graphite flakes

Magnetite (Fe<sub>3</sub>O<sub>4</sub> reduced in H<sub>2</sub>/Ar)

- Combining purified deoxygenated water (25 mL) and HCL (0.85 mL, 12.1 M) addition of FeCl<sub>3</sub> (5.2 g) and FeCl<sub>2</sub> (2.0 g) stirred before dropwise addition of NaOH (1.5 M, 250 mL). Separation using deoxygenated water and HCl (500 mL, 0.01 M) and centrifuging at 4000 rpm.

- washed with purified deoxygenated water

- vacuum drying at 70°C

- reduced in H<sub>2</sub>/Ar (80/20 ml/min) at 600°C for 6 h

(CVD furnace set-up K5-228)

## GROWTH OF CARBON NANOFIBER

- PCNF growth: CVD at 600°C for up to 48h in CO/H<sub>2</sub> (50/12,5 mL/min) (CVD furnace set-up)

with Fe/graphite flakes as catalyst

- PCNF growth: CVD at 600°C for up to 48h in CO/CO<sub>2</sub>/H<sub>2</sub> (50/30/12,5 mL/min - might be slightly altered) (CVD furnace set-up)

Rough estimate of PCNF size:

500-4000 nm long

100-700 nm large

## CHARACTERIZATION OF CATALYSTS AND CARBON SAMPLES

- XRD: Da Vinci 1 Diffractometer, K2-XRD lab

Method for identifying the phases present in unknown polycrystalline powders - performed by comparing diffraction pattern collected from sample with patterns of known compounds.

- Raman Spectroscopy: Horiba Jibin Yvon LabRAM HR800, K5-Raman lab

Method for identifying the crystalline, nanocrystalline, and amorphous carbons using laser beam (laser excitation wavelength of 633 nm).

April-Mai 2020 - preventive measures towards Covid-situation:

1) Switch off procedure for CVD set-up 1 in K5-228 and/or GC 7820A CHD

- Stop the experiment:

Reactor setup: Stop reagents feed, turn off oven and cool down reactor.

GC 7820A: stop sequence and set bakeout method

- Purge the set-up flowing N<sub>2</sub> (CVD)

- Close the vial for gas sampling, if sample is already collected, use fume hood to empty it (CVD)

- Switch off the GC

2) Risk related to shortage of personnel in the labs:

All the lab activities can continue regularly but taking extra-safety measures. I am not able to avoid all toxic gases (must use H<sub>2</sub> and CO) but will carefully monitor gas detectors (both installed on wall and hand held detector). CVD-setup 1 K5-228.

3) Safety measures related to spread of covid19 infection:

- Avoid touching the face

- Wash hands as often as possible

- Keep 2m distance from colleagues

- Use nitrile gloves when touching shared lab set-ups and equipment (GC and oven/MFC in CVD setup)

- Disinfect all surfaces with ethanol before and after touching them with bare hands

## Prerequisites, assumptions and simplifications

The prerequisite for following the HSE requirements is that the laboratories are equipped with sufficient equipment for safety and that everybody working in the laboratories are aware of the HSE regulations. It is also necessary to have good communications with the HSE coordinators and the colleagues working in the lab.

## Attachments

Norges teknisk-naturvitenskapelige universitet (NTNU)

Untatt offentlighet jf. Offentlighetsloven § 14

Print date:

24.07.2020

Printed by:

Maren Wassås Kveinå

Page:

2/19

# Carbon Looping for Metallurgical Processes via Boudouard reaction over Magnetite

---



---

MSDS graphite.pdf  
MSDS iron(III)nitratnonahydrate.pdf  
MSDS CNF.pdf  
MSDS CO.pdf  
MSDS NH3.pdf  
K5\_228\_CVD\_Unit\_1\_Maren\_ApparatusCard.doc

## References

[Ingen registreringer]

# Carbon Looping for Metallurgical Processes via Boudouard reaction over Magnetite







## Summary, result and final evaluation



The summary presents an overview of hazards and incidents, in addition to risk result for each consequence area.



<b>Hazard:</b>	<b>Carbon</b>			
<b>Incident:</b>	<b>Inhalation of carbon particles</b>			
<b>Consequence area:</b>	Helse	Risk before measures:		Risiko after measures:
<b>Incident:</b>	<b>Spillage of carbon materials</b>			
<b>Consequence area:</b>	Helse	Risk before measures:		Risiko after measures:
	Materielle verdier	Risk before measures:		Risiko after measures:
<b>Hazard:</b>	<b>Flamable gas (H2), toxic gas (CO and NH3), oxidiser gas</b>			
<b>Incident:</b>	<b>Gasleak</b>			
<b>Consequence area:</b>	Helse	Risk before measures:		Risiko after measures:
	Ytre miljø	Risk before measures:		Risiko after measures:
<b>Hazard:</b>	<b>High temperature</b>			
<b>Incident:</b>	<b>Contact with elements with high temperature</b>			
<b>Consequence area:</b>	Helse	Risk before measures:		Risiko after measures:
<b>Hazard:</b>	<b>Gases under pressure</b>			
<b>Incident:</b>	<b>Leakage of high-pressure gas</b>			
<b>Consequence area:</b>	Helse	Risk before measures:		Risiko after measures:
	Ytre miljø	Risk before measures:		Risiko after measures:

# Carbon Looping for Metallurgical Processes via Boudouard reaction over Magnetite





<b>Hazard:</b>	<b>Flamable liquids</b>			
<b>Incident:</b>	<b>Spillage/contact flamable liquids</b>			
<b>Consequence area:</b>	Helse	Risk before measures:	 Risiko after measures:	
	Materielle verdier	Risk before measures:	 Risiko after measures:	

<b>Hazard:</b>	<b>Toxic liquids</b>			
<b>Incident:</b>	<b>Spillage/contact toxic liquids</b>			
<b>Consequence area:</b>	Helse	Risk before measures:	 Risiko after measures:	

<b>Hazard:</b>	<b>working in the lab under covid-situation</b>			
<b>Incident:</b>	<b>Getting infected with Covid</b>			
<b>Consequence area:</b>	Helse	Risk before measures:	 Risiko after measures:	

<b>Incident:</b>	<b>Working alone</b>			
<b>Consequence area:</b>	Helse	Risk before measures:	 Risiko after measures:	
	Materielle verdier	Risk before measures:	 Risiko after measures:	

<b>Incident:</b>	<b>Carrier of infection (Covid19)</b>			
<b>Consequence area:</b>	Helse	Risk before measures:	 Risiko after measures:	

**Final evaluation**



## Organizational units and people involved

A risk assessment may apply to one or more organizational units, and involve several people. These are listed below.

### Organizational units which this risk assessment applies to

- Institutt for kjemisk prosesssteknologi

### Participants

Estelle Marie M. Vanhaecke

De Chen

Anne Hoff

Martina Cazzolaro

### Readers

[Ingen registreringer]

### Others involved/stakeholders

[Ingen registreringer]

## The following accept criteria have been decided for the risk area Risikovurdering: Helse, miljø og sikkerhet (HMS):

### Helse



### Materielle verdier



### Omdømme



### Ytre miljø





## Overview of existing relevant measures which have been taken into account

The table below presents existing measures which have been taken into account when assessing the likelihood and consequence of relevant incidents.

Hazard	Incident	Measures taken into account
Carbon	Inhalation of carbon particles	Protective equipment
	Inhalation of carbon particles	Fume hood
	Inhalation of carbon particles	Covering material for tables and equipments
	Spillage of carbon materials	Protective equipment
	Spillage of carbon materials	Fume hood
	Spillage of carbon materials	Covering material for tables and equipments
	Spillage of carbon materials	Waste disposal containers
Flamable gas (H <sub>2</sub> ), toxic gas (CO and NH <sub>3</sub> ), oxidiser gas	Gasleak	Local gas detectors: CO, H <sub>2</sub> , CH <sub>4</sub> , C <sub>3</sub> H <sub>8</sub>
	Gasleak	Portable gas detector for CO and H <sub>2</sub>
	Gasleak	Ventilation box
High temperature	Contact with elements with high temperature	Protective equipment
	Contact with elements with high temperature	Ventilation box
Gases under pressure	Leakage of high-pressure gas	Local gas detectors: CO, H <sub>2</sub> , CH <sub>4</sub> , C <sub>3</sub> H <sub>8</sub>
	Leakage of high-pressure gas	Portable gas detector for CO and H <sub>2</sub>
	Leakage of high-pressure gas	Ventilation box
Flamable liquids	Spillage/contact flammable liquids	Protective equipment
	Spillage/contact flammable liquids	Ventilation box
Toxic liquids	Spillage/contact toxic liquids	Protective equipment
	Spillage/contact toxic liquids	Fume hood
	Spillage/contact toxic liquids	Covering material for tables and equipments
	Spillage/contact toxic liquids	Ventilation box
working in the lab under covid-situation	Getting infected with Covid	Protective equipment
	Getting infected with Covid	Covering material for tables and equipments
	Working alone	Protective equipment
	Working alone	Fume hood
	Working alone	Covering material for tables and equipments
	Working alone	Waste disposal containers
	Working alone	Local gas detectors: CO, H <sub>2</sub> , CH <sub>4</sub> , C <sub>3</sub> H <sub>8</sub>
	Working alone	Portable gas detector for CO and H <sub>2</sub>
Working alone	Ventilation box	

# Carbon Looping for Metallurgical Processes via Boudouard reaction over Magnetite



working in the lab under covid-situation	Working alone	Fire instructions
	Carrier of infection (Covid19)	

## Existing relevant measures with descriptions:

### Protective equipment

When working in the laboratory protective equipment like labcoats, goggles and protective gloves should be accessible and used when required (handling of reagents and equipment in the lab).

### Fume hood

Fume hood for good ventilation when handling chemical compounds that evaporate or spread to the environment through dust etc.

### Covering material for tables and equipments

[Ingen registreringer]

### Waste disposal containers

Specific disposals for different chemicals, compounds

### Local gas detectors: CO, H<sub>2</sub>, CH<sub>4</sub>, C<sub>3</sub>H<sub>8</sub>

[Ingen registreringer]

### Portable gas detector for CO and H<sub>2</sub>

[Ingen registreringer]

### Ventilation box

Rig will be inside ventilation box

### Fire instructions

Fire instructions should be easily accessible and contain information on what to do in case of fire. That includes instructions on notification, escape routes and various extinguishing methods.



## Risk analysis with evaluation of likelihood and consequence

This part of the report presents detailed documentation of hazards, incidents and causes which have been evaluated. A summary of hazards and associated incidents is listed at the beginning.

**The following hazards and incidents has been evaluated in this risk assessment:**

- **Carbon**
  - Inhalation of carbon particles
  - Spillage of carbon materials
- **Flamable gas (H<sub>2</sub>), toxic gas (CO and NH<sub>3</sub>), oxidiser gas**
  - Gasleak
- **High temperature**
  - Contact with elements with high temperature
- **Gases under pressure**
  - Leakage of high-pressure gas
- **Flamable liquids**
  - Spillage/contact flammable liquids
- **Toxic liquids**
  - Spillage/contact toxic liquids
- **working in the lab under covid-situation**
  - Getting infected with Covid
  - Working alone
  - Carrier of infection (Covid19)





## Detailed view of hazards and incidents:

### Hazard: Carbon

---

#### Incident: Inhalation of carbon particles

---

Can cause respiratory irritations.

Likelihood of the incident (common to all consequence areas): **Less likely (2)**

*Kommentar:*

Use of protective equipment makes this "less likely". The laboratories are also equipped with disposable face masks.

#### Consequence area: Helse

Assessed consequence: **Small (1)**

*Comment:* May be some irritation on lungs/skin but the safety measurements should attribute to a small consequence if an incident occurs.

**Risk:**



#### Incident: Spillage of carbon materials

---

Likelihood of the incident (common to all consequence areas): **Likely (3)**

*Kommentar:*

Frequent work with carbon materials (catalyst preparation)

#### Consequence area: Helse

Assessed consequence: **Small (1)**

*Comment:* Personal protection equipment (labcoat, goggles, gloves) in addition to mask when necessary. Fume hood also available. Will not be in contact with the skin, and risk attached to contact is not very high.

**Risk:**



#### Consequence area: Materielle verdier

Assessed consequence: **Small (1)**

*Comment:* Use of covering material for tables and equipment, fume hood, waste disposal containers nearby working area. If incident occurs materials and equipment will not be highly affected.

**Risk:**



# Carbon Looping for Metallurgical Processes via Boudouard reaction over Magnetite



---

## Hazard: Flammable gas (H2), toxic gas (CO and NH3), oxidiser gas

---

### Incident: Gasleak

---

Leak of flammable/toxic/oxidiser gas

Likelihood of the incident (common to all consequence areas): **Less likely (2)**

Kommentar:

Leak testing with inert gases before experiment

### Consequence area: Helse

Assessed consequence: **Small (1)**

Comment: The rig is placed in a ventilated box. Will not work with high amounts of gas.

Risk:



### Consequence area: Ytre miljø

Assessed consequence: **Small (1)**

Comment: The rig is placed inside a ventilated box. Small amounts of gas.

Risk:



# Carbon Looping for Metallurgical Processes via Boudouard reaction over Magnetite



---

## Hazard: High temperature

---

### Incident: Contact with elements with high temperature

---

Likelihood of the incident (common to all consequence areas): **Less likely (2)**

Kommentar:

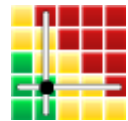
The elements of high temperature is isolated in ventilation box

### Consequence area: Helse

Assessed consequence: **Medium (2)**

Comment: Use of protective equipment and ventilation box

**Risk:**





---

## Hazard: Gases under pressure

---

### Incident: Leakage of high-pressure gas

---

Likelihood of the incident (common to all consequence areas): **Less likely (2)**

Kommentar:

Leak might happen but leak tests are done continuously during experiment.

### Consequence area: Helse

Assessed consequence: **Small (1)**

Comment: Rig inside ventilation box in addition to gas detectors.

Risk:



### Consequence area: Ytre miljø

Assessed consequence: **Small (1)**

Comment: Rig inside ventilated box.

Risk:



# Carbon Looping for Metallurgical Processes via Boudouard reaction over Magnetite



---

## Hazard: Flammable liquids

---

### Incident: Spillage/contact flammable liquids

---

Likelihood of the incident (common to all consequence areas): **Likely (3)**

Kommentar:

Frequent work with flammable chemicals.

### Consequence area: Helse

Assessed consequence: **Small (1)**

Comment: Work under fume hood and use of personal protective equipment. Contact with skin prevented by gloves.

**Risk:**



### Consequence area: Materielle verdier

Assessed consequence: **Small (1)**

Comment: Work will be done in fume hood or under point ventilation. Protective materials placed on working area (bench). Will keep flammable liquids away from high temperature equipment.

**Risk:**



# Carbon Looping for Metallurgical Processes via Boudouard reaction over Magnetite



---

**Hazard: Toxic liquids**

---

**Incident: Spillage/contact toxic liquids**

---

Likelihood of the incident (common to all consequence areas): **Likely (3)**

*Kommentar:*

Frequent work with toxic chemicals.

**Consequence area: Helse**

Assessed consequence: **Small (1)**

*Comment:* Protective equipment and use of fume hood/ventilated box in addition to covering material for equipment and tables making clean-up easier/safer.

**Risk:**





## Hazard: working in the lab under covid-situation

---

### Incident: Getting infected with Covid

---

*Cause:* Contact with infected person

*Likelihood of the incident (common to all consequence areas):* **Unlikely (1)**

*Kommentar:*

Will keep a good distance (minimum 2 meters) from other personell on lab. In case of touching equipment with bare hands, I will wash my hands and use Ethanol on the equipment.

### Consequence area: Helse

*Assessed consequence:* **Medium (2)**

*Comment:* Considering my age, the health conseqense for me personally is not big. However, if I infect others it might be - Medium.

**Risk:**



### Incident: Working alone

---

*Cause:* Accident in lab when working alone

*Description:*

Accidents (spillage of toxic liquids/leakage of toxic gas/) and how to handle them when working alone

*Likelihood of the incident (common to all consequence areas):* **Less likely (2)**

*Kommentar:*

Doing experiments I have done routinely during the entire project, familiar with all risks and how to avoid them.

### Consequence area: Helse

*Assessed consequence:* **Small (1)**

*Comment:* There could be damage to health when working alone if for example toxic liquids spills or toxic gas leak, however, I am not working with toxic liquids and use gas detectors regularly when working with toxic gases. In addition, if a leak occurs, the amount will be quite small when it is detected, and is therefore not very hazardous to my health.

**Risk:**



# Carbon Looping for Metallurgical Processes via Boudouard reaction over Magnetite



## Consequence area: Materielle verdier

Assessed consequence: **Small (1)**

*Comment:* The rig I am using toxic gases in is an enclosed space so material assets are separated from the leak.

**Risk:**



## Incident: Carrier of infection (Covid19)

---

*Cause:* Meeting people

*Description:*

From going to store, on walks and on lab etc.

*Likelihood of the incident (common to all consequence areas):* **Unlikely (1)**

*Kommentar:*

I am following all advice given by the WHO (keeping distance, washing hands regularly, no gatherings with more than 5 people etc.)

## Consequence area: Helse

Assessed consequence: **Large (3)**

*Comment:* The consequence of being a carrier of the virus is large considering I will not know that I am spreading the virus.

**Risk:**







---

**Overview of risk mitigating measures which have been decided:**

Below is an overview of risk mitigating measures, which are intended to contribute towards minimizing the likelihood and/or consequence of incidents:

**Overview of risk mitigating measures which have been decided, with description:**



**Detailed view of assessed risk for each hazard/incident before and after mitigating measures**

